

TRACKER-AWARE DETECTION:
A THEORETICAL AND AN EXPERIMENTAL STUDY

A THESIS SUBMITTED TO
THE GRADUATE SCHOOL OF NATURAL AND APPLIED SCIENCES
OF
MIDDLE EAST TECHNICAL UNIVERSITY

BY

MURAT ŞAMİL ASLAN

IN PARTIAL FULFILLMENT OF THE REQUIREMENTS
FOR
THE DEGREE OF DOCTOR OF PHILOSOPHY
IN
ELECTRICAL AND ELECTRONICS ENGINEERING

FEBRUARY 2009

Approval of the thesis:

**TRACKER-AWARE DETECTION:
A THEORETICAL AND AN EXPERIMENTAL STUDY**

submitted by **MURAT ŞAMİL ASLAN** in partial fulfillment of the requirements for the degree of **Doctor of Philosophy in Electrical and Electronics Engineering Department, Middle East Technical University** by,

Prof. Dr. Canan Özgen _____
Dean, Graduate School of **Natural and Applied Sciences**

Prof. Dr. İsmet Erkmek _____
Head of Department, **Electrical and Electronics Engineering**

Assist. Prof. Dr. Afşar Saranlı _____
Supervisor, **Electrical and Electronics Engineering Dept., METU**

Prof. Dr. Buyurman Baykal _____
Co-supervisor, **Electrical and Electronics Engineering Dept., METU**

Examining Committee Members:

Prof. Dr. Mübeccel Demirekler _____
Electrical and Electronics Engineering Dept., METU

Assist. Prof. Dr. Afşar Saranlı _____
Electrical and Electronics Engineering Dept., METU

Assoc. Prof. Dr. Tolga Çiloğlu _____
Electrical and Electronics Engineering Dept., METU

Assoc. Prof. Dr. Gökhan Taner _____
TÜBİTAK-UEKAE

Assist. Prof. Dr. Sinan Gezici _____
Electrical and Electronics Engineering Dept., Bilkent University

Date: 17.02.2009

I hereby declare that all information in this document has been obtained and presented in accordance with academic rules and ethical conduct. I also declare that, as required by these rules and conduct, I have fully cited and referenced all material and results that are not original to this work.

Name, Last Name: MURAT ŞAMİL ASLAN

Signature :

ABSTRACT

TRACKER-AWARE DETECTION: A THEORETICAL AND AN EXPERIMENTAL STUDY

Aslan, Murat Şamil

Ph.D., Department of Electrical and Electronics Engineering

Supervisor : Assist. Prof. Dr. Afşar Saranlı

Co-Supervisor : Prof. Dr. Buyurman Baykal

February 2009, 140 pages

A promising line of research attempts to bridge the gap between detector and tracker by means of considering jointly optimal parameter settings for both of these subsystems. Along this fruitful path, this thesis study focuses on the problem of detection threshold optimization in a tracker-aware manner so that a feedback from the tracker to the detector is established to maximize the overall system performance. Special emphasis is given to the optimization schemes based on two non-simulation performance prediction (NSPP) methodologies for the probabilistic data association filter (PDAF), namely, the modified Riccati equation (MRE) and the hybrid conditional averaging (HYCA) algorithm.

The possible improvements are presented in two domains: Non-maneuvering and maneuvering target tracking. In the first domain, a number of algorithmic

and experimental evaluation gaps are identified and newly proposed methods are compared with the existing ones in a unified theoretical and experimental framework. Furthermore, for the MRE based dynamic threshold optimization problem, a closed-form solution is proposed. This solution brings a theoretical lower bound on the operating signal-to-noise ratio (SNR) concerning when the tracking system should be switched to the track before detect (TBD) mode.

As the improvements of the second domain, some of the ideas used in the first domain are extended to the maneuvering target tracking case. The primary contribution is made by extending the dynamic optimization schemes applicable to the PDAF to the interacting multiple model probabilistic data association filter (IMM-PDAF). Resulting in an online feedback from the filter to the detector, this extension makes the tracking system robust against track losses under low SNR values.

Keywords: Tracker-aware detection threshold optimization, modified Riccati equation, hybrid conditional averaging algorithm, interacting multiple model probabilistic data association filter (IMM-PDAF), track before detect approach

ÖZ

İZLEYİCİ-FARKINDA SEZİM: BİR KURAMSAL VE DENEYSEL ÇALIŞMA

Aslan, Murat Şamil

Doktora, Elektrik ve Elektronik Mühendisliği Bölümü

Tez Yöneticisi : Yard. Doç. Dr. Afşar Saranlı

Ortak Tez Yöneticisi : Prof. Dr. Buyurman Baykal

Şubat 2009, 140 sayfa

Umut vaat eden bir araştırma kolu, sezimci ve izleyici arasında, her iki alt sistem için birleşik olarak eniyi parametre ayarlarını gözönüne alarak, bir köprü kurma çabası içindedir. Bu verimli yolda, bu tez çalışması, izleyici-farkında olarak, sezimci eşiği eniyileme problemine odaklanmaktadır. Bu şekilde, izleyiciden sezimciye, tüm sistemin performansını artıracak şekilde bir geri besleme yapılmaktadır. Özel olarak, olasılıksal veri ilişkilendirme süzgeci (PDAF) için geliştirilmiş iki benzetimsiz başarı tahmini (NSPP) yöntemlili olan, değiştirilmiş Riccati denklemi (MRE) ve melez koşullu ortalama alma (HYCA) algoritması yöntemliliklerine dayanan eniyileme tasarımlarına ağırlık verilmektedir.

Olası geliştirimler iki alanda sunulmaktadır: Manevrasız ve manevralı hedef izleme. İlk alanda, bir takım algoritmik ve deneysel değerlendirme boşlukları

belirlenmekte ve birleřtirici bir kuramsal ve deneysel çatı altında, yeni önerilen yöntemler, mevcut olanlarla karşılaştırılmaktadır. Ayrıca, MRE tabanlı dinamik eşik eniyileme problemi için, kapalı bir çözüm önerilmektedir. Bu çözüm, izleme sisteminin ne zaman, sezmeden önce izle (TBD) moduna geçmesi gerektiğine dair, çalışılan işaret gürültü oranı (SNR) üzerinde kuramsal bir alt sınır getirmektedir.

İkinci alandaki geliřtirmeler olarak, ilk alanda kullanılan bazı fikirler, manevralı hedef izleme durumu için genişletilmiştir. Birincil katkı, PDAF için uygulanabilen dinamik eniyileme yaklaşımlarının, etkileşimli çoklu model olasılıksal veri ilişkilendirme süzgeci (IMM-PDAF) için genişletilmesi ile yapılmıştır. Süzgeçten sezimciye çevrim içi bir geri beslemeyi sonuç veren bu genişletme, düşük SNR değerleri altında, izleme sistemini iz kayıplarına karşı gürbüz hale getirmiştir.

Anahtar Kelimeler: İzleyici-farkında sezim eşiđi eniyileme, deđiřtirilmiş Riccati denklemi (MRE), melez koşullu ortalama alma (HYCA) algoritması, çoklu model olasılıksal veri ilişkilendirme süzgeci (IMM-PDAF), sezmeden önce izle yaklaşımı

To Gülistan and Ayşe Naz,

ACKNOWLEDGMENTS

First of all, I would like to thank my thesis supervisor Assist. Prof. Dr. Afşar Saranlı for his sincere and friendly support, encouragement and guidance throughout the thesis work. I greatly appreciate his patience and belief which helped me recover during disappointing periods of the thesis study.

I would also thank my thesis co-supervisor Prof. Dr. Buyurman Baykal for his support and reference at the beginning of my graduate education as well as my business life.

I would like to thank my thesis progress committee members Assoc. Prof. Dr. Tolga Çiloğlu and Assoc. Prof. Dr. Gökhan Tanyer. They have been involved continuously in the progress of the study and their support, encouragement and suggestions have improved the quality of the thesis. I should also thank my thesis defense committee members Prof. Dr. Mübeccel Demirekler and Assist. Prof. Dr. Sinan Gezici for spending their time and effort in reading and evaluation of the thesis.

I should also mention about my office and team at İLTAREN Research and Development Group. I would like to thank Assoc. Prof. Dr. Gökhan Tanyer and my team leader Dr. Murat Akgül for their understanding and friendship.

Moreover, I would like to thank Dr. Umut Orguner for his valuable comments and fruitful discussions at any time that he shared with me.

Finally, of course, I owe much thanks to my wife Gülistan, my daughter Ayşe Naz and my parents who have shared and relieved my stress during this long marathon. I can not forget their altruism and I feel their support and love all my life.

TABLE OF CONTENTS

ABSTRACT	iv
ÖZ	vi
DEDICATION	viii
ACKNOWLEDGMENTS	viii
TABLE OF CONTENTS	x
LIST OF TABLES	xiv
LIST OF FIGURES	xv
LIST OF ABBREVIATIONS	xxii
LIST OF SYMBOLS	xxv
CHAPTERS	
1 INTRODUCTION	1
1.1 Outline of the Thesis	5
1.2 Contributions	6
2 OFFLINE PERFORMANCE EVALUATION OF TRACKING ALGORITHMS	8
2.1 Introduction	8
2.2 An Overview of Non-Simulation Performance Predic- tion (NSPP) Methodologies	10
2.3 Application Areas of NSPP Techniques and Thesis Focus	12
2.4 The Baseline NSPP Tool for the Kalman Filter: The Riccati Equation	13

2.5	NSPP Techniques for the PDAF	16
2.5.1	The Modified Riccati Equation (MRE)	16
2.5.2	The Hybrid Conditional Averaging (HYCA) Algorithm	25
3	A COMPARISON OF TA-DETOP SCHEMES IN A UNIFIED THEORETICAL AND EXPERIMENTAL FRAMEWORK	31
3.1	Static Threshold Optimization (STOP)	32
3.2	Dynamic Threshold Optimization (DTOP)	34
3.2.1	MRE-Based Formulation	34
3.2.2	HYCA-Based Formulation	35
3.3	Simulation Results	35
3.3.1	Obtaining TOC Curves	38
3.3.2	Experiment1: Comparison of STOP with Conventional Approaches	42
3.3.3	Experiment2: Comparison of STOP with the MRE-Based DTOP	47
3.3.4	Experiment3: Comparison of DTOP Schemes	50
3.3.5	Combining the Results	54
3.4	Conclusion	57
4	A CLOSED-FORM SOLUTION FOR THE MRE-BASED DYNAMIC THRESHOLD OPTIMIZATION PROBLEM	58
4.1	Introduction	59
4.2	The Modified Riccati Equation (MRE)	61
4.3	Problem Formulation and Solution	64
4.3.1	Prior Detection Threshold Optimization	65
4.3.2	A Functional Approximation to the IRF	67
4.3.3	Obtaining a Closed-Form Solution	68
4.3.4	Considering Different Detectors	69
4.3.5	Neyman-Pearson (NP) Detector Case	71
4.4	Interpretation of the Result and Practical Issues	72

4.5	Simulation Results	75
4.5.1	Experiment1: Comparison with Conventional Approaches	77
4.5.2	Experiment2: Comparison with Line Search Optimization Schemes	79
4.6	Conclusion	83
5	EXTENSIONS TO MANEUVERING TARGET TRACKING CASE	85
5.1	Introduction	85
5.2	Proposed Optimization Schemes	88
5.2.1	A Heuristic Extension	88
5.2.2	A Multiple Model Filter Integrated Extension	94
5.3	Simulation Results	97
5.3.1	Experiment1: Comparison of Proposed Methods with Conventional Approaches	101
5.3.2	Experiment2: Comparison of MRE and HYCA Based Approaches	104
5.4	Conclusion	104
6	DISCUSSION AND FUTURE WORK	107
	REFERENCES	109
	APPENDICES	
A	TRACKING AND FUSION SIMULATOR (TAFSIM)	117
A.1	Modeling Target Kinematics	120
A.2	Modeling Radar Scanning	121
A.3	Modeling Radar Measurements	122
A.3.1	Generating Target-Originated Measurements	122
A.3.2	Generating the Measurements Due to Clutter	124
A.4	Implemented Tracking Filters	125
B	PROBABILISTIC DATA ASSOCIATION FILTER	128
B.1	Assumptions	128

B.2	Steps of the Algorithm	129
C	INTERACTING MULTIPLE MODEL ESTIMATOR	134
C.1	Assumptions	134
C.2	Steps of the Algorithm	135
VITA	138

LIST OF TABLES

TABLES

Table 3.1	Exponential fit coefficients for STOP curves.	41
Table 3.2	Experiment-I: Compared tracking systems. The name of the proposed system is written in italic.	42
Table 3.3	Experiment-II: Compared tracking systems. The name of the proposed system is written in italic.	47
Table 3.4	Experiment-III: Compared tracking systems. The system whose name is written in italic is proposed in this study.	50
Table 4.1	Experiment I: Compared tracking systems.	77
Table 4.2	Experiment II: Compared tracking systems.	79
Table 5.1	Minimum and maximum SNR values for different values of the SNR constant, C_{ζ}	99
Table 5.2	Experiment-I: Compared tracking systems.	101
Table 5.3	Experiment-II: Compared tracking systems.	104

LIST OF FIGURES

FIGURES

- Figure 1.1 The block diagram of a conventional tracking system. This block diagram is rather generic in the sense that the sensor can be either an active one such as an active sonar, a radar or a ladar (laser detection and ranging), or a passive one such as an electro-optical (EO), an infrared (IR), or a passive sonar sensor. In the case of an active sensor, the energy flow in the channel is *bidirectional*. The type of energy can be either *electromagnetic* as in the case of radar, ladar, EO and IR sensors, or *acoustic* as in the case of a (active/passive) sonar. The focus of the thesis, as shown in the figure, is to a large extent independent of the sensor type used except when a specific detector is used as an example. However, to be more focused, the presentation in this thesis is in the context of a radar sensor. 2
- Figure 1.2 The algorithmic space of tracker-aware detector threshold optimization (TA-DETOP) schemes for the PDAF. The schemes written in bold are proposed in this thesis. Here, the abbreviations TOC, LUT, LS and CF correspond to “tracker operating characteristic”, “look-up table”, “line search” and “closed-form”, respectively. 5

Figure 2.1	Dependence of information reduction factor on average number of false alarms for various detection probabilities. The plot is obtained for two dimensional measurement vector, i.e., $n_z = 2$, and $g = 4$ sigma gate.	20
Figure 2.2	The algorithmic flow of obtaining the tracker operating characteristic (TOC) curves from the offline modified Riccati recursion.	22
Figure 2.3	Illustration of (a): TOC curves obtained as steady-state RMS position error contours, (b): ROC curves for a CA-CFAR detector	24
Figure 2.4	The superimposition of TOC and ROC curves.	25
Figure 2.5	Block diagrams of two offline covariance recursion algorithms for the PDAF: HYCA (left) and MRE (right). The corresponding output of each algorithm, denoted by $\bar{P}_{HYCA}(k k)$ and $\bar{P}_{MRE}(k k)$, is a deterministic approximation to the filter calculated covariance, $P(k k)$ of the PDAF.	27
Figure 3.1	The flow of static threshold optimization (STOP) for graphical (TOC-curve) approach. The procedure given in this figure is repeated for different SNR values to obtain the optimum operating curve on P_{FA} - P_D plane. Then, this optimum operating curve is used together with ROC curve relation to find the STOP curve which is the ultimate goal of STOP. The STOP curve provides an SNR-dependent optimum P_{FA} setting which makes the threshold optimization online possible under varying SNR conditions. A numerical example is given in Section 3.3.1.	33
Figure 3.2	Scenario geometry: Assumed constant SNR target trajectories and location of the radar.	37

Figure 3.3	STOP using TOC curves. Note that, the instability region for the HYCA case has a slightly larger area than that of MRE. One can fit a line equation for the optimum operating curves in both approaches. Then this equation together with the ROC curve relation determine STOP curve which can be used to find the optimum operating point for an arbitrary SNR value.	40
Figure 3.4	STOP curves for MRE and HYCA approaches. Note that for a practical range of operating SNR values, the HYCA based approach consistently suggests a higher P_{FA} .	41
Figure 3.5	Experiment-I: The effect of selecting different operating P_{FA} values on downstream tracking: (a) The transient RMS position error plots ($\zeta = 10$ dB case), (b) track loss percentages, (c) the average and (d) the steady-state, RMS position error levels. In each subfigure, the performance of the corresponding Kalman filter (KF) which uses <i>perfect data association</i> is also shown as a baseline.	43
Figure 3.6	Experiment-I: The performance comparison of statically optimized systems and the best heuristic system in terms of (a) average and (b) steady-state, RMS position error levels.	45
Figure 3.7	Experiment-I: The optimum operating P_{FA} values suggested by STOP schemes for different SNR values.	46
Figure 3.8	Experiment-I: The performance comparison of statically optimized and heuristic tracking systems in terms of TLP.	46
Figure 3.9	Experiment-II: Performance comparison of STOP schemes with the MRE-based DTOP scheme presented in [1] in terms of (a) average (b) steady-state, RMS position error levels and (c) TLP. The average operating P_{FA} values suggested by the optimization schemes are also shown in (d).	48
Figure 3.10	Experiment-III: The transient RMS position error levels for 10 dB scenario.	51

Figure 3.11 Experiment-III: The optimum operating P_{FA} values of the TA-DETOP schemes for $\zeta = 10$ dB scenario.	51
Figure 3.12 Experiment-III: The average P_{FA} values suggested by the DTOP schemes as a function of SNR. Except for the lowest SNR case, HYCA based method suggests marginally higher P_{FA} values on the average (over transient and steady-state regions).	52
Figure 3.13 Experiment-III: Performance comparison of DTOP schemes in terms of RMS position error and TLP. Note that the plots given in (a) and (c) represent the trade-off between achieving a low steady-state RMS position error level versus having a low TLP.	53
Figure 3.14 Algorithms on the performance plane: The steady-state RMS position error versus TLP. Here, the prefixes “H”, “S” and “D” correspond to “heuristic”, “static” and “dynamic” approaches, respectively. Note that, as SNR increases, the performance of the algorithms gets closer to each other and to the the best achievable performance point, the Kalman filter with perfect data association.	55
Figure 3.15 The performance of the algorithms in 5 dB case. At some portions of the performance trajectory of heuristic approaches, there are sharp bends, resulting in a significant change in the performance. Therefore, in general one can not guarantee a reliable performance with an heuristic approach.	56
Figure 4.1 Dependence of information reduction factor on average number of false alarms for various detection probabilities. The plot is obtained for 2-dimensional measurement vector with $g = 4$ sigma gate. Result of a functional approximation to these curves is shown with dashed lines.	68

Figure 4.2 (a) The surface of optimal P_{FA} values as a function of ζ and N_C , (b) P_{FA} contours in the practical operating region. The region where the optimization suggests $P_{FA} = 1$ is also shown in (b) as a shaded area. Note that this region corresponds to applying no thresholding at all, where the whole system operates in <i>track before detect</i> (TBD) mode.	73
Figure 4.3 Scenario geometry: Assumed constant SNR target trajectories and location of the radar.	76
Figure 4.4 Impact of various detector false alarm probability settings on RMS position errors of their downstream tracking filters. For all SNR scenarios, the tracking system PDAF-OP, which uses the proposed detector threshold adaptation scheme, gives the best performance in terms of both RMS position error and TLP.	78
Figure 4.5 Variation of the IRF $q_2(P_{FA}N_C(k), P_D)$ and its functional approximation $\hat{q}_2(P_{FA}N_C(k), P_D)$ over a NP detector ROC curve for $N_C = 10$ and $\zeta = 10$ dB case.	80
Figure 4.6 Comparison of tracking systems for $\mathcal{I}_e = [-8, 0]$ and $\Delta_e = 0.01$. Although there is no notable difference in terms of RMS position error and TLP, the closed-form approach (PDAF-OP) is computationally much more efficient than the iterative algorithms.	82
Figure 5.1 The operating modes of the proposed heuristic approach over the variation of model probabilities of the IMM-PDAF. The white regions corresponds to the transition mode E_0	91
Figure 5.2 A sample Air Traffic Control (ATC) scenario: “T” and “R” denote initial aircraft (or target) position and radar location, respectively.	98
Figure 5.3 The variation of the range between target and radar, and that of SNR for $C_\zeta = 4 \times 10^{17}$ case.	98

Figure 5.4	TLPs [%] (the above table), and average RMS position errors [m] (the below table) for different values of the SNR constant, C_ζ .	102
Figure 5.5	The false alarm probabilities suggested by the proposed DTOP schemes for (a) $C_\zeta = 1 \times 10^{18} m^4$, (b) $C_\zeta = 9 \times 10^{17} m^4$, (c) $C_\zeta = 8 \times 10^{17} m^4$ and (d) $C_\zeta = 7 \times 10^{17} m^4$ cases. Note that except from the transition mode, E_0 the false alarm probabilities suggested by SWITCHING-PDAF are close to those suggested by IMM-PDAF-OP algorithm.	103
Figure 5.6	The performances of the algorithms in terms of TLP and average RMS position error. The point “EX” denotes the performance of the conventional system for which the desired false alarm probability is set to 10^{-X} .	105
Figure 5.7	The suggested false alarm probabilities of the proposed solutions.	105
Figure A.1	Tracking and Fusion Simulator (TAFSIM): Main window. The right and the left part of the GUI is related with the radar and target properties, respectively. At the middle, there is a main tracking screen showing an animated target tracking if single simulation with animation is selected. The upper part of the GUI consists of some buttons for loading and saving the configuration. In the lower part, there exists analysis buttons which allows user to see and analyze some performance measures like RMS position error, RMS velocity error etc.	118
Figure A.2	2D radar surveillance region, the square and diamond markers correspond to the radar and targets, respectively.	119
Figure A.3	Radar scanning parameters.	121
Figure A.4	Target-originated measurement: (a) True range, r and true bearing, ψ , and (b) radar resolution cell.	123
Figure A.5	Pulse and beam width parameters.	124

Figure A.6 A sample configuration file for TAFSIM. From this file, the user can define the scenario of the experiment, tracking filters and radar parameters. Note that, several tracking filters can be added for each radar. This artificial structure is useful especially when a comparison of several filters with the same measurement set is required. 127

Figure B.1 Block diagram of the probabilistic data association filtering algorithm. 130

LIST OF ABBREVIATIONS

2D	Two Dimensional
3D	Three Dimensional
A/D	Analog-to-Digital
ATC	Air Traffic Control
CA-CFAR	Cell Averaging Constant False Alarm Rate
CF	Closed-Form
CFAR	Constant False Alarm Rate
CT	Coordinated Turn
DETOP	Detector Threshold Optimization
DTOP	Dynamic Threshold Optimization
EKF	Extended Kalman Filter
EO	Electro-Optical
GUI	Graphical User Interface
HYCA	Hybrid Conditional Averaging
IMM	Interacting Multiple Model
IR	Infrared
IRF	Information Reduction Factor
JMLS	Jump Markov Linear System
JPDAF	Joint Probabilistic Data Association Filter
KF	Kalman Filter

LCT	Linear Coordinated Turn
LS	Line Search
LTI	Linear Time-Invariant
LUT	Look-Up Table
MHT	Multiple Hypothesis Tracking
MMSE	Minimum Mean Square Error
MRE	Modified Riccati Equation
MSPDAF	Multisensor Probabilistic Data Association Filter
NCT	Nearly Coordinated Turn
NNF	Nearest Neighbor Filter
NNJPDAF	Nearest Neighbor Joint Probabilistic Data Association Filter
NP	Neyman-Pearson
NPD	Neyman-Pearson Detector
NSPP	Non-Simulation Performance Prediction
OS-CFAR	Order Statistic Constant False Alarm Rate
pdf	Probability Density Function
pmf	Probability Mass Function
PDA	Probabilistic Data Association
PDAF	Probabilistic Data Association Filter
RMS	Root Mean Square
ROC	Receiver Operating Characteristic
SNF	Strongest Neighbor Filter
SNR	Signal-to-Noise Ratio
SQL	Square Law
SRE	Standard Riccati Equation
STOP	Static Threshold Optimization
TA	Tracker-Aware
TA-DETOP	Tracker-Aware Detector Threshold Optimization

TAFSIM	Tracking and Fusion Simulator
TBD	Track Before Detect
TLP	Track Loss Percentage
TOC	Tracker Operating Characteristic
TWS	Track-While-Scan
WNA	White Noise Acceleration
WPA	Wiener Process Acceleration

LIST OF SYMBOLS

\mathbf{c}	($N + 1$) dimensional constant column vector with all entries being equal to 1
c_{n_z}	Volume of n_z -dimensional unit hypersphere (i.e., $c_1 = 2, c_2 = \pi, c_3 = 4\pi/3$, etc.), $c_{n_z} \triangleq \pi^{n_z/2} / \Gamma(n_z/2 + 1)$
C	Cholesky factor (a square root) of a matrix
C_ζ	A constant representing all the factors except from range to target in the SNR equation
$E[\cdot]$	Expectation operator
$E_0(k)$	Complementary event of $\{E_1(k) \text{ or } E_2(k)\}$
$E_j(k), j > 0$	The event that the j th model probability exceeds a certain threshold at time step k , $E_j(k) \triangleq \{\mu_j(k) \geq 1 - \epsilon\}$
$f_{FA}(\cdot), f_D(\cdot, \cdot)$	Analytical functions for ROC curve (parameterized-form)
$f_{HYCA}(\cdot)$	The STOP curve obtained by HYCA methodology
$f_{MRE}(\cdot)$	The STOP curve obtained by MRE methodology
$f_{ROC}(\cdot, \cdot)$	Analytical function for ROC curve (closed-form)
$f_S(\cdot), f_S[\cdot]$	Any scalar measure that can be deduced from a matrix, such as determinant, trace, etc.
$F(k)$	State transition matrix at time step k
g	The number of sigmas (or standard deviations) of the validation gate, $g \triangleq \sqrt{\gamma G}$
$G(k)$	Process noise gain or input gain matrix at time step k
$H(k)$	Measurement matrix at time step k

\mathcal{H}	The Hamiltonian matrix of a given state-space description
$\text{HOG}_I^{\text{SQL}}$	Represents the joint assumption of <i>homogeneous</i> and <i>Gaussian</i> background detector noise, a Swerling-I target fluctuation and <i>square-law</i> detection scheme
$I_2(\cdot, \cdot, \cdot)$	Folded integral term in IRF
$\mathcal{I}_{P_{FA}}, \mathcal{I}_e$	Initial interval of uncertainty for P_{FA} and exponent of P_{FA} (used in line search optimization algorithms)
$\mathcal{I}_{P_{FA}}$	Initial interval of uncertainty for P_{FA} (used in line search optimization algorithms)
\mathcal{J}	Cost function
k	Time step
l_R	Radar location
L	Eigenvector matrix of \mathcal{H}
L_{ij}	Partitions of matrix L
m_k	Number of validated measurements at time step k
m_F	Number of false measurements
n_x, n_z	Dimensions of state space and measurement space
$M(k)$	Modal state at time step k which represents the <i>system mode</i> at k (i.e., the model in effect <i>during</i> the sampling period ending at time step k)
$M_j(k)$	The event that the j th model is in effect at time k , $M_j(k) \triangleq \{M(k) = j\}$
N	Number of possible hypothesis, a parameter of HYCA algorithm.
\mathbb{N}	Set of natural numbers
$N_C(k)$	Number of resolution cells enclosed by the validation gate at time step k
$N_C^j(k)$	Number of resolution cells enclosed by the validation gate defined by the j th model at time step k
N_{MC}	Number of Monte Carlo runs
N_R	Number of reference cells used in a CFAR detection scheme

N_{TL}	Number of Monte Carlo runs that result in track loss
$\mathcal{N}(\bar{x}, \Sigma)$	(Multivariate) Gaussian probability density function with mean \bar{x} and covariance Σ
$p_T(k)$	Target position at time step k .
$\bar{p}_{MRE}^{ii}(P_{FA}, P_D)$	i th diagonal element of $\bar{P}_{MRE}(P_{FA}, P_D)$
\mathbf{p}	$(N + 1)$ dimensional column vector whose j th entry is $\Pr\{m_{k-1} = j\}$
P	Steady-state value of $P(k + 1 k)$, $P \triangleq \lim_{k \rightarrow \infty} P(k + 1 k)$
$\tilde{P}(k)$	Spread of innovations term in the covariance update of the PDAF at time step k
$P(0 0)$	Initial covariance. (a priori knowledge reflecting the initial <i>degree of belief</i>)
$P(k k)$	Estimation error covariance at time step k , the covariance associated with $\hat{x}(k k)$, or covariance of $\tilde{x}(k k)$
$P^j(k k)$	Estimation error covariance at time step k corresponding to the j th model-matched filter
$P(k + 1 k)$	State prediction error covariance at time step $k + 1$, or the covariance associated with $\hat{x}(k + 1 k)$
$P^M(k k)$	Estimation error covariance associated with $\hat{x}^M(k k)$
$P^Q(k k)$	Estimation error covariance associated with $\hat{x}^Q(k k)$
$P^{IMM-PDAF}(k k)$	Estimation error covariance associated with $\hat{x}^{IMM-PDAF}(k k)$
$\bar{P}(k k)$	A deterministic approximation of $P(k k)$
$\bar{P}(k + 1 k)$	A deterministic approximation of $P(k + 1 k)$
$\bar{P}(k + 1 k, m_k)$	Conditional expectation of $P(k + 1 k)$ given that there are m_k validated measurements at time step k , $\bar{P}(k + 1 k, m_k) \triangleq \mathbb{E}\left[P(k + 1 k) \middle Z^k, m_k\right]$
$\bar{P}(k k, m_{k-1}, m_k)$	Conditional expectation of $P(k k)$ given that there are m_k validated measurements at time step k and m_{k-1} validated measurements at time step $k - 1$, $\bar{P}(k k, m_k) \triangleq \mathbb{E}\left[P(k k) \middle Z^k, m_k, m_{k-1}\right]$
$\bar{P}^j(k k)$	A deterministic approximation of $P^j(k k)$

$\bar{P}_{HYCA}(k k)$	Output of HYCA algorithm at time step k
$\bar{P}_{HYCA}(P_{FA}, P_D)$	Steady-state output of HYCA algorithm for a specific (P_{FA}, P_D) pair
$\bar{P}_{MRE}(k k)$	Output of MRE at time step k
$\bar{P}_{MRE}(P_{FA}, P_D)$	Steady-state output of MRE for a specific (P_{FA}, P_D) pair
$\bar{P}_{NSPP}(k k)$	A deterministic approximation of $P(k k)$ obtained by NSPP methodologies
\bar{P}_{NSPP}	Steady-state output of a NSPP methodology
$\bar{P}_{NSPP}^M(k k)$	$\bar{P}_{NSPP}(k k)$ based on maneuvering model
$\bar{P}_{NSPP}^Q(k k)$	$\bar{P}_{NSPP}(k k)$ based on quiescent model
P_D	Probability of detection
P_D^*	Optimum detection probability
P_{FA}	False alarm probability
P_{FA}^*	Optimum false alarm probability
(P_{FA}^*, P_D^*)	Optimum detector operating point
P_{FA}^d	Desired false alarm probability
P_{FA}^{NPD}	Optimum desired false alarm probability at time step k for an NPD concatenated with a PDAF
P_G	Gate probability, the probability that the target-originated measurement falls inside the validation gate given that the target is detected
Pr	Probability operator
$\text{Pr}\{m_k\}$	The probability that having m_k validated measurements at time step k
$\text{Pr}\{m_k m_{k-1}\}$	The probability that having m_k validated measurements at time step k given that there were m_{k-1} validated measurements at time step $k - 1$
q	Variance of each process noise component
$q_2(\cdot), q_2(\cdot, \cdot)$	IRF in MRE
$\hat{q}_2(\cdot, \cdot)$	An analytical approximation for $q_2(\cdot, \cdot)$
$Q(k)$	Process noise covariance matrix at time step k

$Q_2^{LUT}(\cdot, \cdot)$	2D-LUT obtained offline from $q_2(\cdot, \cdot)$
$r(k)$	Range to target at time step k
r_{min}, r_{max}	Minimum and maximum target range
r_{ij}	i th row and j th column element of the matrix $R \triangleq [r_{ij}]$
$R(k)$	Measurement noise covariance matrix at time step k
$S(k)$	Innovation covariance matrix at time step k , $S(k) \triangleq H(k)P(k k-1)H^T(k) + R(k)$
$\bar{S}(k)$	Offline-calculated innovation covariance at time step k
$\bar{S}(k, m_{k-1})$	Offline-calculated innovation covariance at time step k conditioned on the hypothesis that there were m_{k-1} val- idated measurements at time step $k-1$
$S^j(k)$	Innovation covariance associated with the j th model- matched filter at time step k
\mathcal{S}_{POS}	Set of state vector indices corresponding to position com- ponents
t_k	Measurement time stamp corresponding to k th sampling period
T	Sampling period, update period of tracking filter, or re- visit interval
\mathbf{T}_B	$(N+1)$ by $(N+1)$ diagonal matrix with the i th diago- nal element being equal to $\text{tr}\{\bar{B}(k, i)\}$ where $\bar{B}(k, i) \triangleq$ $\bar{W}(k, i)\bar{S}(k, i)\bar{W}^T(k, i)$
\mathbf{T}_P	$(N+1)$ by $(N+1)$ diagonal matrix with the i th diagonal element being equal to $\text{tr}\{\bar{P}(k k-1, i)\}$
TLP	TLP, $TLP \triangleq N_{TL}/N_{MC} \times 100$
$\text{tr}\{\cdot\}$	Trace operator
$\mathbf{U} = [u_{ij}]$	$(N+1)$ by $(N+1)$ matrix with $u_{ij} \triangleq u_2(\lambda\bar{V}(k, i), P_D, j)$
$u_2(\cdot, \cdot), u_2(\cdot, \cdot, \cdot)$	IRF in HYCA algorithm
$U_2^{LUT}(\cdot, \cdot)$	3D-LUT obtained offline from $u_2(\cdot, \cdot, \cdot)$
$\{v(k)\}, k \in \mathbb{N}$	Process noise sequence
$v_T(k)$	Target velocity at time step k .

$v_\eta(k), v_\xi(k)$	North and East component of the process noise at time step k
$V(k)$	Validation region (or gate) volume at time step k , $V(k) \triangleq c_{n_z} g^{n_z} S(k) ^{1/2}$
$\bar{V}(k)$	Offline-calculated gate volume at time step k
$\bar{V}(k, m_{k-1})$	Offline-calculated gate volume at time step k conditioned on the hypothesis that there were m_{k-1} validated measurements at time step $k - 1$
V_C	The resolution (or detection) cell volume
$V_G(k, \gamma_G)$	Validation region (or gate) defined by γ_G at time step k
\bar{x}	Mean (or expected value) of x
$\{x(k)\}, k \in \mathbb{N}$	True (target) state sequence
$\hat{x}(0 0)$	Initial state (a priori knowledge reflecting the initial <i>degree of belief</i>)
$\hat{x}(k k), \hat{x}^{MMSE}(k k)$	MMSE estimate of $x(k)$
$\tilde{x}(k k)$	Estimation error at time step k , $\tilde{x}(k k) \triangleq x(k) - \hat{x}(k k)$
$\hat{x}(k+1 k)$	Predicted state at time step $k+1$, or one-step prediction of $\hat{x}(k k)$
$\hat{x}^M(k k)$	$\hat{x}(k k)$ obtained from maneuvering model
$\hat{x}^Q(k k)$	$\hat{x}(k k)$ obtained from quiescent model
$\hat{x}^{IMM-PDAF}(k k)$	The state estimated by a IMM-PDAF at time step k
$\{w(k)\}, k \in \mathbb{Z}^+$	Measurement noise sequence
$w_\eta(k), w_\xi(k)$	North and East component of the measurement noise at time step k
$W(k)$	Kalman gain at time step k , $W(k) \triangleq P(k k-1)H^T(k)S^{-1}(k)$
$W^j(k)$	Kalman gain associated with the j th model-matched filter at time step k
$\bar{W}(k)$	Offline-calculated Kalman gain at time step k ,
$\bar{W}(k, m_{k-1})$	Offline-calculated Kalman gain at time step k conditioned on the hypothesis that there were m_{k-1} validated measurements at time step $k - 1$
$\{z(k)\}, k \in \mathbb{Z}^+$	Measurement (or observation) sequence

$\hat{z}(k k-1)$	Predicted measurement at time step k
$z_i(k)$	i th validated measurement at time step k
$Z(k)$	Set of validated measurements at time step k , $Z(k) \triangleq \{z_i(k)\}_{i=1}^{m_k}$
Z^k	Cumulative set of all (validated) measurements through time step k , $Z^k \triangleq \{Z(1), Z(2), \dots, Z(k)\}$
\mathbb{Z}^+	Set of positive integers
$\arg \max$	Argument that maximizes
$\arg \min$	Argument that minimizes
α	The threshold multiplier defined in OS-CFAR ROC curve
$\beta_0(k)$	The probability that none of the validated measurements is target originated at time step k
$\beta_i(k)$	The probability that the i th validated measurement is target originated at time step k
$\Delta r_\eta, \Delta r_\xi$	Range resolutions in North and East directions
$\Delta P_{FA}, \Delta_e$] Maximum error tolerance for P_{FA} and exponent of P_{FA} (used as a stop condition in line search algorithms)
ϵ_{POS}^i	Average position estimation error for the i th Monte Carlo run
γ_G	Gate threshold
$\Gamma(\cdot)$	The gamma function
$\eta(k), \dot{\eta}(k), \eta^m(k)$	North component of true target position, true target velocity and measured target position at time step k
λ	Spatial (random) clutter density, $\lambda \triangleq P_{FA}/V_C$
λ_F	Expected number of false measurements
$\mu_F(\cdot, \cdot)$	Poisson pmf for m_F
$\mu_j(k), j > 0$	j th model probability, posterior probability that j th model is in effect at time step k
$\mu_j(k k-1)$	Predicted model probability of the j th model, $\mu_j(k k-1) \triangleq \Pr\{M_j(k) Z^{k-1}\}$
$\Pi = [p_{ij}]$	$(N+1)$ by $(N+1)$ probability matrix with $p_{ij} \triangleq \Pr\{m_k = i m_{k-1} = j\}$

ρ	Measurement error level, $\rho \triangleq \sqrt{\text{tr}\{R\}}$
σ_{POS}	RMS position estimation error
σ_{POS}^{ss}	Steady-state RMS position error
$\bar{\sigma}_{POS}^{ss}(P_{FA}, P_D)$	Offline-calculated σ_{POS}^{ss} for a specific (P_{FA}, P_D) pair
Σ	Covariance matrix
τ_M, τ_Q	Expected <i>sojourn times</i> (in unit of sampling interval) of the underlying Markov chain in maneuvering and quiescent modes
Ω	The turn rate (of a coordinated turn motion)
$\xi(k), \dot{\xi}(k), \xi^m(k)$	East component of true target position, true target velocity and measured target position at time step k
$\zeta(k)$	Detection (or enhanced signal) SNR at time step k
$\zeta_R(k)$	Raw signal SNR at time step k
0	Scalar zero, zero vector, zero matrix
\in	Element of
$(\cdot)^{-1}, \{\cdot\}^{-1}, [\cdot]^{-1}$	Matrix inverse
$ \cdot $	Determinant of a matrix, or magnitude of a scalar
$\ \cdot\ $	Norm of a matrix or vector
$(\cdot)^T, \{\cdot\}^T, [\cdot]^T$	Transposition (of a matrix or a vector)
\sim	Distributed as

CHAPTER 1

INTRODUCTION

Radar systems are one of the most important remote sensing equipment of today. They are used everywhere including civilian, military and space applications and are indispensable for sustaining modern way of life.

Radar systems typically radiate a pulse of electromagnetic energy and capture and digitize the returning echo for the purpose of determining the location, velocity and other state information of a “target” of interest. To achieve this goal, the captured electromagnetic echo is first converted to an electrical signal and passed through a signal processing stage which includes *signal conditioning*¹ [2] and *detection*. This is usually followed by an *information processing*² (i.e., *tracking*) stage [4], as illustrated in Fig. 1.1.

Following this conventional treatment, through the years, the research about radar signal and data processing has been conducted along two distinct paths, namely “detection theory” and “tracking theory” with little interaction between them. The tracking literature mostly assumed that the detection stage is a prior and isolated process, providing *measurements* for the tracking stage. The detection literature, in a similar way assumed no incoming information from the downstream tracking algorithms.

¹ This includes the processing blocks prior to detection such as analog-to-digital (A/D) conversion, beamforming, pulse compression, clutter filtering and Doppler processing [2].

² This stage is also called frequently as *data processing*, see for example [2], [3].

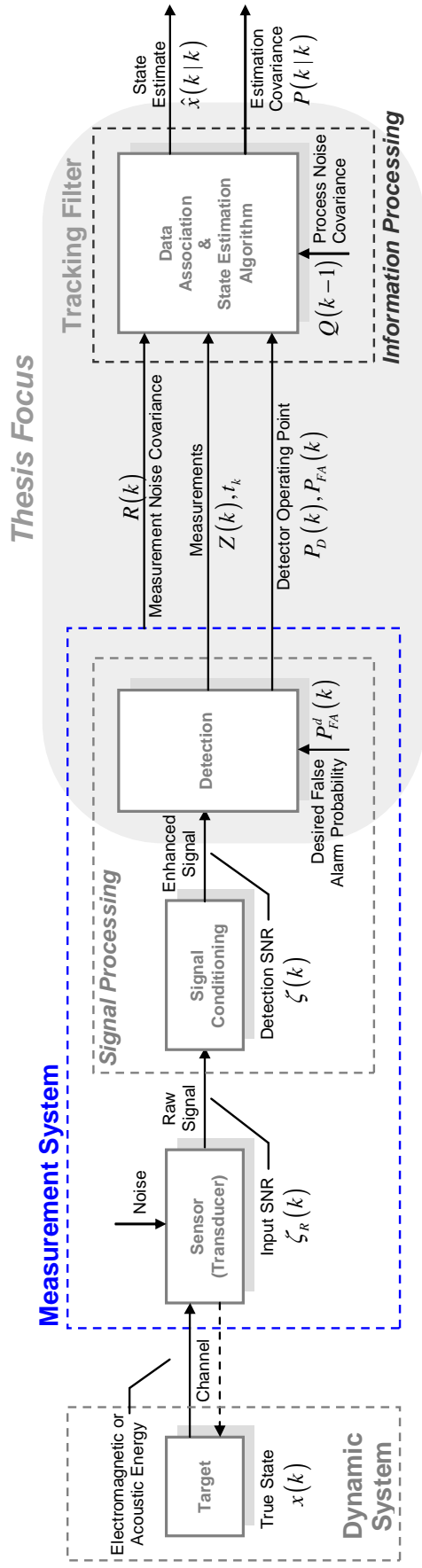


Figure 1.1: The block diagram of a conventional tracking system. This block diagram is rather generic in the sense that the sensor can be either an active one such as an active sonar, a radar or a ladar (laser detection and ranging), or a passive one such as an electro-optical (EO), an infrared (IR), or a passive sonar sensor. In the case of an active sensor, the energy flow in the channel is *bidirectional*. The type of energy can be either *electromagnetic* as in the case of radar, ladar, EO and IR sensors, or *acoustic* as in the case of a (active/passive) sonar. The focus of the thesis, as shown in the figure, is to a large extent independent of the sensor type used except when a specific detector is used as an example. However, to be more focused, the presentation in this thesis is in the context of a radar sensor.

A reasonable and challenging question is whether parameter decisions made for the detector and tracker subsystems are optimal for the combined performance of the overall radar system. This question, which is also the focus of this thesis, has been first addressed by the work of Fortmann et al. [5], where they introduced a feedback mechanism from the downstream information processing (tracking) subsystem to the upstream signal processing (detection) subsystem. The main contributions of [5] are the so-called *modified Riccati equation* (MRE) and its by-product, *tracker operating characteristic* (TOC) curves. Fortmann et al. have shown that for a given signal-to-noise ratio (SNR), one can determine the optimum detector operating point by finding the tangential intersection point between TOC and the corresponding receiver operating characteristic (ROC) curve. Furthermore, the introduced MRE provides a *steady-state* non-simulation performance prediction (NSPP) for the probabilistic data association filter (PDAF) in clutter, in a way similar to how the standard Riccati equation (SRE) does for the Kalman filter in clutter-free environments. Inspired from this work, Li et al. have introduced a more sophisticated approach [6], known as *hybrid conditional averaging* (HYCA) algorithm, which has extended the idea in [5] to the *transient* performance (e.g., track loss) prediction, and applied this technique for optimization of detection thresholds [7].

Another equally important question is whether these subsystem level parameters really have to be statically optimized or should they rather be adaptive in space and time. One strongly feels that some adaptation is necessary since the motion of the target changes both the spatial context and the SNR. Indeed, in [1], Gelfand et al. have formulated and solved threshold optimization problem dynamically for each time step which led to a temporal adaptation of the detection threshold. Another approach was presented in [8] by Willett et al. where they fed the spatial *a posteriori* information of the tracking filter, back to a Bayesian detector as an *a priori* information. This results in a spatially adaptive detection threshold adjustment scheme such that the threshold

is decreased near locations where the target is expected and increased near locations where it is unexpected.

A line of recent articles [9, 10] show the growing interest into the concept of *cognitive radar* [11], which aims to make a radar system smarter and more adaptive by dynamically optimizing the “transmitter” as well. We should note however that steps towards this goal are not entirely new. In the context of overall system optimization, the optimization of transmitter waveforms was first introduced in [12] and applied to the PDAF in [13]. Another recent study is [14] where the design of waveform and detection threshold for range and range-rate tracking in clutter is formulated and numerically solved as a finite horizon optimization problem. The concept of waveform optimization for tracking is well summarized in [15].

In the present thesis, we consider these exciting theoretical and experimental steps towards the goal of spatially and temporally adaptive radar. In particular, we focus on the interaction between the detector and the tracker subsystems and consider the problem of *tracker-aware* (TA) optimization of detector threshold per target track and per resolution cell. We strongly believe that this is an important subarea of the research consisting of steps that are necessary for the ultimate goal of *cognitive radar*. We build on two important NSPP methodologies for the PDAF, namely, MRE of Fortmann [5] and HYCA of Li [6]. For each methodology, we consider both static (offline) and dynamic (online) threshold optimization schemes in a *unified* theoretical and experimental framework. Fig. 1.2 illustrates the algorithmic space of research for these optimization schemes with highlights on those introduced in the present study.

		OPTIMIZATION APPROACH	
		STATIC	DYNAMIC
NSPP	MRE	STATIC-MRE-TOC	DYNAMIC-MRE-LS DYNAMIC-MRE-CF
	HYCA	STATIC-HYCA-LUT STATIC-HYCA-TOC	DYNAMIC-HYCA-LS

Figure 1.2: The algorithmic space of tracker-aware detector threshold optimization (TA-DETOP) schemes for the PDAF. The schemes written in bold are proposed in this thesis. Here, the abbreviations TOC, LUT, LS and CF correspond to “tracker operating characteristic”, “look-up table”, “line search” and “closed-form”, respectively.

1.1 Outline of the Thesis

The thesis is organized as follows. In Chapter 2, NSPP methodologies in general and for the PDAF in particular are given. This chapter constitutes a preliminary information for the rest of the thesis. In Chapter 3, tracker-aware detector threshold optimization (TA-DETOP) schemes based on NSPP methodologies are explained. Both static and dynamic formulations of the problem are given. Furthermore, a comprehensive comparison of existing and newly proposed TA-DETOP schemes is made in a unified theoretical and experimental framework. The simulation results showed that there is a trade-off between having a low steady-state root mean square (RMS) estimation error (i.e. good steady-state performance) versus having a low track loss percentage (TLP) (i.e., good transient performance). Although the dynamic threshold optimization (DTOP) schemes are found to be well-located on this trade-off plane, it is noted that they are computationally expensive. To partially overcome this problem, in Chapter 4, an approximate closed-form solution is presented for the MRE-based DTOP problem for a special detector type. The proposed solution, dramatically reduces the computational complexity and hence increases the feasibility for an online application of the approach. Furthermore, it is shown that the proposed closed-form solution possess a the-

oretical lower bound on the operating SNR concerning when the whole system should be switched to the track before detect (TBD) mode. In Chapter 5, TA-DETOP problem is extended to the maneuvering target tracking case. One heuristic and one theoretically rigorous solution are proposed. It is shown that the rigorous solution is well-integrated into the multiple model filtering algorithms and improves robustness of the famous interacting multiple model probabilistic data association filter (IMM-PDAF) against track loss. In Chapter 6, the important results of the thesis are summarized and possible future studies from the present point are discussed. Finally, the structure of the developed software — tracking and fusion simulator (TAFSIM) and other related background materials on the PDAF and the interacting multiple model (IMM) estimator are given in the appendices.

1.2 Contributions

The primary contributions of the thesis can be summarized as follows:

- A comprehensive comparison of TA-DETOP schemes is made in a unified experimental and theoretical framework. Within the presented framework, the TOC curves are experimentally obtained for the HYCA approach leading to the optimization scheme *STATIC-HYCA-TOC*. This is an extension to the work presented in [7], where threshold optimization based on HYCA was made using look-up tables (*STATIC-HYCA-LUT* [7]). Moreover, for the dynamic optimization case, a new method, named as *DYNAMIC-HYCA-LS*, is proposed by formulating and solving the problem for the HYCA approach. This is done within the same unified framework such that results are directly comparable with those of the MRE approach (*DYNAMIC-MRE-LS* [1]).
- For the MRE-based dynamic threshold optimization, an alternative closed-form solution (*DYNAMIC-MRE-CF*) is introduced. The proposed solu-

tion is shown to be computationally much more efficient than the existing schemes (DYNAMIC-MRE-LS [1]).

- A theoretical lower bound on the operating SNR is found for the tracking system, which consists of a Neyman-Pearson detector (NPD) and a PDAF, concerning when the system should be switched to the track before detect (TBD) mode.
- TA-DETOP problem is formulated and solved for tracking maneuvering targets. Two extensions are presented: A heuristic one and a multiple model filter integrated one. It is shown that the integrated extension makes IMM-PDAF more robust against track loss.

Overall, we present a comprehensive comparative study of all the newly proposed methods and the existing ones through extensive simulation experiments. To the best of author's knowledge, such a comparative study has not been done before in the literature.

CHAPTER 2

OFFLINE PERFORMANCE EVALUATION OF TRACKING ALGORITHMS

2.1 Introduction

Involving both *continuous* and *discrete* uncertainties,¹ real-world tracking is a *hybrid* [19] estimation problem. Tracking algorithms which operate under these uncertainties are necessarily stochastic. As the performance of these algorithms can not be evaluated *confidently* with a single run, the common practice for performance evaluation is to run extensive number of Monte Carlo simulations and take the ensemble average of a performance measure(s) over the runs.

Although this methodology is very simple and straightforward, it may be very time-consuming and costly in some cases. More importantly, if a design, an *optimization*² or a sensitivity analysis of a tracking algorithm is of interest, Monte Carlo simulations based approach does not give much insight into the

¹ Examples of continuous uncertainties are inaccuracy in the measurements and “small” perturbations in the target motion which are usually modeled as an additive measurement noise and process noise, respectively. These type of uncertainties are well-understood and solved in the literature over the past four decades under the title of *classical state estimation* [16], [17], [18]. However, major challenges of tracking arise from two discrete-valued uncertainties: Measurement origin uncertainty, which is, in the words of Li and Bar-Shalom [6], the *crux* of tracking, and target maneuver which appears as an *abrupt* and “large” deviation in the target motion.

² In this thesis, we consider this aspect, i.e., *tracker-aware optimization of detection thresholds* where we extensively use offline performance evaluation tools. This is actually why we reserve a separate chapter for this topic here.

problem. In such a case, analytic expressions and deterministic tools are much more useful. Therefore, the techniques for performance evaluation that do not require stochastic simulations are needed.

The title “offline performance evaluation of a tracking algorithm” is related to this need, and defined as to evaluate the performance of a tracking filter without recourse to extensive and expensive Monte Carlo simulations. There are numerous works done in this context in the literature. However, the available tools for offline evaluation of the performance can be roughly classified into three categories [20]:

- **Error Bounding Techniques:** These techniques are the most popular offline performance evaluation tools. They provide Cramér-Rao like bounds on the performance. There are lots of works done under different titles (possibly having much in common), such as nonlinear filtering [21], [22], [23], [24], filtering with intermittent observations [25], [26], [24], [27], [28], [29], tracking in clutter [30], [31], [32], bearing-only tracking [30], [33], [34], multitarget tracking [35], [36], [37], [38] and maneuvering target tracking [34], [39]. Rather than predicting the filter performance, these techniques put some *best-achievable* borders for the problem at hand. The tightness of such bounds is usually not known and questionable. In this aspect, they can provide at most semi-quantitative measures for offline performance evaluation of a tracking filter.
- **Analytic Model Approach:** The second class of tools is referred to as analytic model approach [20]. In this methodology, the aim is to establish some (possibly approximate) analytic relationships between the performance measure and some “key” parameters of the algorithm (see, e.g. [40], [41], [42]). Although these techniques provide analytically useful expressions, they are obtained along several assumptions and approximations due to complexity of the big picture. Therefore, their accuracies are still not good as the performance prediction approach.

- **Performance Prediction Approach:** This is an algorithmic approach. It aims to obtain an offline (or a deterministic) algorithm for calculation of one of the performance measures of the tracking filter, usually the estimation error covariance matrix. Developing such a deterministic algorithm for the covariance propagation is in general a hard task. However, this methodology is proven to produce much more accurate results as compared to the previous two techniques mentioned above (see, for example, [5], [6] and [43]).

In this chapter (and also in the entire thesis), our focus will be on the performance prediction category. From now on, we refer to this category as *non-simulation performance prediction* (NSPP) methodologies.

2.2 An Overview of Non-Simulation Performance Prediction (NSPP) Methodologies

Non-simulation performance prediction (NSPP) methodologies are currently the most effective and reliable offline performance evaluation tools among their alternatives. Similar to error bounding or analytic modeling techniques, NSPP approach also aims to evaluate the performance of a tracking filter without recourse to expensive Monte Carlo simulations. However, different from these two techniques, NSPP approach relies on obtaining a well-developed *deterministic* algorithm for the performance measure of interest. Naturally, this measure is often taken as (some function of) the *estimation error covariance* of the tracking filter under concern. Therefore, the key point is to obtain a *deterministic relationship*³ for the *estimation error covariance*, which then can be used to quantify the filter's performance in an offline manner.

³ This is either in the form of a recursive algorithm or, if possible, in the form of a non-recursive expression.

In the simplest case, when there is no clutter and no variation in target dynamics (i.e., no “target maneuver” in tracking terminology), the *Kalman filter* [44] has already a deterministic covariance recursion in the form of a (matrix) *Riccati equation* [16]. However, for the more complex situations in which there is clutter or the target dynamics is time-varying, the error covariance calculation of the filter under concern is no longer deterministic. This is due to the presence of discrete type uncertainties introduced into the problem⁴ which makes the covariance calculation dependent on the measurements received, hence stochastic.

To be able to make a NSPP for the filters in these situations, there are two main methodologies proposed so far. The first methodology, which also pioneered NSPP topic, is the work of Fortmann et al. [5] where both type of uncertainties (discrete and continuous) in the problem are *globally* averaged out. In this pioneering work [5], they applied this methodology for the *probabilistic data association filter* (PDAF) [45] and obtained a Riccati-like recursion for the deterministic calculation of its covariance. This recursion was named as the *modified Riccati equation* (MRE) [5]. The MRE approach is further extended to multi-sensor case (Multisensor PDAF – MSPDAF) by Frei [46], and recently studied in the context of NSPP for Kalman filtering with intermittent observations [29], [25], [26].

Inspired by the work of Fortmann et al., the second methodology was proposed by Li et al. in [6] where only the continuous type of uncertainties are averaged, while the discrete type of uncertainties are retained in the propagation of the covariance. Similar to Fortmann et al, in the proposal paper of their algorithm [6], they first derive it for the PDAF and name it as the *hybrid conditional averaging* (HYCA) algorithm. However, they also note and show that rather than being applicable only for the PDAF, HYCA is actually a methodology that can be applied for NSPP of various hybrid filters, such as, the interacting

⁴ Together with the continuous type of uncertainties, the overall problem is said to be *hybrid* [6] in nature.

multiple model (IMM) filter [43], MSPDAF [46], the nearest neighbor filter (NNF) [47] and the strongest neighbor filter (SNF) [48].

2.3 Application Areas of NSPP Techniques and Thesis Focus

NSPP techniques have found several important application areas in the literature such as detector threshold optimization [5], [7], [1], waveform optimization [12], [13], [49], [14], [50], multisensor tracking (as a sensor selection criteria) [51], [52], [53], multitarget tracking (for the occlusion problem) [54], and multi-function radar resource allocation [55]. Although our research interest extends beyond, in this thesis, we focus on the area of detector threshold optimization.

There are two common properties of the optimization problems that we consider in this thesis: First, they all aim to maximize the performance of a tracking filter over detection thresholds.⁵ Second, the cost (or objective) functions of the optimization problems are all based on an *offline* approximation of the filter's covariance, which is produced by an NSPP methodology.

We investigate the optimization problems in two domains:

- In the first domain, the problem is investigated for the simplest possible case: Single-sensor tracking of non-maneuvering, *non-crossing*⁶ targets in clutter. One of the most cost effective and popularly used filters in this domain is the PDAF (see, e.g. [4], [3]). Therefore, in this domain, we consider the detector-PDAF pair as the tracking system whose performance is to be maximized.

⁵ This in essence results in a feedback from the tracking filter to the detector. This is why we call these optimization schemes as *tracker-aware* [56], [57], [58], [59].

⁶ The term *non-crossing* targets is used for the targets whose tracking gates have no common validated measurements.

- In the second domain, we relax the “no maneuver” assumption of the first domain and consider maneuvering (but still non-crossing) targets in clutter. In this domain, we investigate the multiple model filtering approach which is the state of the art choice for tracking maneuvering targets. To be able to use the knowledge gained by the NSPP of the PDAF considered in the first domain, we use PDAFs as *modules* [4] (or *elemental filters* [19]) in the multiple model filtering structures in general and the IMM filter structure in particular like in [60].

In any case, in this thesis, we extensively use the NSPP techniques for the PDAF (in either considering a single PDAF, like in the first domain or considering a bank of PDAFs in a multiple model filtering structure such as IMM, in the second domain). Therefore, in the rest of this chapter, our emphasis will be on the NSPP techniques for the PDAF.

The chapter is organized as follows. First, in Section 2.4, we give a brief theoretical background about standard Riccati equation (SRE) which is the baseline NSPP tool for the Kalman filter in classical state estimation problems. Then, we explain two NSPP approaches for the PDAF in detail, namely, the modified Riccati equation (MRE) [5] and the hybrid conditional averaging (HYCA) algorithm [6], in Section 2.5.1 and 2.5.2, respectively.

2.4 The Baseline NSPP Tool for the Kalman Filter: The Riccati Equation

Consider a discrete-time linear time-invariant (LTI) dynamic system, described by the plant and measurement equations

$$x(k+1) = Fx(k) + Gv(k), \quad k = 0, 1, \dots, \quad (2.1)$$

$$z(k) = Hx(k) + w(k), \quad k = 1, 2, \dots, \quad (2.2)$$

where $x(k)$ and $z(k)$ are the state and measurement vectors whose dimensions are n_x and n_z , respectively. The sequences $\{v(k)\}$ and $\{w(k)\}$, known as process and measurement noises, respectively, are assumed to be *white, stationary*⁷ and distributed as

$$v(k) \sim \mathcal{N}(0, Q), \quad (2.3)$$

$$w(k) \sim \mathcal{N}(0, R) \quad (2.4)$$

for all k where the notation $x \sim \mathcal{N}(\bar{x}, \Sigma)$ means that “the random variable x is normally (Gaussian) distributed with mean \bar{x} and covariance Σ .” The initial state $x(0)$, which is generally unknown, is modeled as

$$x(0) \sim \mathcal{N}(\hat{x}(0|0), P(0|0)) \quad (2.5)$$

where the mean $\hat{x}(0|0)$ and the covariance $P(0|0)$ are assumed to be known. Furthermore, two noise sequences $\{v(k)\}$ and $\{w(k)\}$ and the initial state $x(0)$ are assumed to be *mutually independent* for all k .

Under these assumptions, at each time step k , the optimal *minimum mean square error* (MMSE) estimate of the state $x(k)$, which is given by [16]:

$$\hat{x}^{MMSE}(k|k) = \mathbb{E}[x(k)|Z^k] \quad (2.6)$$

with

$$Z^k \triangleq \{z(1), z(2), \dots, z(k)\}, \quad (2.7)$$

can be recursively obtained by the Kalman filter. The Kalman filter provides not only the optimum estimate $\hat{x}(k|k)$, but also the corresponding *estimation error covariance*, defined by

$$P(k|k) \triangleq \mathbb{E}\left[(x(k) - \hat{x}(k|k))(x(k) - \hat{x}(k|k))^T \middle| Z^k\right] \quad (2.8)$$

which reflects how good its estimate is. In standard Kalman filter, this covariance can be recursively calculated from the covariance prediction and update

⁷ Non-stationary case can be treated similarly. In that case covariance matrices of the noise sequences will be time-varying.

equations of the form

$$P(k|k-1) = FP(k-1|k-1)F^T + GQG^T, \quad (2.9)$$

$$P(k|k) = P(k|k-1) - W(k)S(k)W^T(k) \quad (2.10)$$

where $P(k|k-1)$ is the state prediction covariance, and $W(k)$ and $S(k)$, known as the Kalman gain and innovation covariance, respectively, are given by

$$W(k) = P(k|k-1)H^T S^{-1}(k), \quad (2.11)$$

$$S(k) = HP(k|k-1)H^T + R. \quad (2.12)$$

Substituting (2.11) and (2.12) into (2.10) and the result into (2.9), the following deterministic recursion for the state prediction covariance is obtained:

$$\begin{aligned} P(k+1|k) = F & \left[P(k|k-1) - P(k|k-1)H^T \left(HP(k|k-1)H^T + R \right)^{-1} \right. \\ & \left. \times HP(k|k-1) \right] F^T + GQG^T \end{aligned} \quad (2.13)$$

with $P(1|0) \triangleq FP(0|0)F^T + GQG^T$. This is the *discrete-time (difference) matrix Riccati equation* [18]. Note that, to be able to propagate this recursion in time, one needs only F , G , H , Q , R and $P(0|0)$ which are all assumed to be known and independent of the measurement received, therefore it can be performed offline.⁸ The solution converges to a finite steady-state covariance, $P \triangleq \lim_{k \rightarrow \infty} P(k+1|k)$, if,

- The pair $\{F, H\}$ is completely *observable*, and
- The pair $\{F, C\}$, where $GQG^T \triangleq CC^T$, is completely *controllable*.

The steady-state covariance P is a unique positive definite symmetric matrix independent of the initial covariance $P(0|0)$ and is the solution of the following *algebraic matrix Riccati equation*:

$$P = F \left[P - PH^T \left(HPH^T + R \right)^{-1} HP \right] F^T + GQG^T \quad (2.14)$$

⁸ That is, “without recourse to Monte Carlo simulations.”

A *non-recursive* solution of (2.14) is given in [61] as

$$P = L_{21}L_{11}^{-1} \quad (2.15)$$

where L_{ij} 's are the $n_x \times n_x$ partitions of

$$L = \begin{bmatrix} L_{11} & L_{12} \\ L_{21} & L_{22} \end{bmatrix} \quad (2.16)$$

which is the eigenvector matrix for the *Hamiltonian* of the system:

$$\mathcal{H} = \begin{bmatrix} F^{-T} & F^{-T}(H^T R^{-1} H) \\ GQG^T F^{-T} & F + GQG^T F^{-T}(H^T R^{-1} H) \end{bmatrix}. \quad (2.17)$$

The columns of L are the eigenvectors of \mathcal{H} and they should be ordered such that, the first n_x columns are the ones that correspond to unstable (outside the unit circle) eigenvalues of \mathcal{H} .

2.5 NSPP Techniques for the PDAF

2.5.1 The Modified Riccati Equation (MRE)

Thanks to its deterministic nature, the standard Riccati recursion can be performed offline. This property allows us to make NSPP for the Kalman filter in clutter-free environments.

The situation is more complicated for the case of cluttered environments. In a cluttered environment, in addition to continuous-valued uncertainties, such as measurement noise and process noise, there exists a discrete-valued uncertainty, called the *measurement origin uncertainty* [4].⁹ Numerous efforts have

⁹ This is the *cru*x of a tracking problem [6] and poses the greatest challenge for tracking community [19]. As its name suggests, this problem is related to the uncertainty in the origin of the received measurements as whether they are originated from the target of interest, interfering targets, countermeasures, or due to false alarms is not known with certainty. Note that this uncertainty is clearly discrete in nature. The tracking algorithms tackling such discrete uncertainties as well as continuous ones (i.e., process and measurement noises) are referred to as *hybrid* algorithms [6].

been made to deal with this problem over the past three decades. One of the most well-known and accepted algorithm is the *probabilistic data association filter* (PDAF) proposed in [45]. Unlike the conventional Kalman filter, the estimation error covariance of the PDAF is measurement-dependent. This stochastic nature of the covariance recursion comes from its update stage given by [4]:

$$P(k|k) = P(k|k-1) - (1 - \beta_0(k)) W(k) S(k) W^T(k) + \tilde{P}(k) \quad (2.18)$$

where the measurement-dependent¹⁰ terms are $\tilde{P}(k)$ and $\beta_0(k)$. To be able to obtain a deterministic recursion, a solution was first proposed in [5] by replacing $\tilde{P}(k)$ and $\beta_0(k)$ with their conditional expectations,

$$\bar{P}(k) \triangleq \mathbb{E}[\tilde{P}(k)|Z^{k-1}], \quad (2.19)$$

$$\bar{\beta}_0(k) \triangleq \mathbb{E}[\beta_0(k)|Z^{k-1}], \quad (2.20)$$

over both the locations and the number of measurements,¹¹ where

$$Z^k \triangleq \{Z(1), Z(2), \dots, Z(k)\} \quad (2.21)$$

is the cumulative set of *validated measurements*¹² through time step k and

$$Z(k) \triangleq \{z_1(k), z_2(k), \dots, z_{m_k}(k)\} \quad (2.22)$$

is the set of validated measurements at time step k . Note that the notation given in (2.21) has a different meaning than its clutter-free counterpart of (2.7). The new covariance update equation, after some approximations, becomes (see [5] for the details)

$$\begin{aligned} \bar{P}(k|k) &\triangleq \mathbb{E}[P(k|k)|Z^{k-1}] \\ &\approx P(k|k-1) - q_2(k) W(k) S(k) W^T(k) \end{aligned} \quad (2.23)$$

¹⁰ The measurement dependency of these terms is due to their dependency on the measurement innovations. Further details can be found in Appendix B.

¹¹ In HYCA [6] approach, averaging (i.e., expectations) is performed over only *measurement locations* – the continuous part of the uncertainty, while retaining the dependency on the *number of validated measurements* – the discrete part of the uncertainty.

¹² The measurement $z(k)$ is said to be a *validated measurement*, if it is inside a validation gate defined by $V_G(k, \gamma_G) \triangleq [z(k) : (z(k) - \hat{z}(k|k-1))^T S^{-1}(k) (z(k) - \hat{z}(k|k-1)) \leq \gamma_G]$ where γ_G is the *gate threshold* and $\hat{z}(k|k-1) \triangleq HF\hat{x}(k-1|k-1)$ is the *predicted measurement* at time step k [4].

where $\bar{P}(k|k)$ is a deterministic approximation of $P(k|k)$ in which the stochastic terms are averaged out according to (2.19) and (2.20), and $q_2(k)$ is a time-varying scalar taking the values between 0 and 1. Furthermore, if we replace the covariance prediction by

$$\bar{P}(k|k-1) = F\bar{P}(k-1|k-1)F^T + GQG^T, \quad (2.24)$$

then similar to the standard Riccati equation, we obtain an offline recursion of the form

$$\begin{aligned} \bar{P}(k+1|k) = F \left[\bar{P}(k|k-1) - q_2(k)\bar{P}(k|k-1)H^T \left(H\bar{P}(k|k-1)H^T + R \right)^{-1} \right. \\ \left. \times H\bar{P}(k|k-1) \right] F^T + GQG^T \end{aligned} \quad (2.25)$$

with $\bar{P}(1|0) \triangleq FP(0|0)F^T + GQG^T$. This is the *modified Riccati equation* (MRE) [5]. The only modification from the standard Riccati is the scalar factor $q_2(k)$ which is a function of probability of detection (P_D), the spatial clutter density (λ) and offline-calculated gate volume ($\bar{V}(k)$). This scalar is called *information reduction factor* [4] and its functional form is given as [5]

$$\begin{aligned} q_2(\lambda\bar{V}(k), P_D) \triangleq P_D \frac{c_{n_z}}{(2\pi)^{n_z/2}} \sum_{m_k=1}^{\infty} \frac{e^{-\lambda\bar{V}(k)} (\lambda\bar{V}(k))^{m_k-1}}{(m_k-1)!} \left(\frac{n_z}{g^{n_z}} \right)^{m_k-1} \\ \times I_2(\lambda\bar{V}(k), P_D, m_k) \end{aligned} \quad (2.26)$$

with

$$\begin{aligned} I_2(\lambda\bar{V}(k), P_D, m_k) \triangleq \int_0^g \cdots \int_0^g \frac{\exp(-r_1^2)r_1^2}{b(\lambda\bar{V}(k), P_D) + \sum_{j=1}^{m_k} \exp(-r_j^2/2)} \\ \times (r_1 r_2 \cdots r_{m_k})^{n_z-1} dr_1 dr_2 \cdots dr_{m_k} \end{aligned} \quad (2.27)$$

$$b(\lambda\bar{V}(k), P_D) \triangleq (2\pi)^{n_z/2} \frac{\lambda\bar{V}(k) (1 - P_D P_G)}{c_{n_z} g^{n_z} P_D} \quad (2.28)$$

where $c_{n_z} \triangleq \pi^{n_z/2} / \Gamma(n_z/2 + 1)$, with $\Gamma(\cdot)$ being gamma function, is the volume of the n_z -dimensional unit hypersphere ($c_1 = 2, c_2 = \pi, c_3 = 4\pi/3$, etc.), and $g \triangleq \sqrt{\gamma_G}$ is referred to as “number of sigmas” (standard deviations) of the gate and linked to the *gate probability*¹³ via chi-square tables. The offline-calculated

¹³ The gate probability (P_G) is defined as the probability that the target-originated measurement falls inside the validation gate given that the target is detected

volume of the validation gate is given by

$$\bar{V}(k) \triangleq c_{n_z} g^{n_z} |\bar{S}(k)|^{1/2} \quad (2.29)$$

where $\bar{S}(k) \triangleq H\bar{P}(k|k-1)H^T + R$ is the offline-calculated innovation covariance. The relationship between λ and probability of false alarm (P_{FA}) is given by

$$\lambda \triangleq \frac{P_{FA}}{V_C} \quad (2.30)$$

where V_C is the *resolution (or detection) cell volume*.

2.5.1.1 Evaluation of Information Reduction Factor

It is claimed in [5] that the information reduction factor expression given in (2.26) has no closed-form solution, therefore it should be evaluated numerically. A positive fact is that $q_2(\lambda\bar{V}(k), P_D)$ can be evaluated offline, tabulated in the form of a look-up table (LUT) and then used when necessary, as it is independent of the measurement received. However this is not a computationally cheap operation either. It involves m_k -fold integration ($m_k = 1, 2, \dots$). One of the computationally efficient way of taking such integrals is the Monte Carlo integration method. Based on 1×10^6 Monte Carlo integration, the plot of $q_2(\lambda\bar{V}(k), P_D)$ obtained for various values of P_D is shown in Fig. 2.1.

The infinite summation in (2.26) is truncated at $m_k = 15$ similar to [5] and [62]. Note that information reduction factor decreases as the average number of false alarms in the gate ($\lambda\bar{V}$) increases and it increases when P_D increases. Furthermore, for $P_D = 1$ and $\lambda\bar{V} = 0$ (corresponding to the ideal case – no clutter and perfect detection¹⁴), q_2 becomes unity (its maximum value), and for $\lambda\bar{V} \rightarrow \infty$ (corresponding to maximal clutter case), q_2 becomes zero (its minimum value) independent of P_D . For the former case, covariance update equations (2.10) and (2.23) become identical as expected, and for the latter case, the covariance is not updated, that is, there is no information extracted

¹⁴ In that case the gate probability (P_G) is also assumed to be 1.

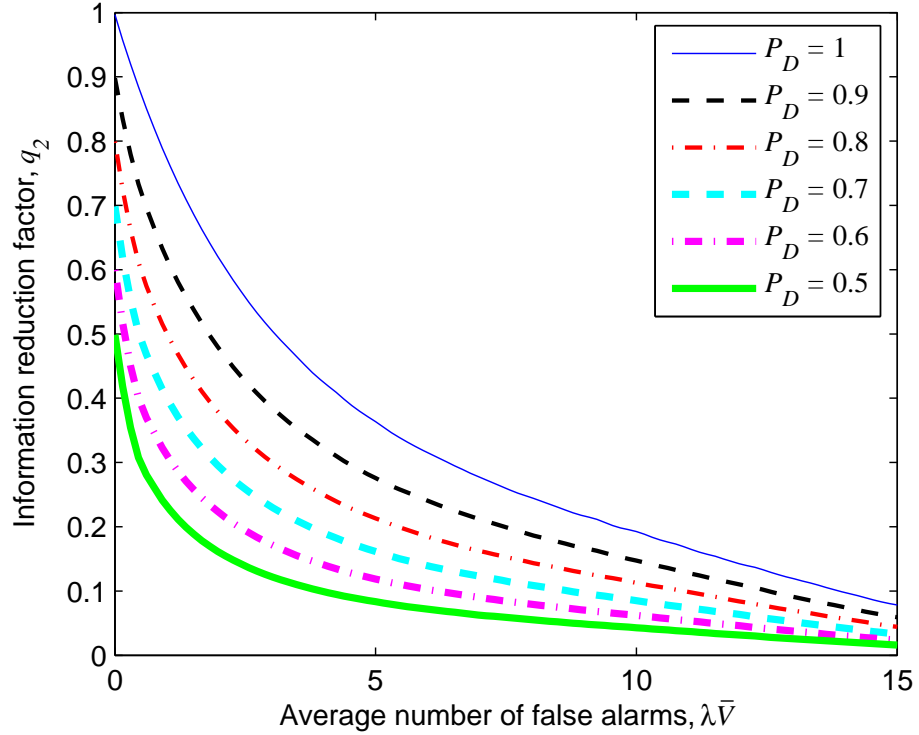


Figure 2.1: Dependence of information reduction factor on average number of false alarms for various detection probabilities. The plot is obtained for two dimensional measurement vector, i.e., $n_z = 2$, and $g = 4$ sigma gate.

from the measurements. These limiting cases illustrate that q_2 can be viewed as an indicator of the amount of information extracted from the measurements but with an inverse relationship, hence the name *information reduction factor*.

2.5.1.2 Stability of the MRE

The standard Riccati equation (2.13) is well-known to be stable, i.e., it will always converge to a steady-state covariance, provided appropriate controllability and observability conditions hold. Furthermore, the solution can be given in a non-recursive form (see (2.15)). This is not the case for the modified Riccati equation. Indeed, the stability analysis of the modified Riccati equation is still a subject of ongoing research. In its most challenging form of (2.25), this analysis seems to be difficult, because the recursion includes the scalar factor $q_2(k)$ which implicitly depends on the solution itself. This

difficulty is clearly stated in [5]. However, only a graphical demonstration is presented, that being for one dimensional state space case. An analysis is still lacking.

More recently, certain theoretical frameworks have been constructed for the simpler version of this equation which arises when there is no clutter ($P_{FA} = 0$) but the measurement is *intermittent* [29], i.e., it is available with a less than unity probability of detection ($P_D < 1$). This tractable problem has been attacked in a number of studies [29], [25], [26]. In this case, the modified Riccati equation simplifies to

$$\begin{aligned} \bar{P}(k+1|k) = F & \left[\bar{P}(k|k-1) - P_D \bar{P}(k|k-1) H^T \left(H \bar{P}(k|k-1) H^T + R \right)^{-1} \right. \\ & \left. \times H \bar{P}(k|k-1) \right] F^T + G Q G^T \end{aligned} \quad (2.31)$$

where the modification is done with the time-invariant scalar P_D which is independent of $\bar{P}(k|k-1)$. This tractable version of the modified Riccati equation resembles the standard one more as compared to (2.25). However, it is still not in the Riccati form, and indeed it was noted that it can not be transformed by smart manipulations into an equation that is of the Riccati form [26]. Therefore, the aforementioned controllability and observability conditions can still not be applied directly for this case, but in [26], some ‘‘Riccati-like’’ properties are reported. In [29], several theorems are proposed for statistical convergence properties of (2.31) showing the existence of a critical value for the arrival rate of the observations, beyond which a transition to an unbounded state error covariance occurs.

2.5.1.3 Offline Recursion of the MRE

Although the stability analysis is not completed theoretically yet, the recursion of the equation (2.25) can still be performed and convergence or divergence phenomena can be observed numerically. The modified Riccati recursion can be performed offline given that $P(0|0)$, P_{FA} , P_D , F , G , Q , H , R , and V_C are

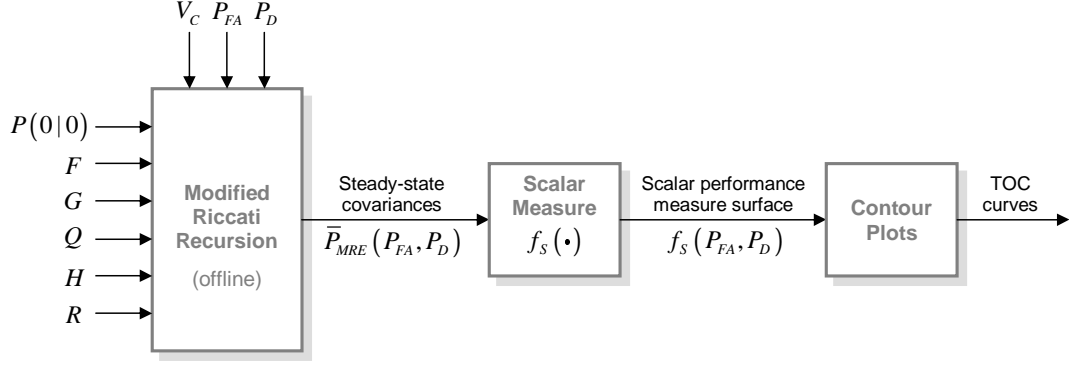


Figure 2.2: The algorithmic flow of obtaining the tracker operating characteristic (TOC) curves from the offline modified Riccati recursion.

known. This is illustrated in Fig. 2.2.

Although algebraically equivalent to (2.25), due to better numerical properties noted [18], the recursion is performed in the following manner:

- **Covariance Update:**

$$\bar{S}(k) = H\bar{P}(k|k-1)H^T + R, \quad (2.32)$$

$$\bar{W}(k) = \bar{P}(k|k-1)H^T\bar{S}^{-1}(k), \quad (2.33)$$

$$\bar{V}(k) = c_{nz}g^{nz}|\bar{S}(k)|^{1/2}, \quad (2.34)$$

$$q_2(k) = Q_2^{LUT}(\lambda\bar{V}(k), P_D), \quad (2.35)$$

$$\begin{aligned} \Sigma(k) &= \left[I - \bar{W}(k)H \right] \bar{P}(k|k-1) \left[I - \bar{W}(k)H \right]^T \\ &\quad + \bar{W}(k)R\bar{W}^T(k), \end{aligned} \quad (2.36)$$

$$\begin{aligned} \bar{P}(k|k) &\triangleq \bar{P}_{MRE}(k|k) \\ &= \left[1 - q_2(k) \right] \bar{P}(k|k-1) - q_2(k)\Sigma(k), \end{aligned} \quad (2.37)$$

- **Covariance Prediction:**

$$\bar{P}(k+1|k) = F\bar{P}(k|k)F^T + GQG^T. \quad (2.38)$$

The MRE recursion is initialized with $\bar{P}(1|0) \triangleq FP(0|0)F^T + GQG^T$. The terms $\bar{S}(k)$, $\bar{W}(k)$, $\bar{P}(k|k-1)$, $\bar{P}(k|k)$ and $\bar{P}(k+1|k)$ are the offline versions of the terms $S(k)$, $W(k)$, $P(k|k-1)$, $P(k|k)$ and $P(k+1|k)$, respectively. At

each time step k , the value of the information reduction factor $q_2(k)$ is obtained from a two dimensional (2D) LUT, $Q_2^{LUT}(\cdot, \cdot)$ via interpolation.

2.5.1.4 Tracker Operating Characteristic (TOC) Curves

The modified Riccati recursion, if it converges, gives a steady-state covariance,

$$\bar{P}_{MRE}(P_{FA}, P_D) \triangleq \lim_{k \rightarrow \infty} \bar{P}(k+1|k) \quad (2.39)$$

where the notation $\bar{P}_{MRE}(P_{FA}, P_D)$ denotes the steady-state covariance matrix obtained for a specific (P_{FA}, P_D) pair. One can deduce several scalar performance measures from $\bar{P}_{MRE}(P_{FA}, P_D)$ such as $\text{tr}\{\bar{P}_{MRE}(P_{FA}, P_D)\}$ and $|\bar{P}_{MRE}(P_{FA}, P_D)|$. Tracker operating characteristic (TOC) curves are defined as the contours on $P_{FA} - P_D$ plane corresponding to *constant values* of these metrics. An example plot is given in Fig. 2.3a for the case of steady-state RMS position error metric, defined by

$$\bar{\sigma}_{POS}^{ss}(P_{FA}, P_D) \triangleq \sqrt{\sum_{i \in \mathcal{S}_{POS}} \bar{p}_{MRE}^{ii}(P_{FA}, P_D)} \quad (2.40)$$

where \mathcal{S}_{POS} is the set of state vector indices corresponding to position components and $\bar{p}_{MRE}^{ii}(P_{FA}, P_D)$ is the i th diagonal element of $\bar{P}_{MRE}(P_{FA}, P_D)$. For example, for $\mathcal{S}_{POS} = \{1, 3\}$, i.e., the first and the third elements of the state vector are the position components, we have

$$\bar{\sigma}_{POS}^{ss}(P_{FA}, P_D) \triangleq \sqrt{\bar{p}_{MRE}^{11}(P_{FA}, P_D) + \bar{p}_{MRE}^{33}(P_{FA}, P_D)} \quad (2.41)$$

Note that in Fig. 2.3a, there exists an instability region, corresponding to low probability of detection and high probability of false alarm (i.e., lower right corner) on $P_{FA} - P_D$ plane. This indicates that in those values of P_{FA} and P_D , the modified Riccati recursion does not converge to a steady state covariance. This region can be viewed as the set of detector operating points causing divergence or track loss for the PDAF.

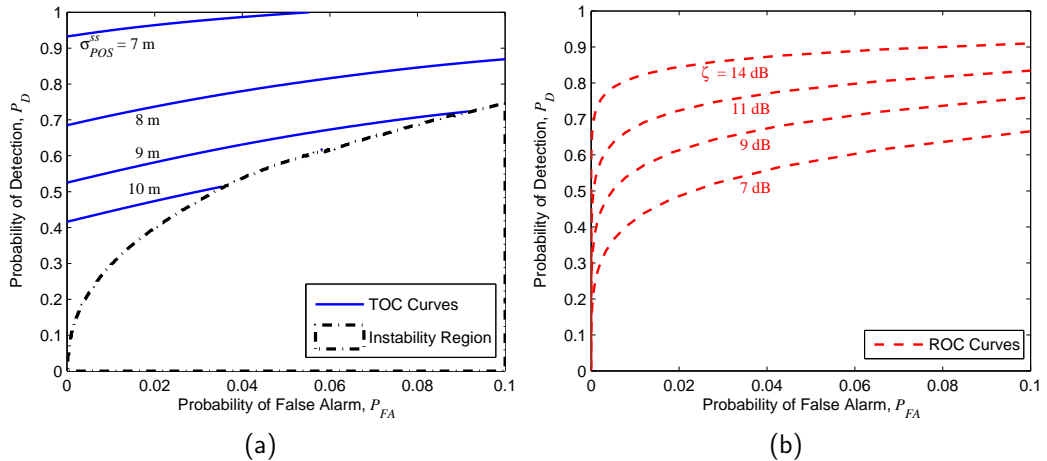


Figure 2.3: Illustration of (a): TOC curves obtained as steady-state RMS position error contours, (b): ROC curves for a CA-CFAR detector

2.5.1.5 Superimposing TOC and ROC Curves

The domain of TOC and ROC curves are the same, i.e., $P_{FA} - P_D$ plane. So they can be superimposed in one plot. This is illustrated in Fig. 2.4.

In this figure, the ROC curves belong to a cell-averaging constant false alarm rate (CA-CFAR) detector with a reference cell length of $N_R = 16$. Their analytic expression is given by

$$P_D = \left(1 + \frac{P_{FA}^{-1/N_R} - 1}{1 + \zeta} \right)^{-N_R} \quad (2.42)$$

where ζ denotes the SNR.

Remark 2.1 *The ROC curve relation given in (2.42) is valid under the assumption of homogeneous and Gaussian background detector noise, a Swerling-I target fluctuation and square-law detection scheme. In radar detection theory, these assumptions are made frequently when obtaining the ROC curves for a specific detector [63]. Therefore, from now on, we refer to this joint assumption shortly as $\text{HOG}_I^{\text{SQL}}$.*

Fig. 2.4 tells us graphically how tracking performance depends on the operating point of the detector (i.e., on the detection threshold). For a given SNR, the optimum detector operating point which gives the minimum steady-state

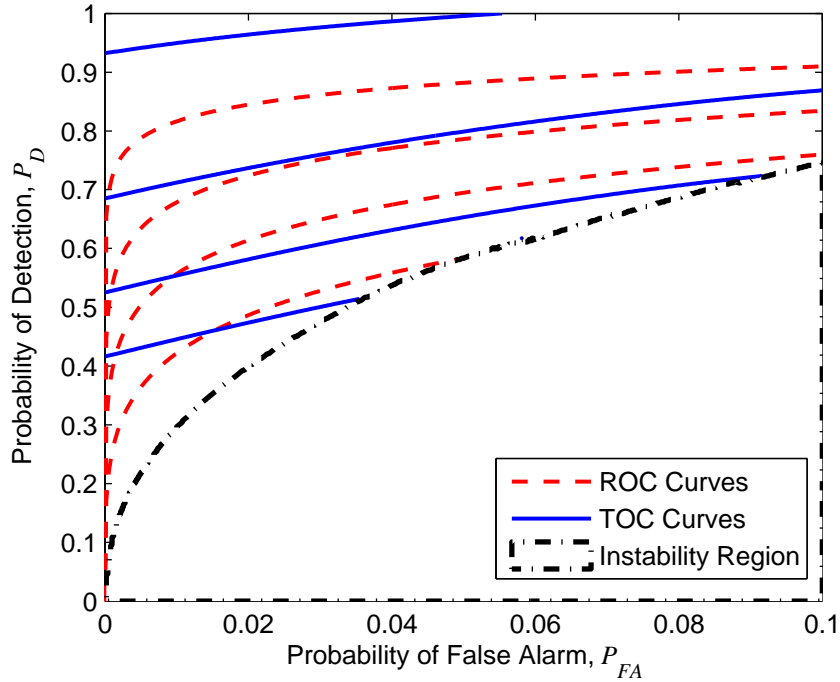


Figure 2.4: The superimposition of TOC and ROC curves.

RMS position error is clearly the tangential point of corresponding TOC and ROC curves.

2.5.2 The Hybrid Conditional Averaging (HYCA) Algorithm

The HYCA algorithm, introduced in [6], extends NSPP capability of MRE [5], which is limited to the steady-state, to the transient. By this feature, HYCA algorithm can quantify some transient phenomena as well, such as, *track loss* and *track lifetime* [6], which are not handled by the MRE approach. The fundamental difference of HYCA from MRE is that, in obtaining deterministic approximations for the stochastic quantities, averaging is performed over only the *continuous* part of the uncertainty, while retaining dependency on the *discrete* part. This is achieved by taking the *conditional* expectations conditioned on each possible value of the discrete uncertainties and propagating (not combining) each expectation as a separate hypothesis with its correspond-

ing likelihood. By this way, the information conveyed by each realization of the discrete uncertainties is retained. This methodology was first applied for NSPP of the PDAF [6]. In this case, the conditional expected values of the state prediction covariances, $P(k+1|k)$; conditioned on each possible value of the *number of validated measurements*, $m_k = 0, 1, \dots, N$; are computed. That is, we have

$$\bar{P}(k+1|k, m_k) \triangleq \mathbb{E}\left[P(k+1|k) \middle| Z^k, m_k\right], \quad (2.43)$$

where the expectation is taken over only *measurement locations*, $z(k)$ (a continuous random variable). Here m_k is a discrete random variable and N is a parameter of the algorithm which limits the number of possible hypothesis.

2.5.2.1 Analogy with the IMM Filtering

In HYCA algorithm, the conditional expectations $\bar{P}(k+1|k, m_k)$ for $m_k = 0, 1, \dots, N$ are recursively propagated together with the marginal probabilities¹⁵ $\Pr\{m_k\}$, $m_k = 0, 1, \dots, N$, so that, at any time step k , they can be combined into one covariance¹⁶ $\bar{P}_{HYCA}(k+1|k)$ for output purposes. In this respect, we argue that the structure and the motivating idea of HYCA algorithm closely resemble those of the so-called *interacting multiple model* (IMM) filtering [64]. For example, in IMM filtering, there are multiple interacting channels in each of which a conditional state estimation, conditioned on one possible value of the *modal state* (discrete uncertainty), is carried out. Similarly, in HYCA algorithm, there are multiple interacting channels in each of which a conditional deterministic covariance approximation, conditioned on one possible value of the *number of validated measurements* is performed. At any time step k , in IMM filtering, the output (the state estimate) can be obtained by combining all channel estimates with the model likelihoods propagated by the algorithm. In a similar way, in HYCA approach, at any time

¹⁵ These are defined as the probabilities of having $m_k = 0, 1, \dots, N$ validated measurements at time step k , respectively.

¹⁶ As shown in Fig. 2.5, depending on the need, the output can be $\bar{P}_{HYCA}(k|k)$ as well.

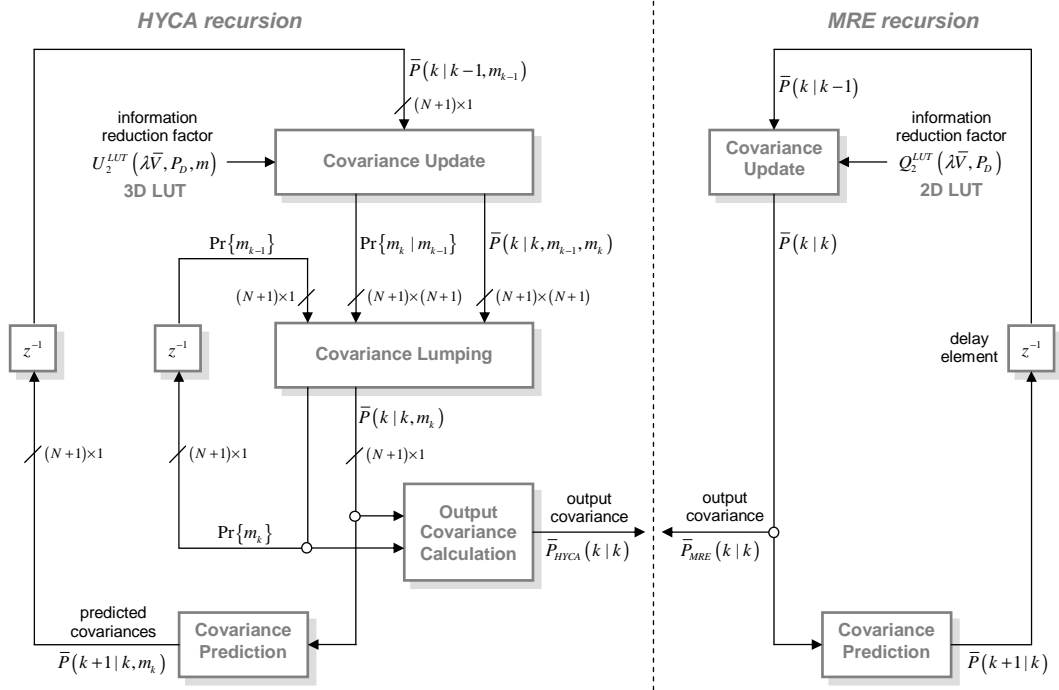


Figure 2.5: Block diagrams of two offline covariance recursion algorithms for the PDAF: HYCA (left) and MRE (right). The corresponding output of each algorithm, denoted by $\bar{P}_{HYCA}(k|k)$ and $\bar{P}_{MRE}(k|k)$, is a deterministic approximation to the filter calculated covariance, $P(k|k)$ of the PDAF.

step k , the output (the deterministic covariance approximation) can be obtained by combining all channel covariance approximations with the marginal probabilities propagated by the algorithm.

2.5.2.2 Offline Recursion of the HYCA Algorithm

The block diagram of HYCA algorithm is given in Fig. 2.5 in comparison with the MRE algorithm. Note that there are two delay elements corresponding to two main recursions in the algorithm:

- The recursion of the prediction covariances $\{\bar{P}(k|k-1, m_{k-1})\}_{m_{k-1}=0}^N$,
- The recursion of the marginal probabilities $\{\Pr\{m_{k-1}\}\}_{m_{k-1}=0}^N$.

Therefore, given $\{\bar{P}(k|k-1, m_{k-1})\}_{m_{k-1}=0}^N$ and $\{\Pr\{m_{k-1}\}\}_{m_{k-1}=0}^N$ at time step $k-1$, one step recursion of HYCA produces $\{\bar{P}(k+1|k, m_k)\}_{m_k=0}^N$ and

$\{\Pr\{m_k\}\}_{m_k=0}^N$ at time step k . The recursions are initialized with $\bar{P}(1|0, m_0) \triangleq FP(0|0)F^T + GQG^T$ and $\Pr\{m_0\} \triangleq 1/(N+1)$ for $m_0 = 0, 1, \dots, N$.

The algorithm consists of four main parts, whose derivations are given in detail in [6]:

- **Covariance Update:** This is the computationally most intensive part of the algorithm. For each $m_{k-1} = 0, 1, \dots, N$, the prediction covariance $\bar{P}(k|k-1, m_{k-1})$ is updated to $\bar{P}(k|k, m_{k-1}, m_k)$ for each $m_k = 0, 1, \dots, N$. That is, all possible updates of all propagated covariances are done in a matrix fashion. Furthermore, for each of these possible update paths from m_{k-1} to m_k , the corresponding conditional probability $\Pr\{m_k|m_{k-1}\}$ is also calculated. For particular values of m_{k-1} and m_k , i.e., for a single entry in that matrix, the computation is done as follows.

$$\bar{S}(k, m_{k-1}) = H\bar{P}(k|k-1, m_{k-1})H^T + R, \quad (2.44)$$

$$\bar{W}(k, m_{k-1}) = \bar{P}(k|k-1, m_{k-1})H^T\bar{S}^{-1}(k, m_{k-1}), \quad (2.45)$$

$$\bar{V}(k, m_{k-1}) = c_{n_z}g^{n_z}|\bar{S}(k, m_{k-1})|^{1/2}, \quad (2.46)$$

$$u_2(k, m_k) = U_2^{LUT}(\lambda\bar{V}(k, m_{k-1}), P_D, m_k), \quad (2.47)$$

$$\begin{aligned} \Sigma(k, m_{k-1}) &= \left[I - \bar{W}(k, m_{k-1})H \right] \bar{P}(k|k-1, m_{k-1}) \\ &\quad \times \left[I - \bar{W}(k, m_{k-1})H \right]^T \\ &\quad + \bar{W}(k, m_{k-1})R\bar{W}^T(k, m_{k-1}), \end{aligned} \quad (2.48)$$

$$\begin{aligned} \bar{P}(k|k, m_{k-1}, m_k) &= \left[1 - u_2(k, m_k) \right] \bar{P}(k|k-1, m_{k-1}) \\ &\quad - u_2(k, m_k)\Sigma(k, m_{k-1}), \end{aligned} \quad (2.49)$$

$$\begin{aligned} \Pr\{m_k|m_{k-1}\} &= \left[1 + P_D P_G \left(\frac{m_k}{\lambda\bar{V}(k, m_{k-1})} - 1 \right) \right] \\ &\quad \times \mu_F(m_k, \lambda\bar{V}(k, m_{k-1})). \end{aligned} \quad (2.50)$$

where

$$\mu_F(m_k, \lambda\bar{V}(k, m_{k-1})) \triangleq \exp(-\lambda\bar{V}(k, m_{k-1})) \frac{(\lambda\bar{V}(k, m_{k-1}))^{m_k}}{m_k!} \quad (2.51)$$

is the Poisson probability mass function (pmf) for the number of false measurements. Note that apart from (2.50), the operations done in the covariance update part of HYCA are very similar to those of MRE given by the equations (2.32)–(2.37). The term $\Pr\{m_k|m_{k-1}\}$ is the conditional probability of the event that having m_k validated measurements at time step k , conditioned on the event that there were m_{k-1} validated measurements at $k-1$. This probability is used for *lumping* the covariances $\bar{P}(k|k, m_{k-1}, m_k)$ to form $\bar{P}(k|k, m_k)$, and can be calculated for different values of m_k as

$$\Pr\{m_k|m_{k-1}\} = \begin{cases} (1 - P_D P_G) \mu_F(m_k, \lambda \bar{V}(k, m_{k-1})), & m_k = 0 \\ (1 - P_D P_G) \mu_F(m_k, \lambda \bar{V}(k, m_{k-1})) \\ + P_D P_G \mu_F(m_k - 1, \lambda \bar{V}(k, m_{k-1})), & m_k = 1, 2, \dots \end{cases} \quad (2.52)$$

It can be shown that this expression can be further simplified to the unified form given in (2.50) by utilizing the definition (2.51). Similar to MRE, in HYCA algorithm, the covariances are updated with an *information reduction factor* $u_2(k, m_k)$ whose functional form is given as [65] (after some manipulations on the original form given in [6])

$$u_2(\lambda \bar{V}(k, m_{k-1}), P_D, m_k) = \frac{m_k}{b(\lambda V(k), P_D) + \frac{1}{c_{n_z}} \left(\frac{2\pi}{g^2}\right)^{n_z/2} P_G m_k} \times \frac{1}{n_z} \left(\frac{n_z}{g^{n_z}}\right)^{m_k} I_2(\lambda V(k), P_D, m_k) \quad (2.53)$$

where the terms $I_2(\cdot, \cdot, \cdot)$ and $b(\cdot, \cdot)$ are previously defined in (2.27) and (2.28), respectively. The three dimensional (3D) LUT, $U_2^{LUT}(\cdot, \cdot, \cdot)$ can be obtained offline by evaluating the information reduction factor expression given in (2.53) over a grid of values.

- **Covariance Lumping:** In this part, first the probabilities $\Pr\{m_{k-1}\}$ are updated to $\Pr\{m_k\}$, then for each $m_k = 0, 1, \dots, N$, updated covariances $\bar{P}(k|k, m_{k-1}, m_k)$ are averaged over m_{k-1} to yield the covariances

$\bar{P}(k|k, m_k)$. That is,

$$\Pr\{m_k\} = \sum_{m_{k-1}} \Pr\{m_k|m_{k-1}\}\Pr\{m_{k-1}\}, \quad (2.54)$$

$$\Pr\{m_{k-1}|m_k\} = \frac{\Pr\{m_{k-1}\}\Pr\{m_k|m_{k-1}\}}{\Pr\{m_k\}}, \quad (2.55)$$

$$\bar{P}(k|k, m_k) = \sum_{m_{k-1}} \bar{P}(k|k, m_{k-1}, m_k)\Pr\{m_{k-1}|m_k\}. \quad (2.56)$$

- **Covariance Prediction:** This is the one-step ahead prediction of the covariances $\bar{P}(k|k, m_k)$ for each $m_k = 0, 1, \dots, N$, i.e.,

$$\bar{P}(k+1|k, m_k) = F\bar{P}(k|k, m_k)F^T + GQG^T. \quad (2.57)$$

- **Output Covariance Calculation:** This is an optional part in the sense that it is only for output purposes – it is not part of the algorithm recursions. The output¹⁷ $\bar{P}_{HYCA}(k|k)$ which is a deterministic approximation to the estimation error covariance $P(k|k)$ of the PDAF is obtained by further averaging of the covariances $\{\bar{P}(k|k, m_k)\}$ over m_k as

$$\bar{P}_{HYCA}(k|k) = \sum_{m_k} \bar{P}(k|k, m_k)\Pr\{m_k\}. \quad (2.58)$$

Note that, in the MRE approach, there is no need for such an outputting block, as it already produces its output in the algorithm recursion.

¹⁷ A similar outputting can be done for the covariances $\{\bar{P}(k+1|k, m_k)\}$ to produce $\bar{P}_{HYCA}(k+1|k)$ which is a deterministic approximation to the prediction error covariance $P(k+1|k)$ of the PDAF.

CHAPTER 3

A COMPARISON OF TA-DETOP SCHEMES IN A UNIFIED THEORETICAL AND EXPERIMENTAL FRAMEWORK

In the conventional approaches to the detection theory such as Neyman-Pearson (NP) and Constant False Alarm Rate (CFAR) formulations, first a desired (acceptable) false alarm probability (P_{FA}^d) value is specified, then the probability of detection (P_D) is maximized with this constraint [63]. The value of P_{FA}^d is usually selected in view of the radar processor's ability in handling maximum number of false alarms. Although this seems a reasonable criterion, it is only a heuristic one in that it doesn't account for the properties of downstream tracker. *Tracker-aware detector threshold optimization* (TA-DETOP) aims at optimally selecting this operating false alarm probability (which in turn determines the detector operating point and the detection threshold), so that the performance of the downstream tracker, hence of the combined target state estimation system, is maximized. The key point is to minimize a cost function based on the deterministic approximation of the tracking filter's covariance matrix. From the practical applications (i.e., causality) point of view, having a deterministic (and therefore *measurement-independent*) covariance is crucial, as it is used in optimization of detection thresholds, which produce measurements.

In the following sections, we introduce a unifying formulation of the problem as

static and dynamic threshold optimization. We claim that the existing studies in the literature can be well-understood and easily extended in this framework.

3.1 Static Threshold Optimization (STOP)

The problem is to determine the optimum operating P_{FA}^* value such that

$$P_{FA}^* = \arg \min_{P_{FA}} \left\{ f_S \left[\bar{P}_{NSPP} \right] \right\}, \quad \text{subject to}$$

$$P_D = f_{ROC}(P_{FA}, \zeta) \quad \text{and} \quad 0 \leq P_{FA} \leq 1. \quad (3.1)$$

Here, $f_S[\cdot]$ is any scalar measure that can be deduced from a matrix (such as, trace or determinant) and \bar{P}_{NSPP} is the steady-state covariance matrix obtained by propagating one of the NSPP recursions, i.e.,

$$\bar{P}_{NSPP} \triangleq \lim_{k \rightarrow \infty} \bar{P}_{NSPP}(k|k), \quad (3.2)$$

where $\bar{P}_{NSPP}(k|k)$ corresponds to the output of either HYCA or MRE approaches at time step k . The equality constraint of the optimization problem is nothing but a ROC curve relation which links P_D to P_{FA} , or vice-versa, through current SNR (ζ), and the inequality constraint ensures that the resultant operating false alarm value is a valid probability. Note that the optimization problem given in (3.1) is a line search. Provided that the cost function is *unimodal*, the global optimum point can be found directly applying well-known numerical techniques, such as, Golden-Section or Fibonacci Search methods [66]. For each function evaluation at an arbitrary point P_{FA}^i , one needs to obtain the steady-state covariance matrix $\bar{P}_{NSPP}(P_{FA}^i, P_D^i)$ from (3.2) with $P_D^i \triangleq f_{ROC}(P_{FA}^i, \zeta)$.

Another alternative is to utilize a graphical approach. In this case, first, the scalar performance measure surface $f_S(P_{FA}, P_D)$ is constructed by evaluating the cost function at each point of a sufficiently fine mesh grid on the P_{FA} - P_D plane. Then, the contours of this surface, which constitute TOC curves [5],

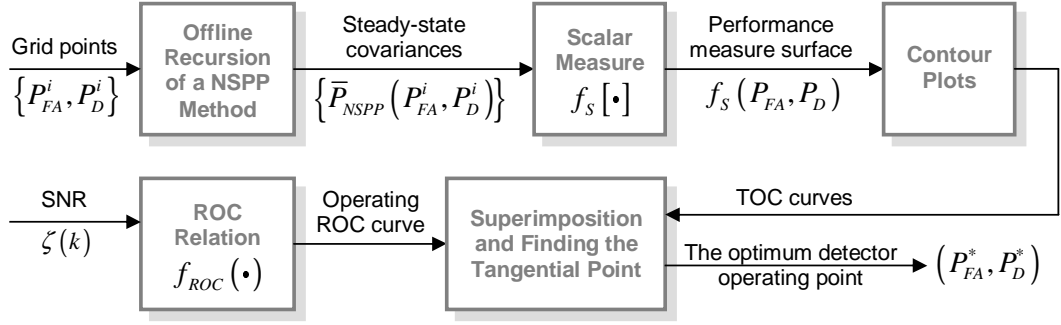


Figure 3.1: The flow of static threshold optimization (STOP) for graphical (TOC-curve) approach. The procedure given in this figure is repeated for different SNR values to obtain the optimum operating curve on P_{FA} - P_D plane. Then, this optimum operating curve is used together with ROC curve relation to find the STOP curve which is the ultimate goal of STOP. The STOP curve provides an SNR-dependent optimum P_{FA} setting which makes the threshold optimization online possible under varying SNR conditions. A numerical example is given in Section 3.3.1.

are obtained. Finally, for the current operating SNR, the tangential point of the corresponding ROC curve with TOC curves is found. This point is the optimum (P_{FA}^*, P_D^*) pair satisfying the ROC curve relation, hence the constraint of the optimization problem. The procedure is summarized in Fig. 3.1.

Although this graphical technique is computationally more expensive, from the practical applicability point of view, this is not a problem since the optimization is made offline and only once. Furthermore, the graphical approach is more preferable compared to the direct utilization of the line search algorithms, as it allows easier interpretation and gives better insight into the problem. For both approaches, however, at some points in the P_{FA} - P_D plane, cost function evaluation may be problematic due to non-existence of the limit given in (3.2), which causes an *instability region* [5].

The TOC-curve approach was first used in [5] for solving the STOP problem for the PDAF case. In this work, MRE is used as an NSPP algorithm leading to threshold optimization scheme STATIC-MRE-TOC (see Fig. 1.2). In this chapter, we apply TOC-curve approach to the HYCA case which results in the optimization scheme *STATIC-HYCA-TOC*. As mentioned before, this is

an extended version of the work given in [7] (HYCA-STATIC-LUT) where the optimization is made using look-up tables. To the best of our knowledge, utilizing the HYCA methodology in this manner is a new look and has not been done in the literature. We believe that the comparison of HYCA and MRE approaches for STOP can be made more reasonably in this unifying framework.

3.2 Dynamic Threshold Optimization (DTOP)

In this case, the problem is to determine the optimum operating $P_{FA}^*(k)$ value such that

$$P_{FA}^*(k) = \arg \min_{P_{FA}} \left\{ f_S \left[\bar{P}_{NSPP}(k|k) \right] \right\}, \quad \text{subject to}$$

$$P_D = f_{ROC}(P_{FA}, \zeta) \quad \text{and} \quad 0 \leq P_{FA} \leq 1. \quad (3.3)$$

Note that the dynamic threshold optimization differs only from its static counterpart in making the optimization not in the steady-state, but at every time step k .

3.2.1 MRE-Based Formulation

The problem formulation based on the MRE approach was first proposed in [1] with the choices of $f_S[\cdot]$ as the trace operator and $\bar{P}_{NSPP}(k|k)$ as the output of the MRE algorithm at time step k . Due to mathematical intractability, the problem was solved by utilizing some line search algorithms that require only the evaluation of the cost function (e.g., Golden-Section or Fibonacci Search methods) [1]. We call this scheme as DYNAMIC-MRE-LS (see Fig. 1.2). A computationally much more efficient alternative to this scheme is the *DYNAMIC-MRE-CF* proposed in [56]. where the same problem is solved in an approximate closed-form. As we will see in the next chapter, by utilizing

such a closed-form solution, one can achieve considerable gain in terms of computational complexity without sacrificing the tracking performance.

3.2.2 HYCA-Based Formulation

Inspired from the formulation for the MRE case by Gelfand [1], we formulate DTOP for HYCA case as follows: Find the optimum operating false alarm probability $P_{FA}^*(k)$ such that

$$P_{FA}^*(k) = \arg \min_{P_{FA}} \left\{ \mathcal{J}(k, P_{FA}) \right\}, \quad \text{subject to}$$

$$P_D = f_{ROC}(P_{FA}, \zeta) \quad \text{and} \quad 0 \leq P_{FA} \leq 1. \quad (3.4)$$

where $\mathcal{J}(k, P_{FA}) \triangleq \text{tr}\{\bar{P}_{HYCA}(k|k)\}$. This problem can be solved by applying line search algorithms, e.g. Fibonacci Search method, which results in the scheme *DYNAMIC-HYCA-LS*. Furthermore, for efficient implementation and avoiding loops, the cost function can be restated in vector-matrix notations as

$$\mathcal{J}(k, P_{FA}) = \mathbf{p}^T(k) \left[\mathbf{T}_P(k) \Pi^T(k, P_{FA}) \mathbf{c} - \mathbf{T}_B(k) \mathbf{U}(k, P_{FA}) \Pi(k, P_{FA}) \right] \quad (3.5)$$

where \mathbf{p} is an $(N + 1)$ dimensional column vector whose j th entry is $p_j \triangleq \text{Pr}\{m_{k-1} = j\}$ for $j = 0, 1, \dots, N$ and \mathbf{c} is an $(N + 1)$ dimensional constant column vector with all entries being equal to 1. \mathbf{T}_P and \mathbf{T}_B are both $(N + 1)$ by $(N + 1)$ diagonal matrices with the i th diagonal elements for $i = 0, 1, \dots, N$ are given by $\text{tr}\{\bar{P}(k|k-1, i)\}$ for \mathbf{T}_P and $\text{tr}\{\bar{B}(k, i)\}$ for \mathbf{T}_B , where $\bar{B}(k, i) \triangleq \bar{W}(k, i) \bar{S}(k, i) \bar{W}^T(k, i)$. Finally, the matrices $\Pi = [p_{ij}]$ and $\mathbf{U} = [u_{ij}]$ are both $(N + 1)$ by $(N + 1)$ with $p_{ij} \triangleq \text{Pr}\{m_k = i | m_{k-1} = j\}$ and $u_{ij} \triangleq u_2(\lambda \bar{V}(k, i), P_D, j)$ for $i, j = 0, 1, \dots, N$.

3.3 Simulation Results

We consider the problem of tracking a single target in clutter using a 2D radar. The target state vector is composed of position and velocity components in

East (ξ) and North (η) directions:

$$x(k) \triangleq \begin{bmatrix} \xi(k) & \dot{\xi}(k) & \eta(k) & \dot{\eta}(k) \end{bmatrix}^T. \quad (3.6)$$

The target motion is a coordinated turn with a constant turn rate:

$$F = \begin{bmatrix} 1 & \frac{\sin(\Omega T)}{\Omega} & 0 & -\frac{1-\cos(\Omega T)}{\Omega} \\ 0 & \cos(\Omega T) & 0 & -\sin(\Omega T) \\ 0 & \frac{1-\cos(\Omega T)}{\Omega} & 1 & \frac{\sin(\Omega T)}{\Omega} \\ 0 & \sin(\Omega T) & 0 & \cos(\Omega T) \end{bmatrix}, \quad G = \begin{bmatrix} T^2/2 & 0 \\ T & 0 \\ 0 & T^2/2 \\ 0 & T \end{bmatrix} \quad (3.7)$$

where the turn rate is selected as $\Omega = 1 \text{ deg/s}$ and the sampling period is $T = 1 \text{ s}$. Note that in the state vector, we do not estimate the turn rate, i.e., it is assumed to be known, therefore the state dynamics is linear. This is adopted to decouple the maneuver problem from the clutter problem on which our focus is. The process noise $v(k) \triangleq [v_\xi(k) \ v_\eta(k)]^T$ is a zero mean white Gaussian random vector sequence with covariance matrix

$$Q = \begin{bmatrix} 1 & 0 \\ 0 & 1 \end{bmatrix} q^2 \quad (3.8)$$

for all k . The factor q is selected as 0.1 m/s^2 .

Measurements are taken from a radar located at the center of the target motion (see Fig. 3.2), and assumed to be consist of position values in East and North directions, i.e.,

$$z(k) \triangleq \begin{bmatrix} \xi^m(k) & \eta^m(k) \end{bmatrix}^T \quad (3.9)$$

which implies

$$H = \begin{bmatrix} 1 & 0 & 0 & 0 \\ 0 & 0 & 1 & 0 \end{bmatrix}. \quad (3.10)$$

Note that the scenario geometry given in Fig. 3.2 ensures the range of the target to be constant during the simulation. Such an artificial scenario is selected to have a constant SNR during the simulation, assuming that the SNR depends only on range as

$$\zeta(r) = \frac{C_\zeta}{r^4} \quad (3.11)$$

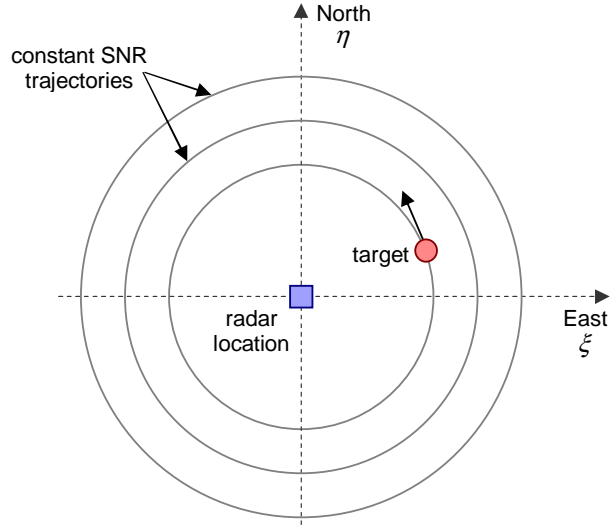


Figure 3.2: Scenario geometry: Assumed constant SNR target trajectories and location of the radar.

where C_ζ is a constant representing all the other factors in the SNR equation and r is the range to the target. To determine C_ζ , ζ is assumed to be 50 for 5 km, which yields $C_\zeta = 3.125 \times 10^{16} m^4$.

The measurement noise $w(k) \triangleq [w_\xi(k) \ w_\eta(k)]^T$ is a zero mean white Gaussian random vector sequence with covariance matrix

$$R = \begin{bmatrix} (\Delta r_\xi / \sqrt{12})^2 & 0 \\ 0 & (\Delta r_\eta / \sqrt{12})^2 \end{bmatrix} \quad (3.12)$$

for all k , where Δr_ξ and Δr_η are the range resolutions in East and North directions, respectively and taken as $\Delta r_\xi = \Delta r_\eta = 50 m$ which results in a resolution cell volume of $V_C = 2500 m^2$. Note that the covariance matrix given in (3.12) is the result of the assumption that the true measurement is uniformly distributed in the resolution cell [4, pp. 472]. The a priori information about the state, i.e., the mean $\hat{x}(0|0)$ and the covariance $P(0|0)$ of the initial state $x(0)$, is obtained by *two point differencing* [18] as

$$\hat{x}(0|0) \triangleq \left[\xi^m(0) \quad \frac{\xi^m(0) - \xi^m(-1)}{T} \quad \eta^m(0) \quad \frac{\eta^m(0) - \eta^m(-1)}{T} \right]^T \quad (3.13)$$

with

$$P(0|0) = \begin{bmatrix} r_{11} & r_{11}/T & 0 & 0 \\ r_{11}/T & 2r_{11}/T^2 & 0 & 0 \\ 0 & 0 & r_{22} & r_{22}/T \\ 0 & 0 & r_{22}/T & 2r_{22}/T^2 \end{bmatrix} \quad (3.14)$$

where $r_{ij} \triangleq R(i, j)$. It is known [18] that such an initialization guarantees the initial *filter consistency*.¹ Note that initialization of the state presumes availability of two measurements $z(-1)$ and $z(0)$. These measurements can be obtained separately before the simulation starts and then used in the initialization of the state in (3.13).

3.3.1 Obtaining TOC Curves

After defining all the necessary variables, TOC curves can be obtained for both MRE and HYCA methodologies, as illustrated in the flow diagram given in Fig. 3.1. The parameter, N of the HYCA algorithm is taken as 15. We run both of the recursions on a 500×500 regular P_{FA} - P_D grid. The borders of the grid are from 0 to 0.1 for P_{FA} and from 0 to 1 for P_D . Both recursions are run over each point in this grid until convergence. As mentioned before, the recursions do not converge to a steady-state covariance for some of the grid points, due to non-existence of the limit given in (3.2). This causes an *instability region* (see Fig. 3.3). Note that this region is located at lower right corner on P_{FA} - P_D plane which corresponds to low P_D and high P_{FA} values.

We define the scalar performance function ($f_S[\cdot]$) as the steady-state position estimation error, i.e.,

$$f_S[\bar{P}_{NSPP}] \triangleq \sigma_{POS}^{ss} = \sqrt{\bar{p}_{NSPP}^{11} + \bar{p}_{NSPP}^{33}} \quad (3.15)$$

where \bar{p}_{NSPP}^{ii} is the i th diagonal element of \bar{P}_{NSPP} . The TOC curves are obtained as the contours of the corresponding performance measure surface.

¹ The consistency of a tracking filter can be viewed as a honesty [18] measure of degree of the filter's statement "I estimate the state with this much error (covariance)."

The superimposition of these curves onto the ROC curves is shown in Fig. 3.3 where the functional form of the ROC curves is given by²

$$P_D = P_{FA}^{1/(1+\zeta)}. \quad (3.16)$$

Note that the collection of optimum operating points for different SNR values, consisting of the tangential points of TOC and ROC curves, are well-behaved. A line fitting works quite well and results in approximations

$$P_D = -9.523P_{FA} + 1.002 \quad \text{for MRE case,} \quad (3.17)$$

$$P_D = -5.943P_{FA} + 0.979 \quad \text{for HYCA case.} \quad (3.18)$$

Each of these optimum operating line equations can be combined with the ROC curve relation given in (3.16) to obtain a relation between P_{FA} and ζ as

$$P_{FA}^{1/(1+\zeta)} + 9.523P_{FA} - 1.002 = 0 \quad \text{for MRE case,} \quad (3.19)$$

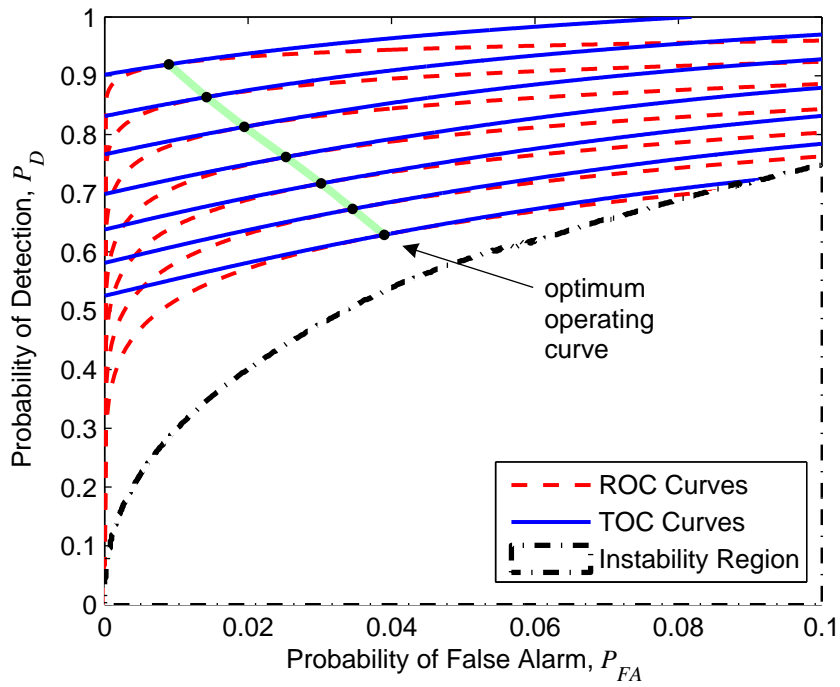
$$P_{FA}^{1/(1+\zeta)} + 5.943P_{FA} - 0.979 = 0 \quad \text{for HYCA case.} \quad (3.20)$$

The numerical solution of these equations constitutes the *static threshold optimization* (STOP) curves given in Fig. 3.4.

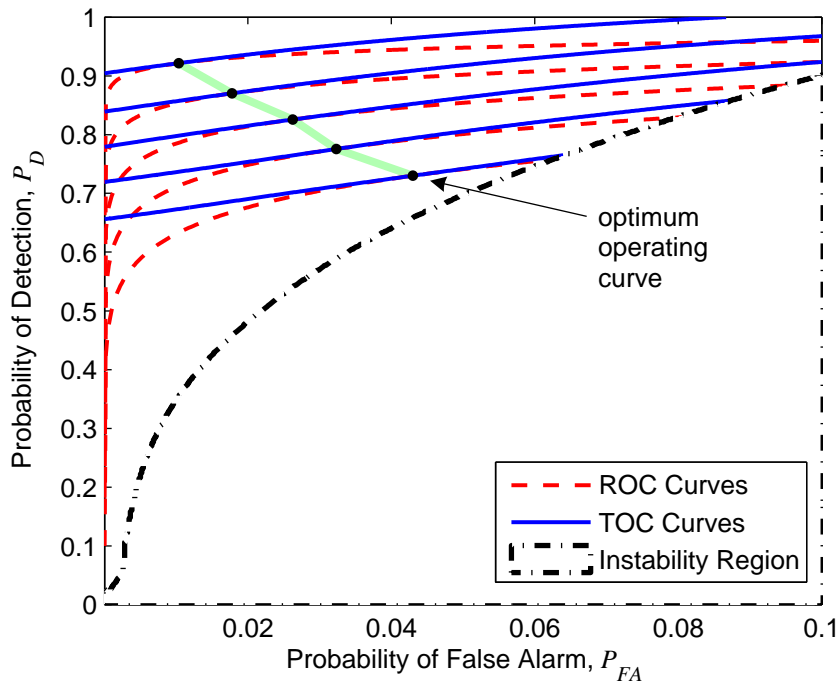
Note that STOP curves suggest that the desired false alarm probability of the detector should be readjusted according to SNR variations. This is different than the conventional approach in which the desired false alarm probabilities are fixed.³ The resulting overall system target tracking performance corresponding to the two static methods is also of interest and is investigated in detail in subsequent experimental sections. At this point however, it can be observed that for a practical range of operating SNR values, HYCA based optimization consistently suggests a higher P_{FA} and therefore results in more false

² This is valid for a special case of a Neyman-Pearson (NP) detector under $\text{HOG}_I^{\text{SQL}}$ where the homogeneous Gaussian background detector noise and Swerling-I target fluctuation are passed through a square-law detection scheme [63].

³ Of course, changing SNR readjusts the detection thresholds in conventional approaches (such as in CA-CFAR), but the desired false alarm probability is not adapted.



(a) MRE case.



(b) HYCA case.

Figure 3.3: STOP using TOC curves. Note that, the instability region for the HYCA case has a slightly larger area than that of MRE. One can fit a line equation for the optimum operating curves in both approaches. Then this equation together with the ROC curve relation determine STOP curve which can be used to find the optimum operating point for an arbitrary SNR value.

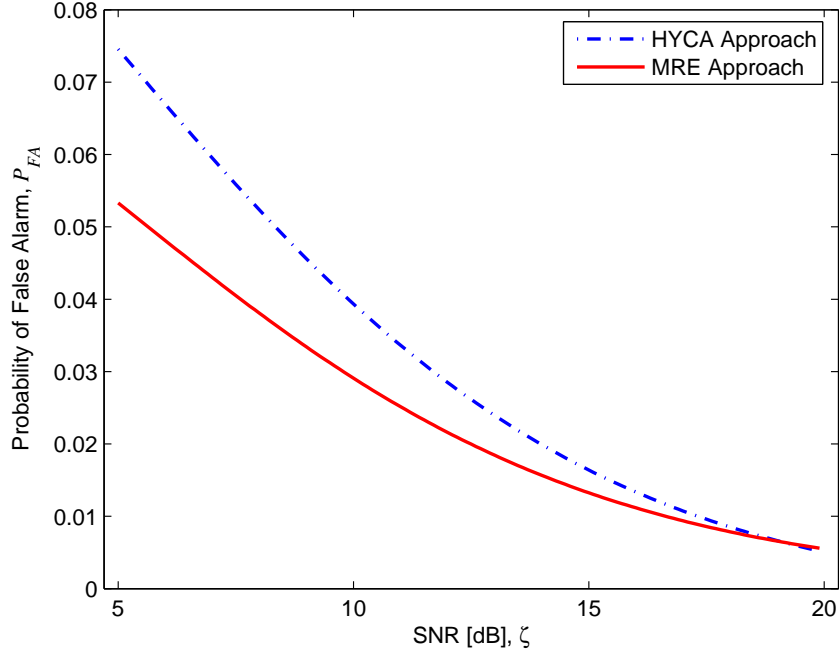


Figure 3.4: STOP curves for MRE and HYCA approaches. Note that for a practical range of operating SNR values, the HYCA based approach consistently suggests a higher P_{FA} .

detections for the radar processor to handle.⁴ For both approaches, STOP curves can be tabulated as a LUT for an online usage (i.e., in varying SNR conditions). A closed form functional approximation to STOP curves can also be considered. In our example, we have verified that an exponential fit of the form $P_{FA}(\zeta) = ae^{b\zeta} + ce^{d\zeta}$ can be found for each STOP curve, with the coefficients given in Table 3.1.

Table 3.1: Exponential fit coefficients for STOP curves.

Methodology	a	b	c	d
MRE	0.1418	-0.1555	-0.0751	-0.3755
HYCA	0.5273	-0.2059	-0.4316	-0.2683

⁴ This is an important practical problem in the radar. Under excessive number of false detections, the radar may initiate lots of false tracks. This causes the radar to allocate its resources, e.g. dwell time, transmission power, unnecessarily and inefficiently. In the scope of this thesis study, we do not consider track initiation and resource allocation problems.

Table 3.2: Experiment-I: Compared tracking systems. The name of the proposed system is written in italic.

System Name	Desired False Alarm Probability, P_{FA}^d
PDAKF-HEURISTIC-E8	$P_{FA}(k) = 10^{-8}$
PDAKF-HEURISTIC-E6	$P_{FA}(k) = 10^{-6}$
PDAKF-HEURISTIC-E4	$P_{FA}(k) = 10^{-4}$
PDAKF-STATIC-MRE [5]	$P_{FA}(k) = f_{MRE}(\zeta(k))$
<i>PDAKF-STATIC-HYCA</i>	$P_{FA}(k) = f_{HYCA}(\zeta(k))$

3.3.2 Experiment1: Comparison of STOP with Conventional Approaches

In this experiment, we compare five tracking systems each consisting of a PDA tracking filter and a Neyman-Pearson (NP) front-end detector. The description of the systems is given in Table 3.2.

In the first three systems, the detectors use conventional (i.e., heuristically selected) constant desired false alarm probabilities of $P_{FA} = 10^{-8}$, $P_{FA} = 10^{-6}$ and $P_{FA} = 10^{-4}$, which are the typical values used in practice [2]. On the other hand, the last two systems utilize tracker-aware (TA) detectors for which the desired false alarm probabilities are determined using STOP curves, $f_{MRE}(\zeta(k))$ and $f_{HYCA}(\zeta(k))$, given in Fig. 3.4. Note that the last system based on HYCA approach is proposed in this study. We choose four different constant SNR scenarios of 5, 10, 15 and 20 dB. In each scenario, the target follows the corresponding constant SNR trajectory for 200 time steps as illustrated in Fig. 3.2. We have conducted 500 Monte Carlo runs for each scenario. Fig. 3.5 shows the simulation results pertaining to the heuristic methods.

In Fig. 3.5a, the RMS position error plots are obtained by ensemble averaging over only the runs that do not result in *track loss*.⁵ The track loss percentage

⁵ Except for the track loss percentage (TLP), in all performance measures presented in the experimental results, we consider only track-loss-free runs. We accept that the track is lost for the i th Monte Carlo run, if $\epsilon_{POS}^i > \rho$ where $\rho \triangleq \sqrt{\text{tr}\{R\}}$ is the measurement error level and ϵ_{POS}^i is the average position estimation error for the i th Monte Carlo run.

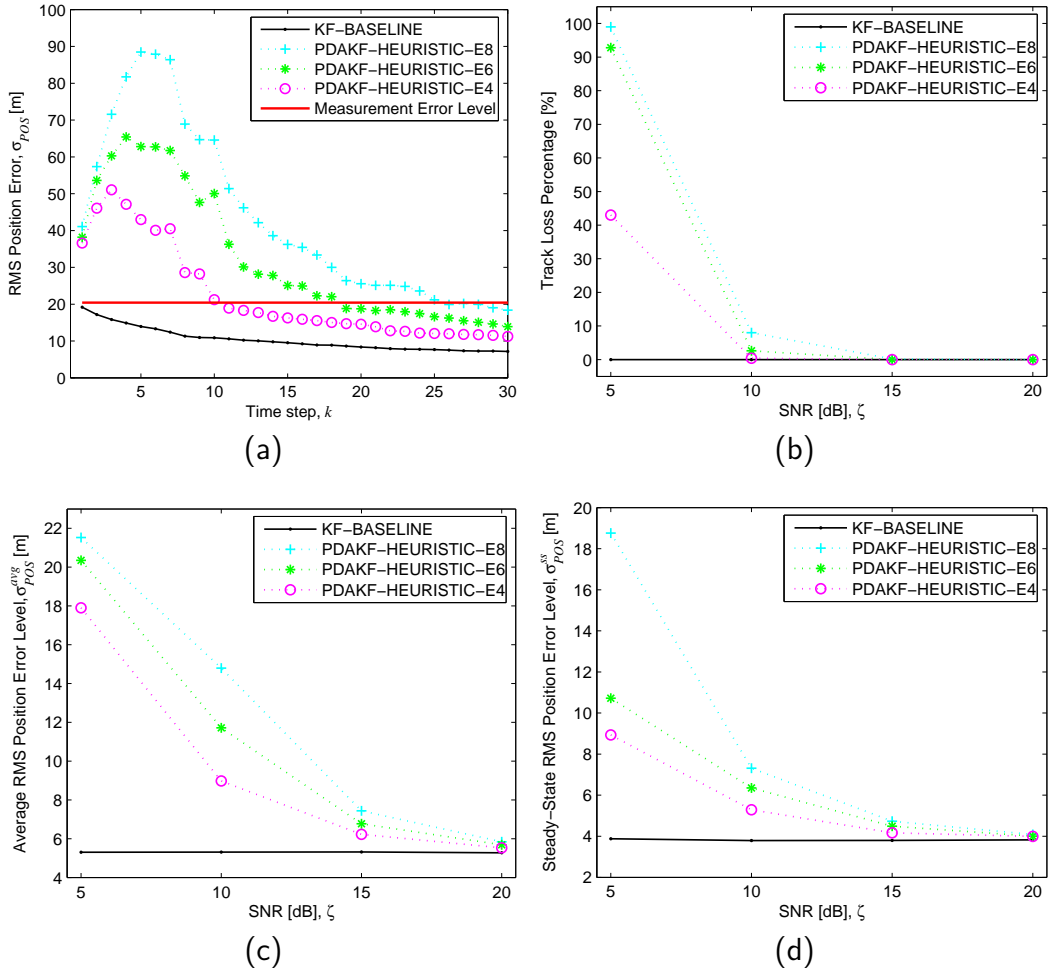


Figure 3.5: Experiment-I: The effect of selecting different operating P_{FA} values on downstream tracking: (a) The transient RMS position error plots ($\zeta = 10$ dB case), (b) track loss percentages, (c) the average and (d) the steady-state, RMS position error levels. In each subfigure, the performance of the corresponding Kalman filter (KF) which uses *perfect data association* is also shown as a baseline.

(TLP) measure is defined as

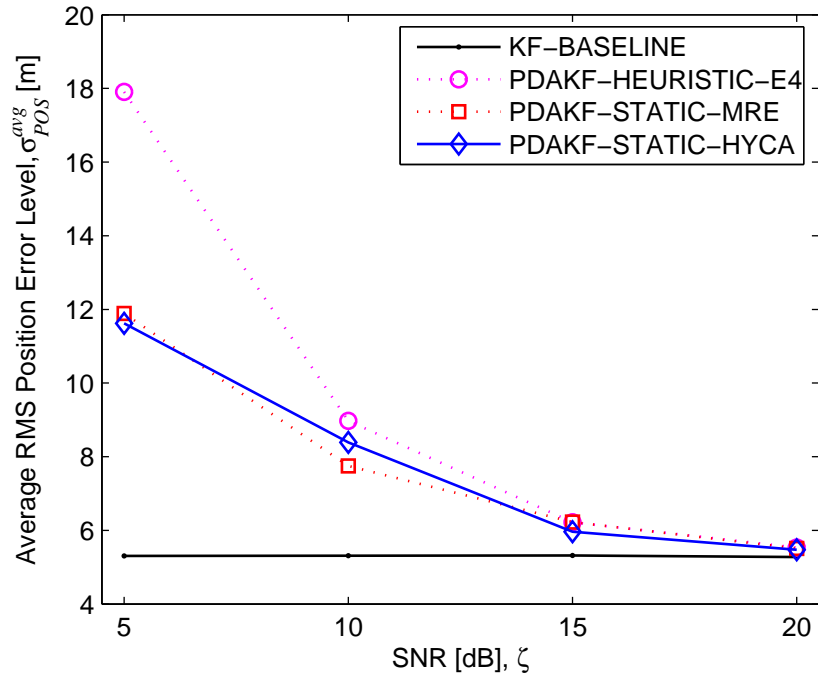
$$TLP \triangleq \frac{N_{TL}}{N_{MC}} \times 100 \quad (3.21)$$

where N_{TL} is the number of Monte Carlo runs that result in track loss and N_{MC} is the total number of Monte Carlo runs performed. TLPs for heuristic approaches are given in Fig. 3.5b. The results show clearly susceptibility of the tracking filter's performance to the selection of the operating P_{FA} value. The selection becomes more critical for low SNR values. For example in 5 dB scenario, selecting P_{FA} as 10^{-4} instead of 10^{-8} saves almost 60 percent of the tracks from being lost (Fig. 3.5b), while it provides approximately 50 percent reduction in the steady-state RMS position error (Fig. 3.5d).

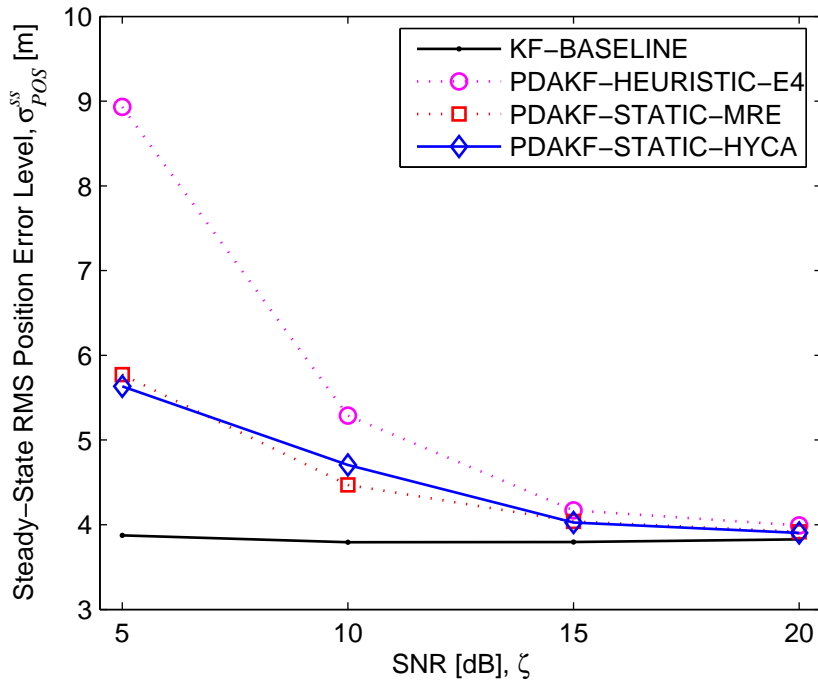
Optimizing operating P_{FA} seems to be promising. Indeed, in terms of RMS position error, both PDAKF-STATIC-MRE [5] and *PDAKF-STATIC-HYCA* perform better than the best heuristic system, PDAKF-HEURISTIC-E4. This is illustrated in Fig. 3.6 where the time-averaged and the steady-state values of the RMS position errors are plotted as a function of SNR. Note that, the improvement gained by STOP is substantial especially when the SNR is low. This is primarily due to the optimization of operating P_{FA} , which renders the extracted measurements to be more informative for downstream tracking.

The optimum operating P_{FA} values suggested by STOP schemes are shown in Fig. 3.7. STOP schemes suggest considerably higher P_{FA} values than those common for a conventional system to achieve optimal system performance. Moreover, it is observed that PDAKF-STATIC-MRE [5] suggests marginally lower P_{FA} values than the proposed scheme *PDAKF-STATIC-HYCA* and achieves still similar performance in terms of RMS position error. This is an advantage since it results in lower load for the radar processor.

If we look at the TLP measure, it is observed that statically optimized systems may not be as good as heuristic ones as illustrated in Fig. 3.8. The system PDAKF-HEURISTIC-E4 has the lowest TLP in all the scenarios considered. However, in low SNR conditions, the system with the highest TLP is also a



(a)



(b)

Figure 3.6: Experiment-I: The performance comparison of statically optimized systems and the best heuristic system in terms of (a) average and (b) steady-state, RMS position error levels.

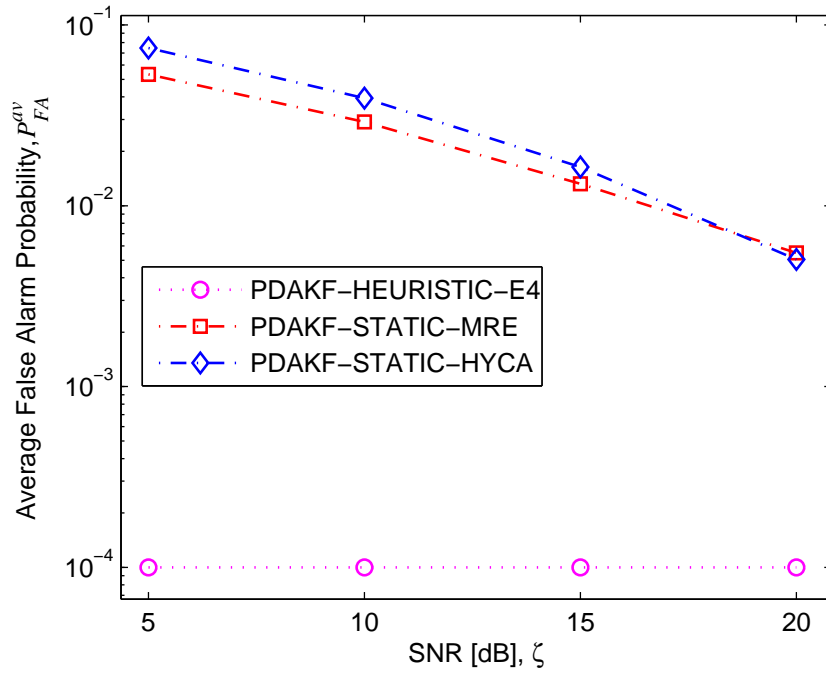


Figure 3.7: Experiment-I: The optimum operating P_{FA} values suggested by STOP schemes for different SNR values.

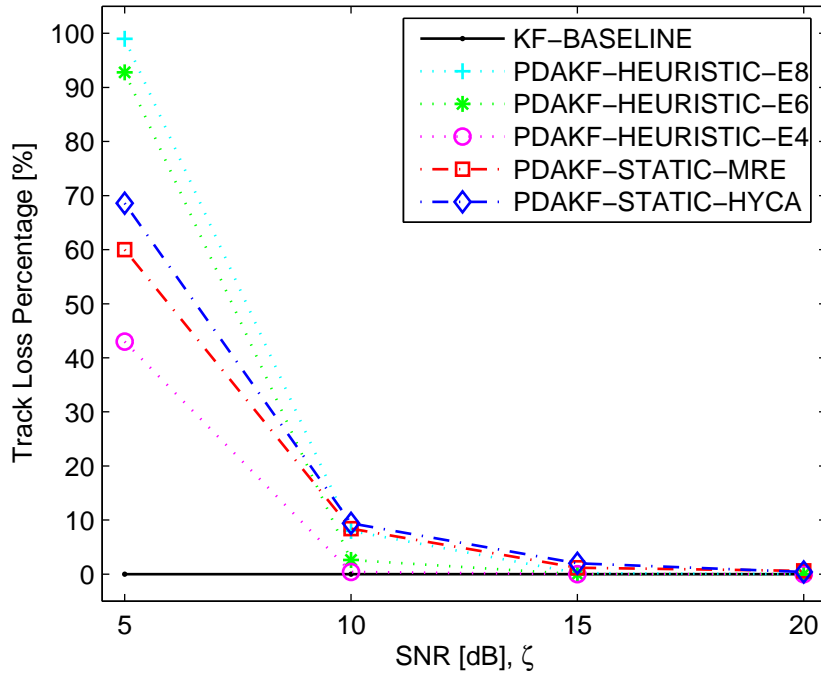


Figure 3.8: Experiment-I: The performance comparison of statically optimized and heuristic tracking systems in terms of TLP.

Table 3.3: Experiment-II: Compared tracking systems. The name of the proposed system is written in italic.

System Name	Desired False Alarm Probability
PDAKF-HEURISTIC-E4	$P_{FA}(k) = 10^{-4}$
PDAKF-STATIC-MRE [5]	$P_{FA}(k) = f_{MRE}(\zeta(k))$
<i>PDAKF-STATIC-HYCA</i>	$P_{FA}(k) = f_{HYCA}(\zeta(k))$
PDAKF-DYNAMIC-MRE [1]	$P_{FA}(k) = \arg \min_{P_{FA}} \text{tr}\{\bar{P}_{MRE}(k k)\}$

heuristic one, suggesting that it may be difficult to achieve this benefit with a heuristic setting. If we compare two tracker-aware optimization schemes, we may conclude that PDAKF-STATIC-MRE [5] performs marginally better than the proposed system *PDAKF-STATIC-HYCA* in terms of TLP.

We conclude that, as compared to heuristics, the systems PDAKF-STATIC-MRE [5] and *PDAKF-STATIC-HYCA*, which are optimized for minimizing the steady-state RMS position error, indeed perform better in terms of average and steady-state RMS position error criteria. On the other hand, they show suboptimal behavior in terms of TLP, suggesting that an optimization which also considers the transient behavior is necessary. As shown by the following experiments, this can be achieved by dynamic threshold optimization (DTOP) schemes, which perform the optimization at every time step, i.e., online.

3.3.3 Experiment2: Comparison of STOP with the MRE-Based DTOP

In this experiment, we compare STOP schemes with the MRE-based DTOP scheme presented in [1]. The HYCA-based DTOP which is a proposal of the present study will be presented in the next experiment.

We compare four tracking systems given in Table 3.3. The first system is the heuristic system which shows the best TLP in the previous experiment. All the other systems utilize TA detectors. Among them, the second and the third

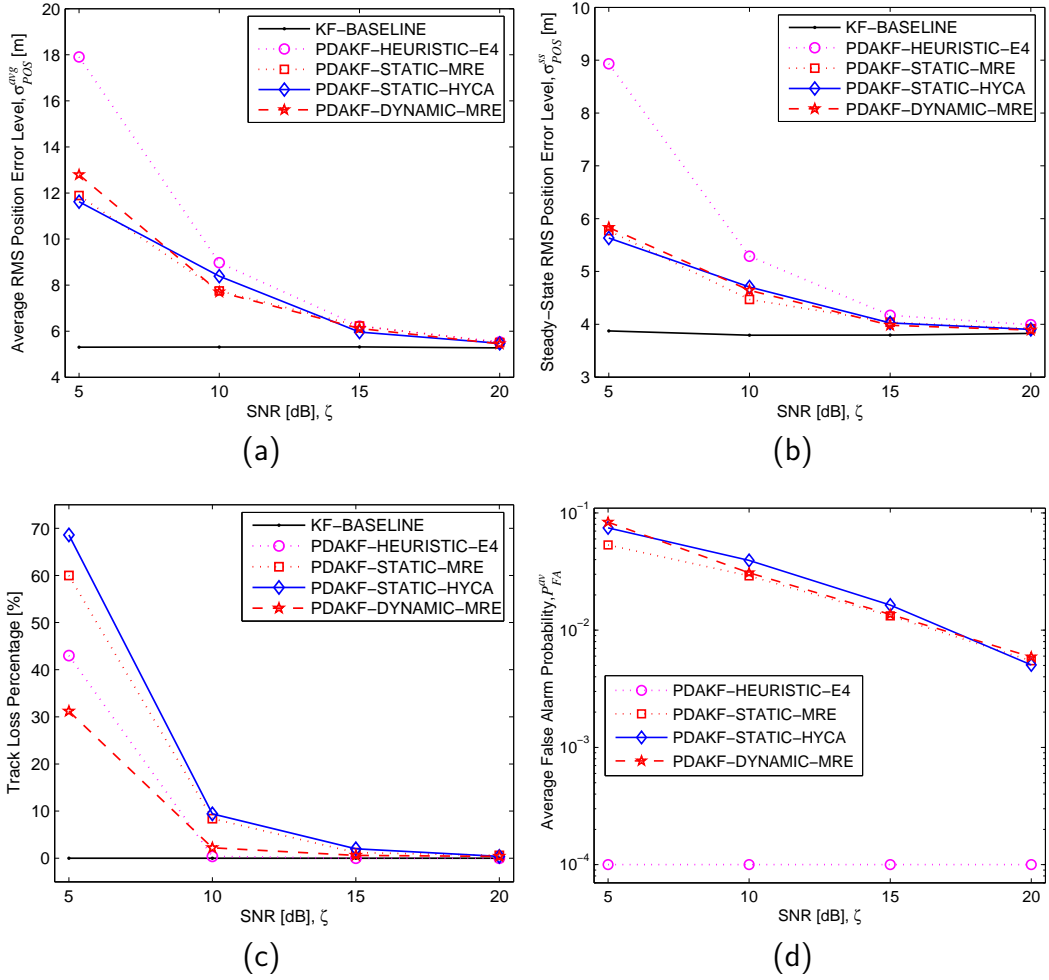


Figure 3.9: Experiment-II: Performance comparison of STOP schemes with the MRE-based DTOP scheme presented in [1] in terms of (a) average (b) steady-state, RMS position error levels and (c) TLP. The average operating P_{FA} values suggested by the optimization schemes are also shown in (d).

one are statically optimized while the last one is dynamically optimized at each time step. The dynamic optimization is solved using Fibonacci Search where we take the initial interval of uncertainty for P_{FA} as $\mathcal{I}_{P_{FA}} \triangleq [10^{-6}, 10^{-1}]$ and the maximum error tolerance⁶ as $\Delta P_{FA} \triangleq 10^{-7}$.

We consider the same set of SNR scenarios given in the previous experiment and perform 500 Monte Carlo runs for each scenario. The results are given in Fig. 3.9. The dynamic approach, PDAKF-DYNAMIC-MRE [1] outperforms the heuristic one and have a similar performance with STOP schemes in terms of RMS position estimation error. Moreover, PDAKF-DYNAMIC-MRE [1] is the best one when TLPs are considered (Fig. 3.9c). This is a powerful aspect of DTOP schemes where the online feedback from the tracker to the detector provides considerable performance improvement in terms of track loss. This transient benefit is achieved while a good RMS position estimation error performance is maintained.

If we consider the optimum operating P_{FA} values suggested by the algorithms, it is observed that the dynamic approach lies between two STOP schemes on the average (see Fig. 3.9d). This means that PDAKF-DYNAMIC-MRE [1] brings moderate processor load in terms of false alarms. However, the actual computational power is needed prior to detection, i.e, in finding the optimum desired P_{FA} value. Indeed, an important aspect of practical applicability of DTOP schemes is their computational complexities. The dynamic approach PDAKF-DYNAMIC-MRE [1] is computationally much more expensive than STOP approaches. This is mainly due to the iterative line search algorithm involved. In a recent study [56], we have presented a step towards alleviating this difficulty where the MRE-based DTOP problem is solved by means of a

⁶ Given an initial interval of uncertainty, $[a, b]$ and the number of function evaluations, N , the Fibonacci Search algorithm reduces the length of the uncertainty interval to $(b - a)/F_N$, where F_N is the $(N + 1)$ th number in the Fibonacci sequence $\{F_n\}$, $n \in \mathbb{N}$. Therefore, given number N , the length of the final uncertainty interval, so the maximum error in finding the extremum point, is determined. Here, we do the other way around. That is, we specify the maximum error tolerance that we are required to have at the end of the algorithm which in turn determines the minimum required number of function evaluations, N .

Table 3.4: Experiment-III: Compared tracking systems. The system whose name is written in *italic* is proposed in this study.

System Name	Desired False Alarm Probability
PDAKF-DYNAMIC-MRE [1]	$P_{FA}(k) = \arg \min_{P_{FA}} \text{tr}\{\bar{P}_{MRE}(k k)\}$
<i>PDAKF-DYNAMIC-HYCA</i>	$P_{FA}(k) = \arg \min_{P_{FA}} \text{tr}\{\bar{P}_{HYCA}(k k)\}$

closed-form approximation for a special NP detector case (DYNAMIC-MRE-CF [56]). This solution is presented in detail in the next chapter.

3.3.4 Experiment3: Comparison of DTOP Schemes

In this experiment, we compare two DTOP schemes based on MRE and HYCA methodologies, the latter one being a formulation and proposal of the present study. We compare the tracking systems given in Table 3.4 under the same SNR scenarios considered in the previous experiments.

For both approaches, the optimization problem is solved using Fibonacci Search method whose parameters $\mathcal{I}_{P_{FA}}$ and ΔP_{FA} are taken as the same with the previous experiment. We have performed 500 Monte Carlo runs in each scenario. As an example, for 10 dB scenario, ensemble averaged (track loss cases excluded) RMS position error plots are shown in Fig. 3.10. Note that in terms of RMS position error, both dynamic optimization schemes have better transient characteristic as compared to static ones. This is an important aspect of DTOP schemes and leads to improved *track loss performance*.

If we examine the optimum P_{FA} sequences given in Fig. 3.11, it is observed that in the steady-state, the optimum P_{FA} values suggested by DTOP schemes get closer to the those of STOP schemes. In this respect, STOP schemes can be regarded as the steady-state versions of their dynamic counterparts. This is a very close analogy to having a dynamic gain versus static one in Kalman and $\alpha-\beta$ filters, respectively. Remember that these gains are obtained from either the current or the steady-state output (i.e., the solution) of the

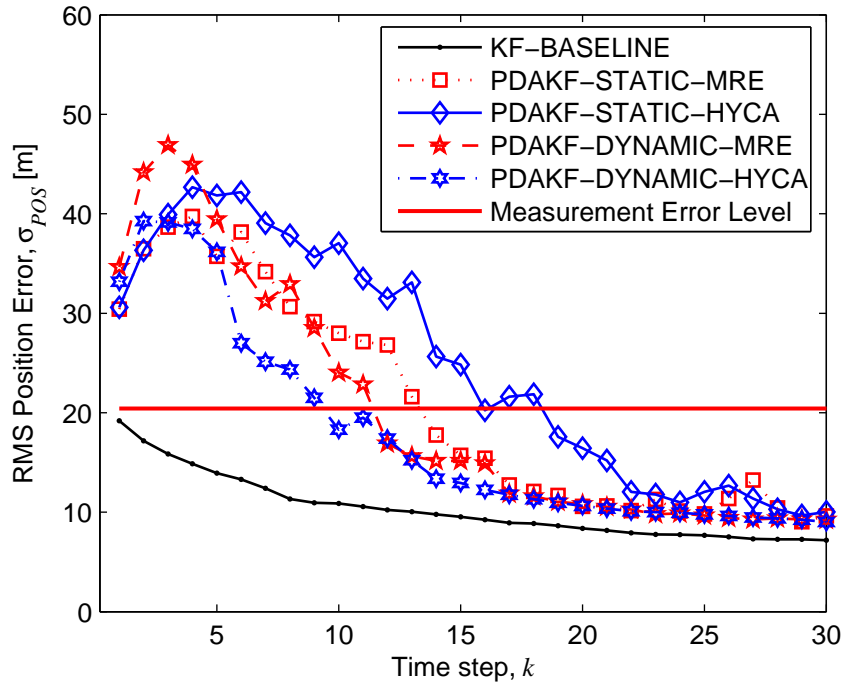


Figure 3.10: Experiment-III: The transient RMS position error levels for 10 dB scenario.

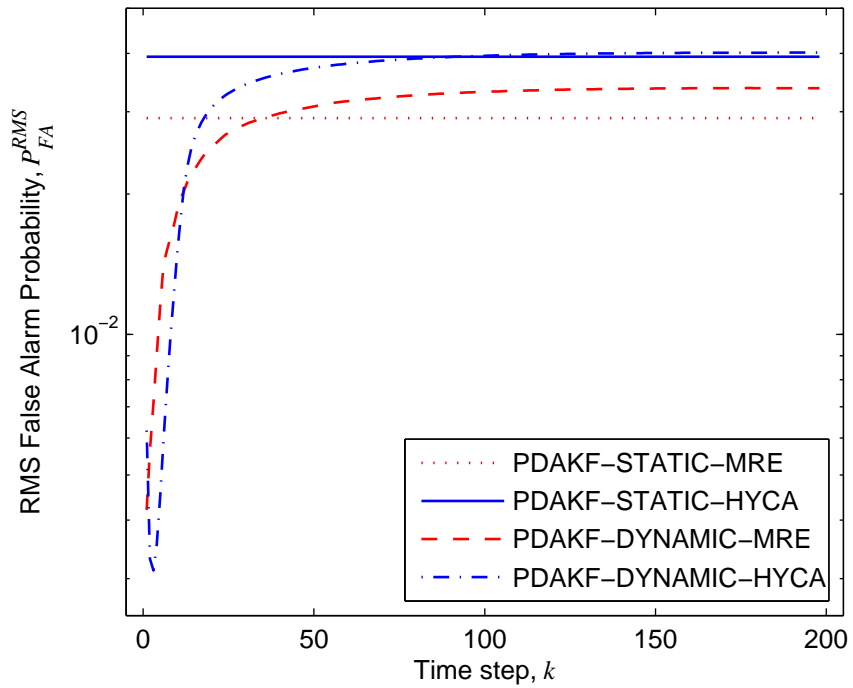


Figure 3.11: Experiment-III: The optimum operating P_{FA} values of the TA-DETOP schemes for $\zeta = 10$ dB scenario.

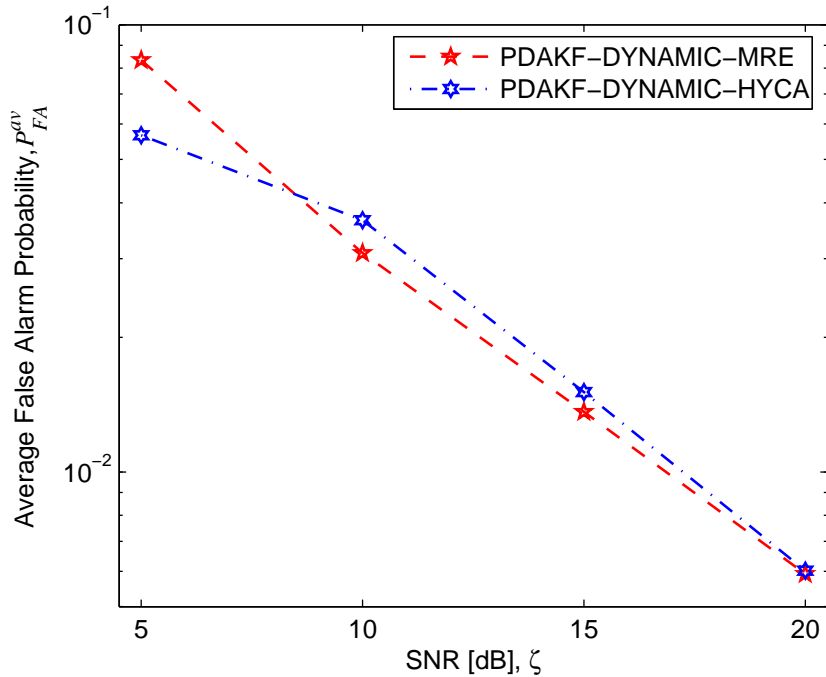


Figure 3.12: Experiment-III: The average P_{FA} values suggested by the DTOP schemes as a function of SNR. Except for the lowest SNR case, HYCA based method suggests marginally higher P_{FA} values on the average (over transient and steady-state regions).

standard Riccati recursion. Here, in the case of threshold optimization, the optimum P_{FA} values are obtained from either the current or the steady-state output of the NSPP recursions (MRE or HYCA). In the transient region, *PDAKF-DYNAMIC-HYCA* suggests lower P_{FA} values than those suggested by *PDAKF-DYNAMIC-MRE* [1], while in the steady-state the situation is reversed (see Fig. 3.11). This is a consistent behavior that we have observed in all scenarios.

The variation of the average operating P_{FA} values suggested by the algorithms over the considered SNR range is shown in Fig. 3.12. Note that for the lowest SNR case, *PDAKF-DYNAMIC-HYCA* suggests a lower P_{FA} value than *PDAKF-DYNAMIC-MRE* [1] and still achieves a lower steady-state RMS position error value (see Fig. 3.13a). This is an advantage in terms of keeping the number of false tracks low which may be very critical in low SNR conditions. The cost paid for this achievement is having marginally higher TLP as shown

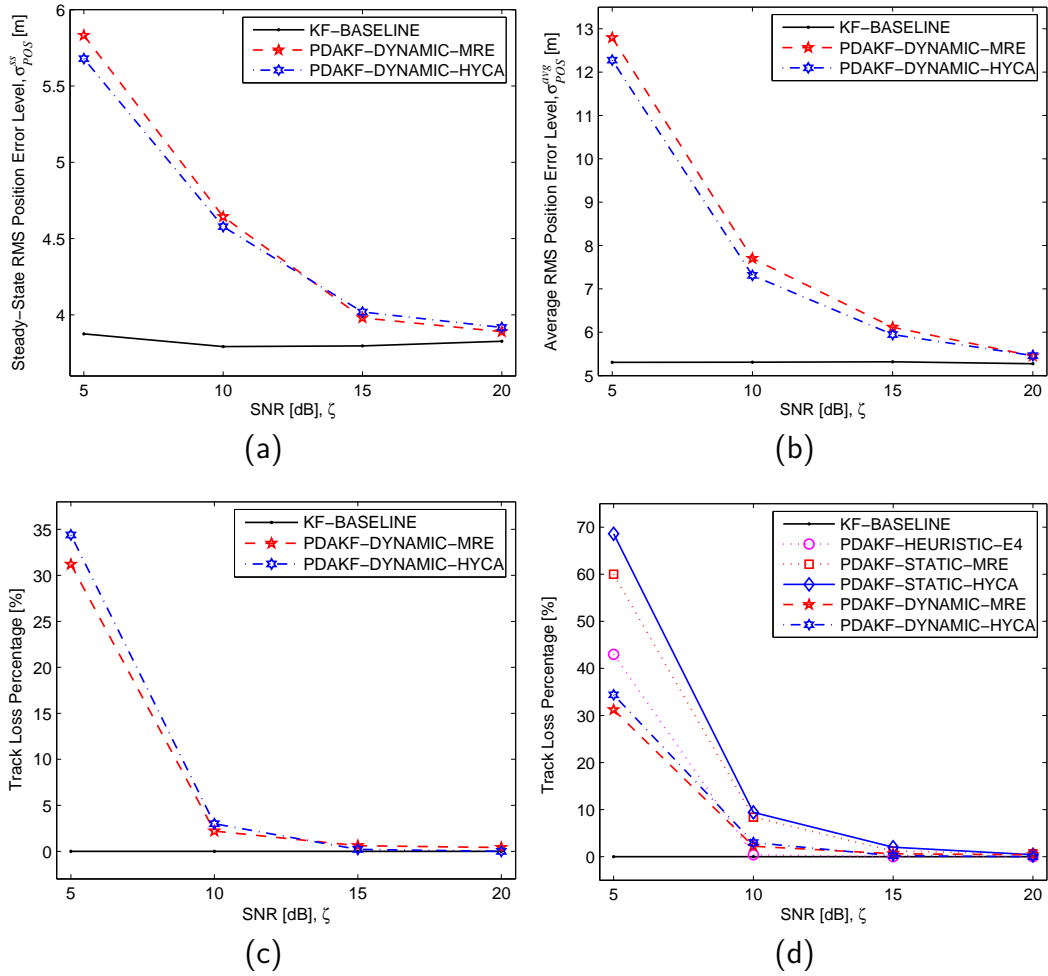


Figure 3.13: Experiment-III: Performance comparison of DTOP schemes in terms of RMS position error and TLP. Note that the plots given in (a) and (c) represent the trade-off between achieving a low steady-state RMS position error level versus having a low TLP.

in Fig. 3.13c. This trade-off is observed for all SNR scenarios and can be seen from examining (a) and (c) parts of the Fig. 3.13. Note also from Fig. 3.13d that, both DTOP approaches are significantly lower TLP values than their statically optimized counterparts and the best heuristic system of the first experiment. This figure clearly shows the robustness of the dynamically optimized systems against track loss.

We were initially motivated to formulate the static and dynamic optimization methods based on HYCA due to its promise in modeling and therefore improving transient behavior of the overall system better than MRE. In practice, we could not observe this improvement to the extent hoped for. Formulating and solving the detector threshold optimization (DETOP) problem based on either MRE or HYCA does not result in a big difference in system performance. However, these methods are not only important because they promise to provide a performance improvement but rather, their formulation and experimental evaluation complete a broad and rigorous evaluation of a family of closely related methods (see Fig. 1.2).

3.3.5 Combining the Results

As a highlight of this chapter, in this section, we combine the results of all the experiments in one plot for each SNR scenario. The axes of this plot are chosen as the steady-state RMS position error and TLP which can be seen as the steady-state and the transient performance measures, respectively. This is motivated by seeing and showing the trade-off between these measures more clearly, although we have already emphasized this trade-off in the experimental results.

The plots corresponding to each SNR scenario are given in Fig. 3.14. In these plots, the lower left corner represents the ultimate performance, i.e., low TLP and low steady-state RMS position error. Note that the points (algorithm

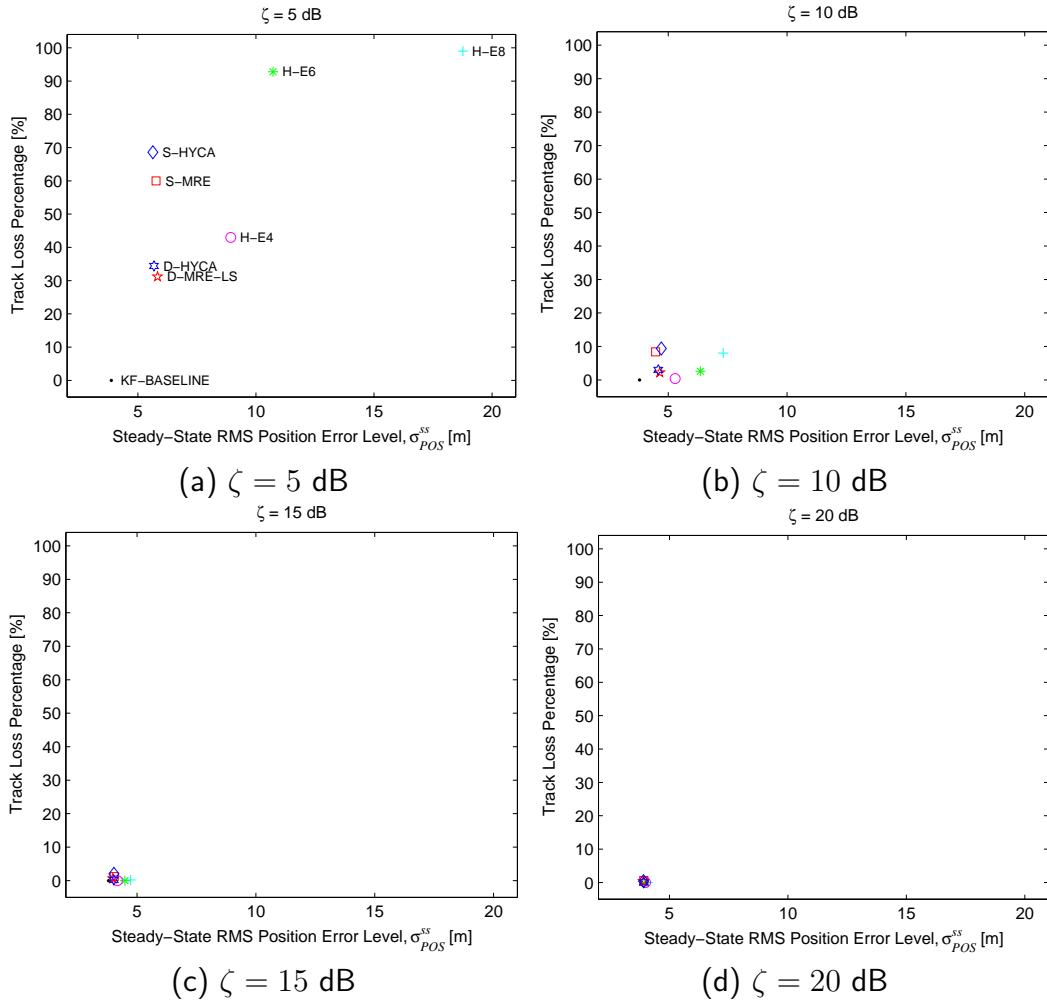


Figure 3.14: Algorithms on the performance plane: The steady-state RMS position error versus TLP. Here, the prefixes “H”, “S” and “D” correspond to “heuristic”, “static” and “dynamic” approaches, respectively. Note that, as SNR increases, the performance of the algorithms gets closer to each other and to the the best achievable performance point, the Kalman filter with perfect data association.

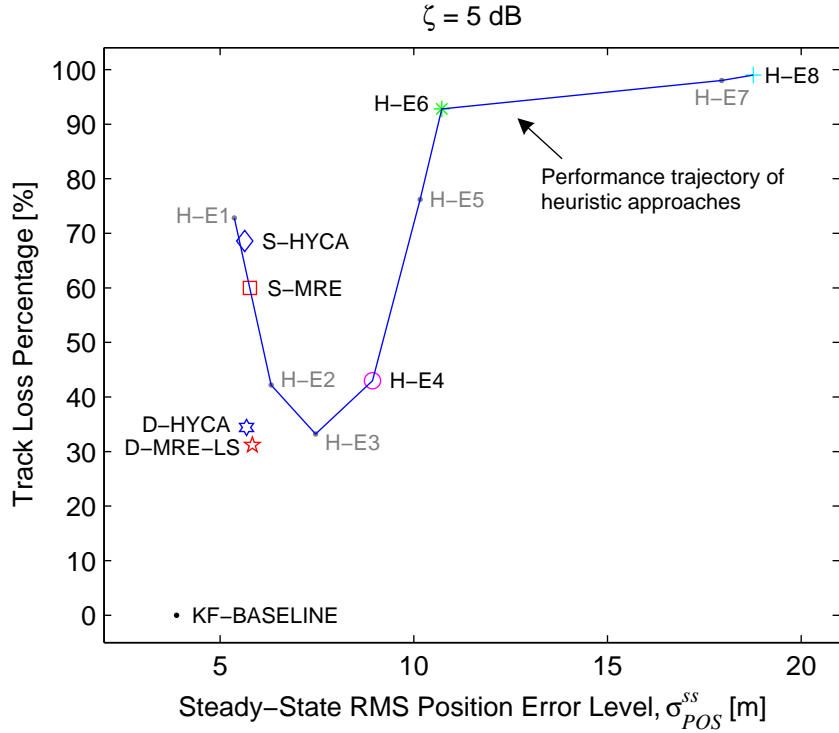


Figure 3.15: The performance of the algorithms in 5 dB case. At some portions of the performance trajectory of heuristic approaches, there are sharp bends, resulting in a significant change in the performance. Therefore, in general one can not guarantee a reliable performance with an heuristic approach.

performances) get closer and eventually converge to the performance of the Kalman filter with perfect data association, when SNR increases. We may conclude that threshold optimization is less critical when the SNR is high, e.g., between 15 and 20 dB. On the other hand, in the lowest SNR scenario, threshold optimization greatly improves the performance. This is obvious from Fig. 3.15 where algorithm performances are well-separated from each other. The superiority of the DTOP schemes is clearly seen from this figure. In fact, they are the only algorithms whose performances are located nearly at the lower left corner of the trade-off plane. Although the static schemes have low steady-state RMS position error level, they may not provide low TLP as shown in the figure.

Note that performance of heuristic approaches can vary widely. Looking at the performance trajectory of heuristic algorithms, it can be seen that DTOP schemes are better than the most successful point in this trajectory. This shows

clearly the power of dynamic threshold optimization. It is observed that STOP schemes correspond to approximately the points on the performance trajectory where the steady-state position error is minimized. But of course, this does not mean that they are the best points in this trajectory, as they can not provide low TLP. In fact, from the practical point of view, the track loss measure is more critical than the steady-state position error measure. So in that respect, DTOP schemes seem to be the only choice in practice.

3.4 Conclusion

By considering both STOP and DTOP schemes in a unified and rigorous simulation based experimental framework, in this chapter, we observed the trade-off between having low steady-state RMS position estimation error vs. having low TLP. DTOP schemes are found to be well-located on this trade-off plane by providing considerably low TLP and low level of steady-state estimation error. The disadvantages of these schemes are their computational complexities.

Apart from a comprehensive experimental survey, a primary contribution of this chapter is the proposal of the static and dynamic threshold optimization schemes based on the HYCA approach which is itself a NNSP technique for the PDAF. Contrary to expectations, the results concluded that only marginal gains can be achieved by HYCA-based approaches as compared to MRE-based ones. However, their formulation and evaluation completes a rigorous evaluation of a closely related family of techniques. To the best of author's knowledge, such a comparative study on threshold optimization schemes has not been done before in the literature.

CHAPTER 4

A CLOSED-FORM SOLUTION FOR THE MRE-BASED DYNAMIC THRESHOLD OPTIMIZATION PROBLEM

As mentioned in the Introduction Chapter, traditionally, the radar data processing chain is usually viewed as a concatenation of two subsystems: Signal processing and information processing. A promising line of research attempts to bridge the gap between these two subsystems by means of considering jointly optimal parameter settings for both of them. In the previous chapter, we have presented and proposed a number of frameworks which fulfill this promise by considering *static* and *dynamic* threshold optimization schemes. The experimental results show that there exists a trade-off between having low steady-state estimation error versus having low track loss percentage (TLP), and the dynamic threshold optimization (DTOP) schemes are found to be well-located on this trade-off plane by providing considerably low TLP and acceptable level of steady-state estimation error.

The primary disadvantage of the dynamic schemes, as compared to static ones, may be their *online* computational requirements. Although, in both dynamic and static schemes, the underlying optimization problem is one dimensional, the dynamic schemes are supposed to make this optimization in *real time*. Therefore, computationally cheaper approaches are preferred. Along this line, in this chapter, we consider one of the dynamic optimization schemes based

on the modified Riccati Equation (MRE) and bring a closed-form solution to the problem. Proposed closed-form solution is approximate but of course, computationally much more efficient than solving the same problem using an iterative optimization algorithm. We will demonstrate this efficiency quantitatively through the experimental results at the end of the chapter. But first, we begin with an introduction which summarizes the literature development of the MRE-based dynamic scheme that we will consider.

4.1 Introduction

Along the line of joint optimization of radar detector and tracker, the pioneering study is the work of Fortmann et al. [5] where for the first time they established a feedback from the information processing subsystem to the signal processing subsystem. The primary motivation in [5] is to find a *deterministic* recursion for the covariance of the probabilistic data association filter (PDAF) [45], similar to the one for the Kalman filter, which is nothing but the standard Riccati equation (SRE). It turns out that the end product, the *modified Riccati equation* (MRE), differs from the SRE only by a scalar variable [5], called the *information reduction factor* (IRF) [4]. This scalar depends explicitly on the probability of false alarm (P_{FA}) and the probability of detection (P_D). Using this dependence, the authors of [5] have introduced a graphical technique (i.e., TOC-curve approach mentioned in the previous chapter) for optimization of the detector thresholds in linear *time-invariant* systems. In this static threshold optimization (STOP) scheme, which is based on iterating the MRE to its steady-state, for a possible range of signal-to-noise ratio (SNR) values, the optimum detector operating points can be found and tabulated offline, and then used when necessary in an online application with varying SNR conditions.

When the steady-state analysis is inappropriate, such as in time-varying or nonlinear systems, a suggested solution is to apply the same methodology by iterating the MRE not to its steady-state but for n steps into the future [5].

In the case of $n = 1$, this leads to a *dynamic*¹ *threshold optimization* (DTOP) scheme.

In [1], Gelfand et al. have proposed two DTOP problems, namely, *prior* and *posterior* threshold optimization which minimize the mean-square state estimation error over detection thresholds, based on the measurements up to the previous and current time step, respectively. It was shown that for the *prior* case, the problem reduces into a single line search which maximizes the IRF [1]. Due to claimed mathematical intractability of obtaining a full closed-form solution, in [1], this problem was solved using iterative numerical optimization techniques, such as Golden Section and Fibonacci Search methods [66].

In this chapter, we consider the *prior* threshold optimization problem proposed in [1] for a special case of Neyman-Pearson (NP) detector. For this detector, we propose a computationally much more efficient alternative solution, based on the functional approximation presented in [62]. We show that this approximate closed-form solution leads to considerable simplification in computational complexity without any noticeable loss in performance. This increases the feasibility of the approach for an online application. Moreover, an analysis made on the proposed closed-form expression reveals that it possess a dynamic criterion on the operating SNR for switching the whole system to the *track before detect* (TBD) mode [67], [68]. These constitute the primary contributions of the present chapter. An early and short version of this work has been discussed in [56].

The chapter is organized as follows: In Section 4.2, we give a brief review of the MRE formulation [5]. In Section 4.3, the formulation of the problem and the proposed closed form solution for an NP detector are given. We present our simulation results in Section 4.5, and finally the concluding remarks are given in Section 5.4.

¹ It is also called *adaptive* [1]

4.2 The Modified Riccati Equation (MRE)

Consider a discrete-time linear time-invariant dynamic system, described by the plant and measurement equations

$$x(k+1) = Fx(k) + Gv(k), \quad k = 0, 1, \dots, \quad (4.1)$$

$$z(k) = Hx(k) + w(k), \quad k = 1, 2, \dots, \quad (4.2)$$

where $x(k)$ and $z(k)$ are the state and measurement vectors whose dimensions are n_x and n_z , respectively. The sequences $\{v(k)\}$ and $\{w(k)\}$, known as process and measurement noises, respectively are assumed to be white, stationary and distributed as $v(k) \sim \mathcal{N}(0, Q)$ and $w(k) \sim \mathcal{N}(0, R)$ for all k . The initial state $x(0)$ is modeled as $x(0) \sim \mathcal{N}(\hat{x}(0|0), P(0|0))$ where the mean $\hat{x}(0|0)$ and the covariance $P(0|0)$ are assumed to be known. Furthermore, two noise sequences $\{v(k)\}$ and $\{w(k)\}$ and the initial state $x(0)$ are assumed to be *mutually independent* for all k .

Under these assumptions, at each time step k , the optimal MMSE estimate of the state $x(k)$, which is defined by [16]:

$$\hat{x}(k|k) = \hat{x}^{MMSE}(k|k) \triangleq \mathbb{E}[x(k)|Z^k] \quad (4.3)$$

with $Z^k \triangleq \{z(1), z(2), \dots, z(k)\}$, can be recursively obtained by the Kalman filter. In the Kalman filter, the covariance corresponding to (4.3), which is defined by

$$P(k|k) \triangleq \mathbb{E}\left[(x(k) - \hat{x}(k|k))(x(k) - \hat{x}(k|k))^T \middle| Z^k\right], \quad (4.4)$$

can also be recursively obtained from the covariance prediction and update equations of the form

$$P(k|k-1) = FP(k-1|k-1)F^T + GQG^T, \quad (4.5)$$

$$P(k|k) = P(k|k-1) - W(k)S(k)W^T(k) \quad (4.6)$$

where $P(k|k-1)$ is the state prediction covariance, and

$$W(k) = P(k|k-1)H^T S^{-1}(k) \quad \text{and} \quad (4.7)$$

$$S(k) = HP(k|k-1)H^T + R \quad (4.8)$$

are called the Kalman gain and innovation covariance, respectively. The equations (4.5)–(4.8) constitute a recursion in $P(k|k-1)$ in the form of a (matrix) Riccati equation whose solution can be obtained uniquely (and even in a non-recursive form [61]) under some *controllability* and *observability* conditions [18]. An important and interesting property is that this recursion is *measurement-independent*. In other words, given only the description of the dynamical system and measurement model, we can have an idea about the filter performance without running the filter. This property allows us to make a non-simulation performance prediction (NSPP) for the Kalman filter in clutter-free environments.

The situation is more complicated in cluttered environments. In this case, the filter performance depends not only on the noise covariances, but also on the uncertainty in the measurement origin [5], which is usually described by the detection parameters, P_{FA} and P_D . Under these situations the covariance calculation of the filter is measurement-dependent, hence stochastic.

Obtaining a deterministic (measurement-independent) recursion for the covariance of the filter is the key to make a NSPP for the filter under concern. Along this line, the first attempt was made in [5] for the PDAF whose covariance recursion is stochastic due to its measurement-dependent covariance update equation [4]:

$$P(k|k) = P(k|k-1) - (1 - \beta_0(k)) W(k) S(k) W^T(k) + \tilde{P}(k) \quad (4.9)$$

where the measurement-dependent terms are $\tilde{P}(k)$ and $\beta_0(k)$. To be able to obtain a deterministic recursion, in [5], these terms were replaced with their

conditional expectations,

$$\bar{P}(k) \triangleq \mathbb{E}[\tilde{P}(k)|Z^{k-1}], \quad (4.10)$$

$$\bar{\beta}_0(k) \triangleq \mathbb{E}[\beta_0(k)|Z^{k-1}], \quad (4.11)$$

over both the locations and the number of measurements where Z^{k-1} is the cumulative set of validated measurements through the time step $k - 1$. The new covariance update equation, after some approximations, becomes [5]

$$\bar{P}(k|k) \triangleq \mathbb{E}[P(k|k)|Z^{k-1}] \approx P(k|k-1) - q_2(k)W(k)S(k)W^T(k) \quad (4.12)$$

where $\bar{P}(k|k)$ is a deterministic approximation of $P(k|k)$ in which the stochastic terms are averaged out according to (4.10) and (4.11), and $q_2(k)$ is a time-varying scalar taking the values between 0 and 1. Furthermore, replacing the covariance prediction of the PDAF with

$$\bar{P}(k|k-1) = F\bar{P}(k-1|k-1)F^T + GQG^T, \quad (4.13)$$

and combining with (4.12) yields a deterministic recursion for the covariance as

$$\begin{aligned} \bar{P}(k+1|k) = & F \left[\bar{P}(k|k-1) - q_2(k)\bar{P}(k|k-1)H^T \left(H\bar{P}(k|k-1)H^T + R \right)^{-1} \right. \\ & \left. \times H\bar{P}(k|k-1) \right] F^T + GQG^T \end{aligned} \quad (4.14)$$

with $\bar{P}(0|-1) \triangleq FP(0|0)F^T + GQG^T$. This is the *modified Riccati equation* (MRE) [5]. The only modification from the standard Riccati is the time-varying scalar $q_2(k)$ which is called the *information reduction factor* (IRF) [4]. The functional form of the IRF is given as [5]

$$\begin{aligned} q_2(P_{FAN_C}(k), P_D) \triangleq & \frac{P_D c_{n_z}}{(2\pi)^{n_z/2}} \sum_{m_k=1}^{\infty} \mu_F(m_k - 1, P_{FAN_C}(k)) \left(\frac{n_z}{g^{n_z}} \right)^{m_k-1} \\ & \times I_2(P_{FAN_C}(k), P_D, m_k) \end{aligned} \quad (4.15)$$

with

$$I_2(P_{FAN_C}(k), P_D, m_k) \triangleq \int_0^g \cdots \int_0^g \frac{\exp(-r_1^2)r_1^2}{b(P_{FAN_C}(k), P_D) + \sum_{j=1}^{m_k} \exp(-r_j^2/2)} \times (r_1 r_2 \cdots r_{m_k})^{n_z-1} dr_1 dr_2 \cdots dr_{m_k} \quad (4.16)$$

$$b(P_{FAN_C}(k), P_D) \triangleq (2\pi)^{n_z/2} \frac{P_{FAN_C}(k) (1 - P_D P_G)}{c_{n_z} g^{n_z} P_D} \quad (4.17)$$

where $c_{n_z} \triangleq \pi^{n_z/2} / \Gamma(n_z/2 + 1)$, with $\Gamma(\cdot)$ being gamma function, is the volume of the n_z -dimensional unit hypersphere ($c_1 = 2, c_2 = \pi, c_3 = 4\pi/3$, etc.) and

$$\mu_F(m_F, \lambda_F) \triangleq \frac{\exp(-\lambda_F) (\lambda_F)^{m_F}}{m_F!} \quad (4.18)$$

is the Poisson probability mass function (pmf) for the number of false measurements (m_F) with mean λ_F . Furthermore,

$$N_C(k) \triangleq \frac{\bar{V}(k)}{V_C} \quad (4.19)$$

is the number of resolution cells enclosed by the validation gate at time step k where

$$\bar{V}(k) \triangleq c_{n_z} g^{n_z} |\bar{S}(k)|^{1/2} \quad (4.20)$$

is the *offline-calculated*² gate volume, V_C is the *resolution (or detection) cell volume* and $g \triangleq \sqrt{\gamma_G}$ is the *gate size*.³

4.3 Problem Formulation and Solution

Our aim is to set optimally the operating P_{FA} value of a detector, which is concatenated with a PDAF, so that the performance of the overall target tracking system is maximized. This problem was first investigated and solved in [5] using a *static* optimization scheme. As an extension to this work, in [1], Gelfand et al. attacked the same problem in the DTOP domain. The authors

² This is based on the offline-calculated innovation covariance defined by $\bar{S}(k) \triangleq H\bar{P}(k|k-1)H^T + R$.

³ This is linked to the *gate probability* P_G via chi-square tables where P_G is defined as the probability that the correct measurement falls inside the validation gate given that it is detected.

of [1] formulated and solved the problem in two versions, namely, *prior* and *posterior* threshold optimization. In the following sections, we reconsider the *prior* threshold optimization case and bring an alternative solution to the problem.

4.3.1 Prior Detection Threshold Optimization

This problem was first formulated in [1]. We redefine the same problem with a minor change in the notation as follows. Our aim is to find an optimum operating $P_{FA}^*(k)$ value such that

$$P_{FA}^*(k) = \arg \min_{P_{FA}} \left\{ \mathbb{E} \left[\|x(k) - \hat{x}(k|k)\|^2 \middle| Z^{k-1} \right] \right\}, \quad \text{subject to}$$

$$P_D = f_{ROC}(P_{FA}, \zeta) \quad \text{and} \quad 0 \leq P_{FA} \leq 1 \quad (4.21)$$

where $\hat{x}(k|k)$ is the state estimated by a PDAF at time step k and Z^{k-1} is the cumulative set of validated measurements up to $k-1$ (i.e., *prior* to k).⁴ The equality constraint of the optimization problem is nothing but the receiver operating characteristic (ROC) curve which links P_D to P_{FA} , or vice-versa, through current SNR value (ζ), and the inequality constraint ensures that the resultant operating false alarm value is a valid probability. This optimization problem can be restated in another equivalent but more useful form [1]. For the sake of clarity, we emphasize this important result as a separate lemma.

Lemma 4.1 *The optimization problem given in (4.21) is equivalent to,*

$$P_{FA}^*(k) = \arg \max_{P_{FA}} q_2(P_{FAN_C}(k), P_D), \quad \text{subject to}$$

$$P_D = f_{ROC}(P_{FA}, \zeta) \quad \text{and} \quad 0 \leq P_{FA} \leq 1 \quad (4.22)$$

where $q_2(P_{FAN_C}(k), P_D)$ is the IRF given in (4.15).

⁴ In the *posterior* threshold optimization, the conditioning is made on Z^k [1]. In other words, in the *posterior* case we optimize the detector thresholds based on the measurements which will be produced by these thresholds. This is a noncausal operation and therefore the use of *posterior* threshold optimization is not feasible in practice. However, it can still be simulated and constitutes an upper bound for the best performance that can be obtained by detection threshold optimization [1].

Proof The cost function $\mathcal{J}(k, P_{FA}) \triangleq \mathbb{E}[\|x(k) - \hat{x}(k|k)\|^2 | Z^{k-1}]$, given in (4.21), can be rewritten as

$$\begin{aligned}
\mathcal{J}(k, P_{FA}) &= \mathbb{E} \left[\text{tr} \left\{ \|x(k) - \hat{x}(k|k)\|^2 \right\} \middle| Z^{k-1} \right] \\
&= \mathbb{E} \left[\text{tr} \left\{ (x(k) - \hat{x}(k|k))^T (x(k) - \hat{x}(k|k)) \right\} \middle| Z^{k-1} \right] \\
&= \mathbb{E} \left[\text{tr} \left\{ (x(k) - \hat{x}(k|k)) (x(k) - \hat{x}(k|k))^T \right\} \middle| Z^{k-1} \right] \\
&= \text{tr} \left\{ \mathbb{E} \left[(x(k) - \hat{x}(k|k)) (x(k) - \hat{x}(k|k))^T \middle| Z^{k-1} \right] \right\} \\
&= \text{tr} \left\{ \mathbb{E} \left[\mathbb{E} \left[(x(k) - \hat{x}(k|k)) (x(k) - \hat{x}(k|k))^T \middle| Z^k \right] \middle| Z^{k-1} \right] \right\} \\
&= \text{tr} \{ \mathbb{E}[P(k|k) | Z^{k-1}] \} \\
&= \text{tr} \{ \bar{P}(k|k) \} \\
&= \text{tr} \{ P(k|k-1) \} - q_2(P_{FAN_C}(k), P_D) \text{tr} \{ W(k)S(k)W^T(k) \}
\end{aligned}$$

where the first equality is due to the property that the trace of a scalar is itself, the third one is due the property that $\text{tr}\{AB\} = \text{tr}\{BA\}$, the fourth one is due to linearity of $\text{tr}\{\cdot\}$ and $\mathbb{E}[\cdot]$ operators and the fifth one follows from the *smoothing property*⁵ of expectations. Note that $W(k)S(k)W^T(k) \geq 0$ implies $\text{tr} \{ W(k)S(k)W^T(k) \} \geq 0$ and $q_2(P_{FAN_C}(k), P_D)$ is the only term that depends on P_{FA} . Hence the minimization of $\mathcal{J}(k, P_{FA})$ can be achieved by maximizing $q_2(P_{FAN_C}(k), P_D)$ over P_{FA} , which completes the proof. \square

Remark 4.1 Note that the prior threshold optimization problem given in (4.21) (and hence in (4.22)) is a line search. Furthermore, the above proof clearly shows that it is a special case of DTOP problem defined in (3.3) with the choices of $f_S[\cdot] \triangleq \text{tr}\{\cdot\}$ and $\bar{P}_{NSPP}(k|k) \triangleq \bar{P}(k|k)$, i.e., the output of the MRE algorithm at time step k .

The functional form of $q_2(P_{FAN_C}(k), P_D)$, which is given in (4.15), is mathematically intractable to take derivative over P_{FA} , however, it can be evaluated

⁵ The smoothing property of expectations states that the expected value of a conditional expected value is the unconditional expected value [18]. That is to say, $\mathbb{E}[\mathbb{E}[x|y]] = \mathbb{E}[x]$ where an additional conditioning in the outer expectation is also permissible.

numerically at any point of interest. Therefore any line search algorithm that requires only the values of the function to be maximized, such as, Golden-Section or Fibonacci Search methods [66], can be applied to this problem. Provided that the cost function is *unimodal*,⁶ these algorithms converge to the global optimum. Arguing along these lines, the problem is solved in [1] using line search algorithms.

In the present work, we adopt a different approach. Instead of using iterative solution algorithms, we attempt to obtain an approximate closed-form solution by using a functional approximation proposed in [62].

4.3.2 A Functional Approximation to the IRF

Although the functional form of $q_2(P_{FA}N_C(k), P_D)$ seems very complicated, when numerically evaluated and plotted it can be seen that it has a monotonic and nice behaviour (see Fig. 2.1). This makes a functional approximation to the IRF feasible. Indeed, in [62], the following closed-form approximation was suggested:

$$\hat{q}_2(\lambda\bar{V}(k), P_D) = \frac{0.997P_D}{1 + 0.37P_D^{-1.57}\lambda\bar{V}(k)} \quad (4.23)$$

where $\lambda \triangleq P_{FA}/V_C$ is the spatial clutter density. This expression can be used for online calculation purposes of the IRF without performing Monte-Carlo integration procedure mentioned previously in Section 2.5.1.1.

The plot of the approximation given in (4.23) together with the actual IRF curves are shown in Fig. 4.1. Note that the approximation is good enough when the average number of false alarms is less than 10 (i.e., $\lambda\bar{V} = P_{FA}N_C < 10$).

⁶ It can be experimentally verified that this requirement is satisfied for $q_2(P_{FA}N_C(k), P_D)$ (see, e.g. Fig. 4.5).

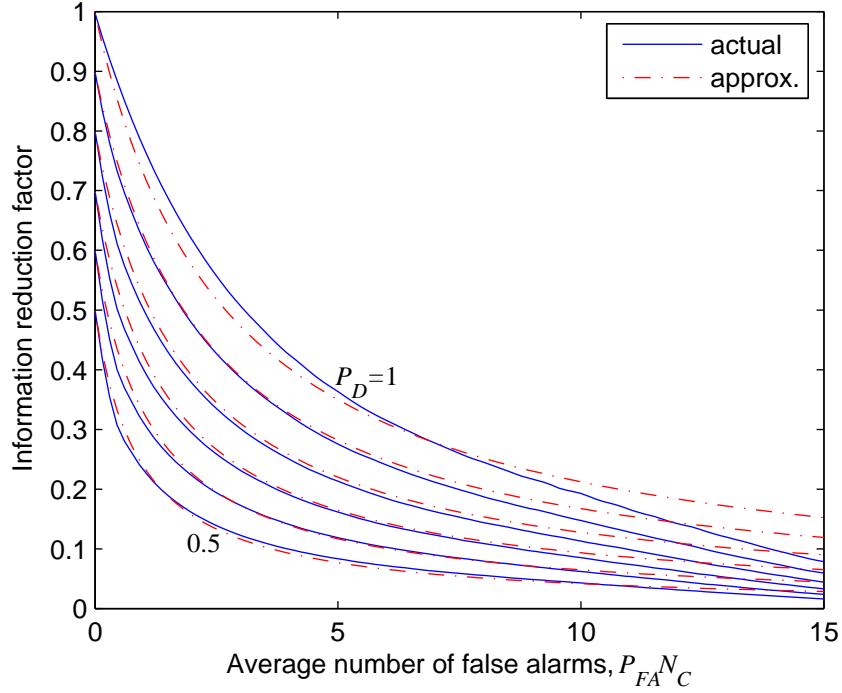


Figure 4.1: Dependence of information reduction factor on average number of false alarms for various detection probabilities. The plot is obtained for 2-dimensional measurement vector with $g = 4$ sigma gate. Result of a functional approximation to these curves is shown with dashed lines.

4.3.3 Obtaining a Closed-Form Solution

Being a mathematically-tractable expression, now it is a reasonable idea to try to find the maximum of the functional approximation given in (4.23) in closed-form. Although this seems quite a simple idea, to the best of author's knowledge, no one tries this way in the literature. In this respect, the work of [1], where the prior optimization problem given in (4.21) and (4.22) was first proposed, and the work of [62], where the functional approximation given in (4.23) was suggested, seem to be unaware of each other. So, as a “close” alternative to (4.22), we propose the following optimization problem:

$$\begin{aligned}
 P_{FA}^*(k) &= \arg \max_{P_{FA}} \hat{q}_2(P_{FA}N_C(k), P_D), \quad \text{subject to} \\
 P_D &= f_{ROC}(P_{FA}, \zeta) \quad \text{and} \quad 0 \leq P_{FA} \leq 1
 \end{aligned} \tag{4.24}$$

where

$$\hat{q}_2(P_{FA}N_C(k), P_D) = \frac{0.997P_D}{1 + 0.37N_C(k)P_D^{-1.57}P_{FA}} \quad (4.25)$$

which can easily be obtained from (4.23) by making the substitution $\lambda\bar{V}(k) = P_{FA}N_C(k)$. To find the single maximum,⁷ we apply the necessary condition for existence of an extremum, namely we take the derivative of both sides of (4.25) with respect to P_{FA} and equate to zero:

$$\begin{aligned} \frac{d\hat{q}_2}{dP_{FA}} &= \frac{0.997 \frac{dP_D}{dP_{FA}} \left[1 + 0.37N_C(k)P_D^{-1.57}P_{FA} \right]}{\left[1 + 0.37N_C(k)P_D^{-1.57}P_{FA} \right]^2} \\ &\quad - \frac{0.997P_D \times 0.37N_C(k) \left[-1.57P_D^{-2.57} \frac{dP_D}{dP_{FA}} P_{FA} + P_D^{-1.57} \right]}{\left[1 + 0.37N_C(k)P_D^{-1.57}P_{FA} \right]^2} = 0. \end{aligned} \quad (4.26)$$

Equating the numerator to zero and rearranging the terms gives the following differential equation for P_D :

$$\left[1 + 2.57 \times 0.37N_C(k)P_D^{-1.57}P_{FA} \right] \frac{dP_D}{dP_{FA}} - 0.37N_C(k)P_D^{-0.57} = 0 \quad (4.27)$$

where the derivative term dP_D/dP_{FA} can be evaluated from a given detector's ROC curve of the form $P_D = f_{ROC}(P_{FA}, \zeta)$.

4.3.4 Considering Different Detectors

Note that the differential equation given in (4.27) is general (i.e., independent of the detector used), while the ROC curve is clearly *detector-specific*. The joint solution of these two equations provides the optimum false alarm probability P_{FA}^* for a specific detector-PDAF pair. At this point, one can try to find a closed-form solution for various type of detectors, each having a different ROC curve expression. However, the problem turns out to be very difficult for

⁷ We know from the shape (see Fig. 4.5) of the cost function $\hat{q}_2(P_{FA}N_C(k), P_D)$ that it is *unimodal*, and for practical values of N_C and P_D , it has a single local maximum in the interior of the P_{FA} domain of interest (typically the interval $[10^{-8}, 1]$). Therefore, in this section we only look at the necessary condition according to *Fermat's Theorem* and skip the "second derivative test."

some of the cases considered. For example, the ROC curve of the famous Cell-Averaging Constant False Alarm Rate (CA-CFAR) detector, which is, under $\text{HOG}_I^{\text{SQL}}$, given by [63]

$$P_D = \left[1 + \frac{P_{FA}^{(-1/N_R)} - 1}{1 + \zeta} \right]^{-N_R} \quad (4.28)$$

where N_R is the *reference window size* [69], is quite complex to be able to obtain a closed-form solution for P_{FA} in (4.27). Such a difficulty also arises when we pick the detectors whose ROC curves can not be given in a closed-form relation of the form $P_D = f_{ROC}(P_{FA}, \zeta)$, but rather they are expressed as a combination of two parameterized equations for P_{FA} and P_D as

$$P_{FA} = f_{FA}(\alpha) \quad (4.29)$$

$$P_D = f_D(\alpha, \zeta) \quad (4.30)$$

where α is a scale factor or *threshold multiplier* [2] used to determine the thresholding level. An example of this kind of ROC curve is that of the Order Statistic Constant False Alarm Rate (OS-CFAR) detector, which is, under $\text{HOG}_I^{\text{SQL}}$, given by

$$P_{FA} = f_{FA}(\alpha) = \prod_{j=0}^{K-1} \frac{N_R - j}{N_R - j + \alpha} \quad (4.31)$$

$$P_D = f_D(\alpha, \zeta) = \prod_{j=0}^{K-1} \frac{N_R - j}{N_R - j + \alpha/(1 + \zeta)} \quad (4.32)$$

where K is the *order number*. Again, it seems very difficult to obtain a closed-form solution for P_{FA} in (4.27).

Remark 4.2 *In any difficulty case mentioned above, the problem can still be solved using optimization algorithms. But remember that our concern in this chapter, is to obtain a closed-form solution for the problem.*

After such pessimistic examples, now we can switch to the Neyman-Pearson (NP) detector case for which it is possible to solve the problem in closed-form.

4.3.5 Neyman-Pearson (NP) Detector Case

Under $\text{HOG}_I^{\text{SQL}}$, the ROC curve for the optimum Neyman-Pearson (NP) detector is given by the following famous relation [63]

$$P_D = P_{FA}^{1/(1+\zeta)}. \quad (4.33)$$

Note that this ROC curve relation is very simple (may be the most simple one among all detectors). This increases the possibility of obtaining a closed-form solution for the optimization problem defined in (4.24). Indeed, if we proceed from (4.33), we get

$$\frac{dP_D}{dP_{FA}} = \frac{1}{1+\zeta} P_{FA}^{-\zeta/(1+\zeta)} \quad (4.34)$$

and substituting P_D and dP_D/dP_{FA} terms into (4.27) we obtain

$$\left[1 + 2.57 \times 0.37 N_C(k) P_{FA}^{-1.57/(1+\zeta)} P_{FA} \right] \frac{1}{1+\zeta} P_{FA}^{-\zeta/(1+\zeta)} = 0.37 N_C(k) P_{FA}^{-0.57/(1+\zeta)}. \quad (4.35)$$

This equation can be solved for P_{FA} in closed-form as

$$P_{FA}(k) = \left[0.37 N_C(k) (\zeta - 1.57) \right]^{(1+\zeta)/(0.57-\zeta)}. \quad (4.36)$$

Note that this solution already satisfies the equality constraint (i.e., the ROC curve) of the optimization problem defined in (4.24). For the inequality constraint, we should have $P_{FA} \in [0, 1]$. For $P_{FA} \geq 0$ part, the base term of (4.36) should be non-negative. Since N_C is by definition always strictly positive, we should have $\zeta \geq 1.57$ for $P_{FA} \geq 0$. Note that with this constraint on the SNR, the exponent term $(1+\zeta)/(0.57-\zeta)$ is strictly negative. Therefore, for $P_{FA} \leq 1$ part, the base term should be greater than or equal to 1, or we should have $\zeta \geq 1.57 + 1/(0.37 N_C)$. Joint consideration of this last constraint and the previous one, i.e., $\zeta \geq 1.57$, yields that we should have $\zeta \geq 1.57 + 1/(0.37 N_C)$ for $P_{FA} \in [0, 1]$. Hence, we propose the following optimal setting for the operating P_{FA} value:

$$P_{FA}(k) = \begin{cases} \left[0.37 N_C(k) (\zeta - 1.57) \right]^{(1+\zeta)/(0.57-\zeta)} & \text{if } \zeta \geq 1.57 + 1/[0.37 N_C(k)] \\ 1 & \text{otherwise.} \end{cases} \quad (4.37)$$

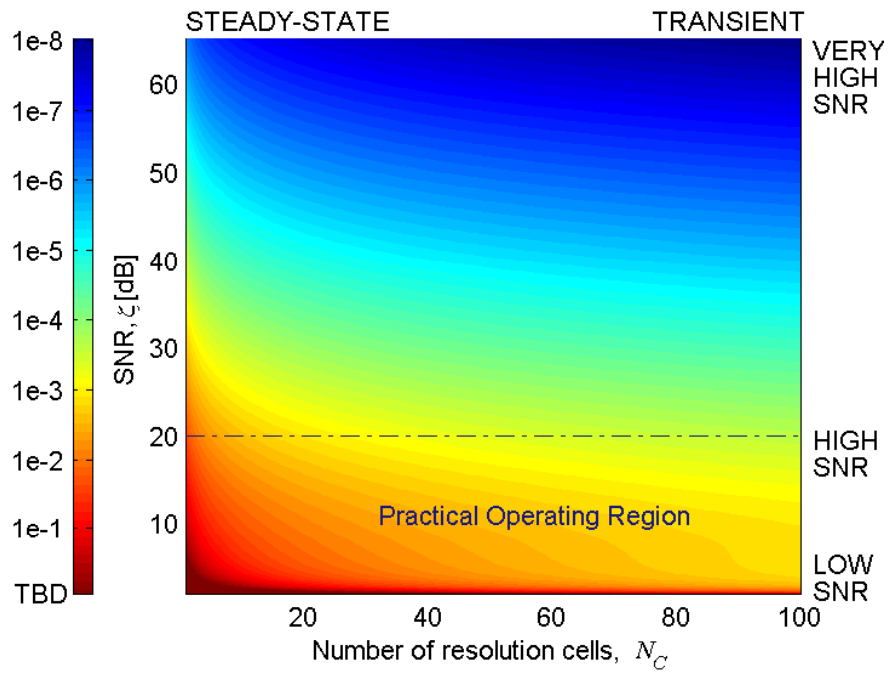
4.4 Interpretation of the Result and Practical Issues

The optimal P_{FA} setting proposed in (4.37) gives some useful insights into *prior* detection threshold optimization. Firstly, this expression provides an optimum operating false alarm probability for an NP detector, which is concatenated with a PDAF, under the assumption of $\text{HOG}_1^{\text{SQL}}$. Furthermore, this setting is valid for the measurement spaces of dimension $n_z = 2$ and when the validation is performed with a gate size of $g = 4$.⁸ The optimal operating false alarm probability P_{FA} is computed at every time step by taking into account of current SNR (ζ) and the number of resolution cells enclosed by the validation gate, denoted by N_C . Note that such a setting for P_{FA} is *tracker-dependent*, and it is totally different than the traditional detection theoretic approach where the operating false alarm probabilities are selected on the basis of experience, intuition and/or other system constraints such as tolerable false alarm limit of the radar data processor.

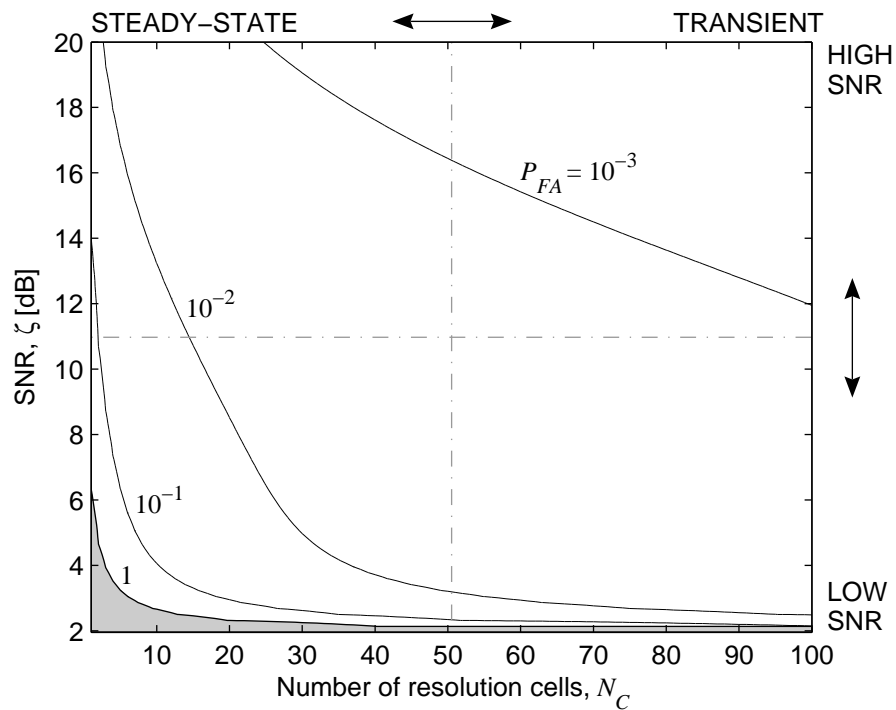
One can argue that NP detector has no practical usage due to its unrealistic assumption of constant and known detection noise power level [2]. Although this is true and so the ROC curve given in (4.33) is not attainable in the real-world, many popularly used practical detection systems operate on some other ROC curves which approximate this optimal one, such as those of CFAR detectors. Hence, the ROC curve given in (4.33) is still of special attention and importance.

Now consider the plot of optimal P_{FA} surface as a function of ζ and N_C which is illustrated in Fig. 4.2a where the third data dimension (optimal P_{FA} values) are represented by colors.

⁸ These assumptions do not originate from the present study but rather from those for obtaining the IRF and the corresponding functional approximation in [62]. For the other values of n_z and g , the extension is conceptually easy but the whole procedure (i.e., obtaining the IRF and the corresponding functional approximation) should be repeated.



(a)



(b)

Figure 4.2: (a) The surface of optimal P_{FA} values as a function of ζ and N_C , (b) P_{FA} contours in the practical operating region. The region where the optimization suggests $P_{FA} = 1$ is also shown in (b) as a shaded area. Note that this region corresponds to applying no thresholding at all, where the whole system operates in *track before detect* (TBD) mode.

Note that the optimization consistently suggests to increase P_{FA} when the SNR decreases or the filter goes from its transient operation to its steady-state operation.⁹ Note also that, considering a practical operating region, where SNR values are below 20 dB, the threshold optimization suggests considerably higher P_{FA} values than the ones used commonly in practice (i.e., between 10^{-8} and 10^{-4} [2]). Similar values like 10^{-8} are only suggested when the SNR is very high (> 60 dB) and the gate volume is large, i.e. in the transient phase of the filter. This clearly shows that the practically chosen P_{FA} values are far from an optimal setting in terms of the overall radar system tracking performance. The main reason for choosing considerably low P_{FA} values in practice is the computational limitations of the radar data processor in handling large number of false alarms. Although this may still be of considerable concern today, it is our belief that diminishing silicon prices and increasing computational power will enable performance optimal algorithms to be the choice over heuristic approaches. At low SNR values, the tracking performance gain of operating at these high but optimal false alarm values may be substantial as illustrated by the experimental results that follow.

A very interesting result of the proposed closed-form expression can also be observed from Fig. 4.2. Namely, the solution is also a generalization of the *track before detect* (TBD) approach suggested in the literature for very low SNR scenarios [67], [68]. Note that in some portion of the $N_C - \zeta$ plane, P_{FA} is set to 1. This means that the optimal solution applies no thresholding on the raw radar signals, effectively making a seamless and automatic transition to the TBD approach, which appears as a degenerate case of the optimal P_{FA} setting given in (4.37).

⁹ It can be argued that a decreasing value of N_C , namely decreasing number of resolution cells falling inside a validation gate, suggests that the gate volume (hence the Gaussian hyper-ellipse suggested by the filter covariance) is diminishing. This in turn suggests the convergence of the filter to its steady-state although this may not be guaranteed to be the correct state estimate. Conversely, by the same argument, a large value of N_C suggests a large gate volume, which in turn suggests that the filter is comparatively in its transient phase.

4.5 Simulation Results

Here, we consider exactly the same tracking problem as in the previous chapter with the same simulation parameters. For the sake of completeness, it is repeated in this section.

We consider the problem of tracking a single target in clutter using a 2D radar. The target state vector is composed of position and velocity components in East (ξ) and North (η) directions:

$$x(k) \triangleq \begin{bmatrix} \xi(k) & \dot{\xi}(k) & \eta(k) & \dot{\eta}(k) \end{bmatrix}^T \quad (4.38)$$

and we assume to measure the target position in Cartesian coordinates,¹⁰ i.e., $z(k) \triangleq [\xi^m(k) \quad \eta^m(k)]^T$.

Remember that the optimal P_{FA} setting proposed in (4.37) depends on two variables, namely, the SNR (ζ) and N_C . To be able to analyze the effects of these parameters independently, first we fix the SNR during a specific scenario and let the threshold optimization be made by considering this fixed SNR and time-varying N_C value, then we repeat this procedure for different constant SNR scenarios. In other words, we change the SNR from scenario to scenario, while N_C changes in each scenario. Again we assume that the SNR depends only on range as given in (3.11) with the same constant factor (i.e., $C_\zeta = 3.125 \times 10^{16} \text{ m}^4$).

Note that such an artificial geometry ensures the range of the target, hence the SNR, to be constant during a specific scenario. To determine C_ζ , which represents all the other factors in the SNR equation, ζ is assumed to be 50 (16.99 dB) for 5 km, which yields $C_\zeta = 3.125 \times 10^{16} \text{ m}^4$.

¹⁰ In a typical 2D radar, the measurements are normally in polar coordinates (range and azimuth). Here, the Cartesian measurements are used to have a linear measurement model. For further discussion on coordinate conversions, see [4, ch. 1, pp. 36] and [18, ch. 10, pp. 397].

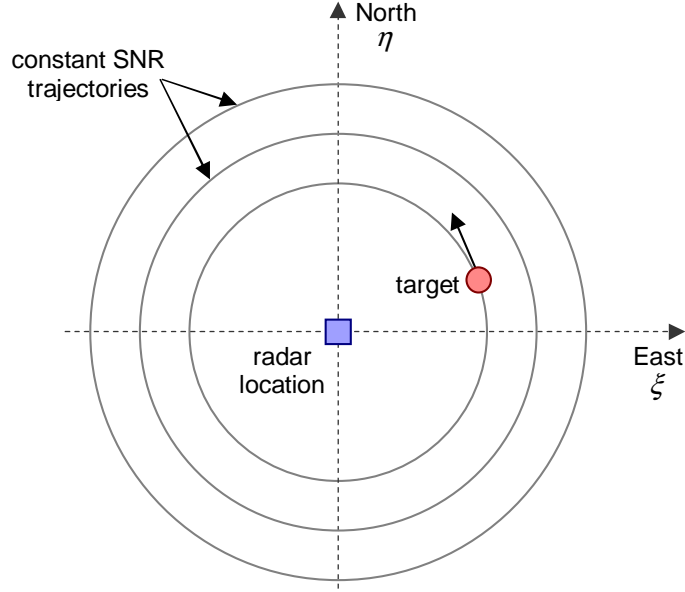


Figure 4.3: Scenario geometry: Assumed constant SNR target trajectories and location of the radar.

The circular target motion given in Fig. 4.3 is modeled by a coordinated turn:

$$F = \begin{bmatrix} 1 & \frac{\sin(\Omega T)}{\Omega} & 0 & -\frac{1-\cos(\Omega T)}{\Omega} \\ 0 & \cos(\Omega T) & 0 & -\sin(\Omega T) \\ 0 & \frac{1-\cos(\Omega T)}{\Omega} & 1 & \frac{\sin(\Omega T)}{\Omega} \\ 0 & \sin(\Omega T) & 0 & \cos(\Omega T) \end{bmatrix}, \quad G = \begin{bmatrix} T^2/2 & 0 \\ T & 0 \\ 0 & T^2/2 \\ 0 & T \end{bmatrix} \quad (4.39)$$

where the turn rate is selected as $\Omega = 1 \text{ deg/s}$ and the sampling period is $T = 1 \text{ s}$. Note that in the state vector, we do not estimate the turn rate, i.e., it is assumed to be known, therefore the state dynamics is also linear. This is adopted to decouple the maneuver problem from the clutter problem on which our focus is.

The process noise $v(k) \triangleq [v_\xi(k) \ v_\eta(k)]^T$ and the measurement noise $w(k) \triangleq [w_\xi(k) \ w_\eta(k)]^T$ are both zero mean white Gaussian sequences with covariance matrixes,

$$Q = \begin{bmatrix} 1 & 0 \\ 0 & 1 \end{bmatrix} q^2 \quad \text{and} \quad R = \begin{bmatrix} (\Delta r_\xi/\sqrt{12})^2 & 0 \\ 0 & (\Delta r_\eta/\sqrt{12})^2 \end{bmatrix}, \quad (4.40)$$

respectively, where the factor q is selected as 0.1 m/s^2 and the range resolutions in East (Δr_ξ) and North (Δr_η) directions are taken as 50 m which yields a

Table 4.1: Experiment I: Compared tracking systems.

System Name	Desired False Alarm Probability, P_{FA}^d
PDAF-E8	$P_{FA}(k) = 10^{-8}$
PDAF-E6	$P_{FA}(k) = 10^{-6}$
PDAF-E4	$P_{FA}(k) = 10^{-4}$
PDAF-OP	$P_{FA}(k) = [0.37N_C(k)(\zeta - 1.57)]^{(1+\zeta)/(0.57-\zeta)}$

resolution cell volume of $V_C = 2500 \text{ m}^2$. Note that the measurement covariance matrix given in (4.40) is the result of the assumption that the true measurement is uniformly distributed in the resolution cell [4, ch. 8, pp. 472]. Finally, the a priori information about the state, i.e., the mean $\hat{x}(0|0)$ and the covariance $P(0|0)$ of the initial state $x(0)$, is obtained by *two point differencing* [18], similar to the previous chapter.

4.5.1 Experiment 1: Comparison with Conventional Approaches

The objective of this experiment is to demonstrate how much is gained in overall system tracking performance by the use of an optimal approach to threshold selection, in particular our approximate closed-form formulation. We leave the discussion of how much is gained computationally by this approximate closed-form method to the next experiment.

We compare four tracking systems given in Table 4.1 each consisting of a probabilistic data association (PDA) tracking filter and an NP front-end detector with particular choices of the operating P_{FA} values. The first three systems use constant and conventionally selected desired P_{FA} values of 10^{-8} , 10^{-6} and 10^{-4} which are the typical values used in practice [2]. On the other hand, the last system has a tracker-aware optimal detector for which the desired P_{FA} value is determined according to the proposed closed-form expression (4.37). The corresponding P_D values for each system can be obtained from their common

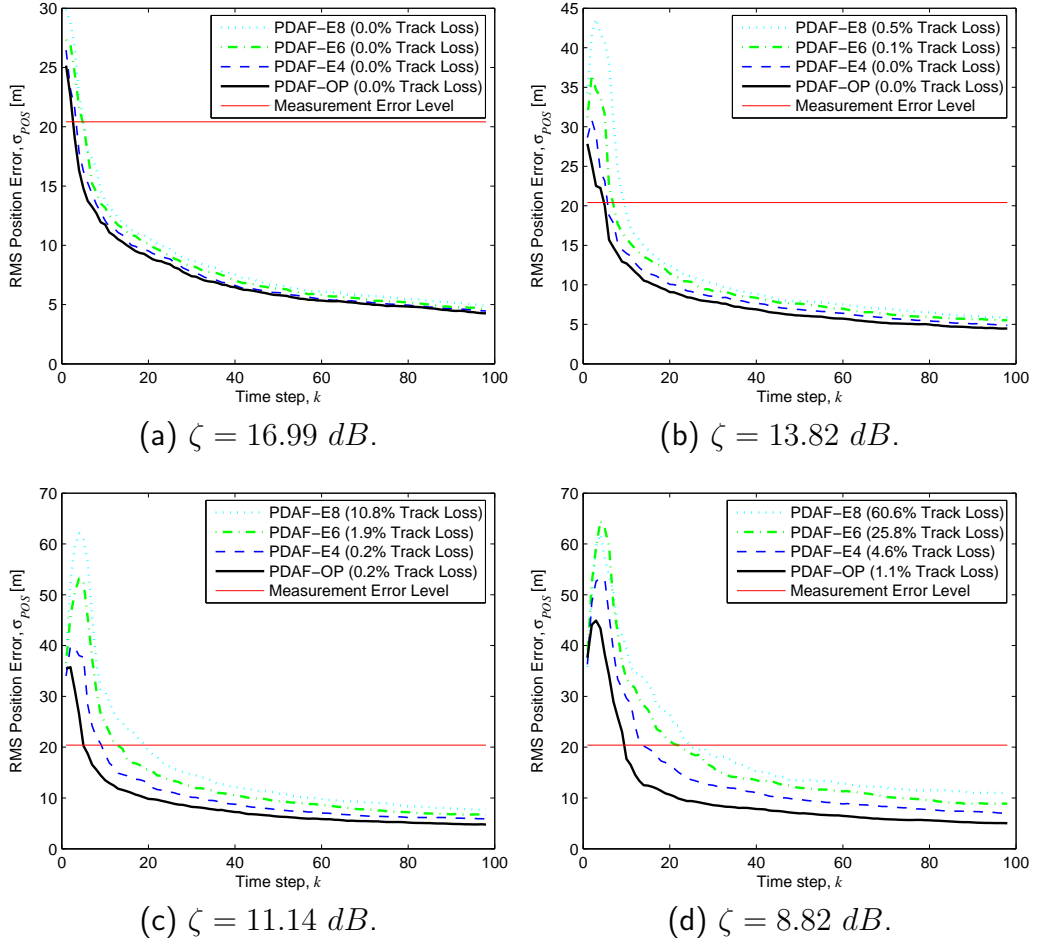


Figure 4.4: Impact of various detector false alarm probability settings on RMS position errors of their downstream tracking filters. For all SNR scenarios, the tracking system PDAF-OP, which uses the proposed detector threshold adaptation scheme, gives the best performance in terms of both RMS position error and TLP.

Table 4.2: Experiment II: Compared tracking systems.

System Name	Desired False Alarm Probability, P_{FA}^d
PDAF-OP-GOL [1]	$P_{FA}(k) = \arg \max_{P_{FA}} q_2 (P_{FA} N_C(k), P_D)$ (solved using Golden-Section Search)
PDAF-OP-FIB [1]	$P_{FA}(k) = \arg \max_{P_{FA}} q_2 (P_{FA} N_C(k), P_D)$ (solved using Fibonacci Search)
PDAF-OP	$P_{FA}(k) = \arg \max_{P_{FA}} \hat{q}_2 (P_{FA} N_C(k), P_D)$ $= [0.37 N_C(k) (\zeta - 1.57)]^{(1+\zeta)/(0.57-\zeta)}$

ROC curve (4.33) for a given SNR. We consider four constant SNR scenarios: 16.99, 13.82, 11.14 and 8.82 dB. In each scenario, the target follows the corresponding constant SNR trajectory (see Fig. 4.3) for 100 time steps. We have conducted 1000 Monte Carlo runs for each scenario. The RMS position error plots, averaged over *track-loss free* runs, are shown in Fig. 4.4.

It can be observed that for all SNR scenarios, the tracking system PDAF-OP shows the best performance in terms of RMS position error and TLP. Note that feeding the desired P_{FA} value back to the detector in a tracker-aware manner significantly improves track loss performance and makes the system more robust against SNR variations. The improvements are more evident and becomes more important for low SNR conditions.

4.5.2 Experiment2: Comparison with Line Search Optimization Schemes

The objective of this second experiment is to now make a comparison between online optimal threshold selection methods only, in particular between the iterative line-search based methods used in [1] and the approximate closed-form solution proposed in the present study.

We compare three optimal tracking systems given in Table 4.2 in terms of overall tracking performance and computational complexity. Each tracking system

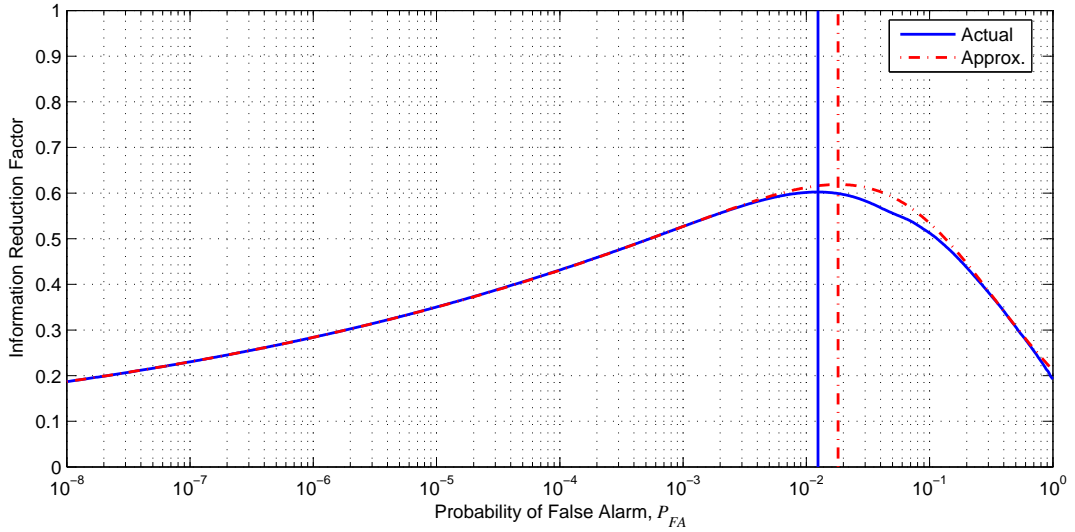


Figure 4.5: Variation of the IRF $q_2(P_{FA}N_C(k), P_D)$ and its functional approximation $\hat{q}_2(P_{FA}N_C(k), P_D)$ over a NP detector ROC curve for $N_C = 10$ and $\zeta = 10$ dB case.

consists of a PDA tracking filter and an NP detector. In each system, the optimum P_{FA} value found by threshold optimization is fed to the detector at every time step. The main differences between these tracking systems are threshold optimization problem formulations that they consider and their solution methodology. For example, PDAF-OP-GOL [1] and PDAF-OP-FIB [1] solve the threshold optimization problem defined in (4.22) using Golden-Section and Fibonacci Search methods, respectively. On the other hand, PDAF-OP, which is proposed in the present study, solves the optimization problem defined in (4.24) in closed-form.

Two cost functions, $q_2(P_{FA}N_C(k), P_D)$ and $\hat{q}_2(P_{FA}N_C(k), P_D)$ are illustrated in Fig. 4.5. Both cost functions are evaluated on the NP detector ROC curve given in (4.33) and for $N_C = 10$ and $\zeta = 10$ dB values. Note that the true cost function $q_2(P_{FA}N_C(k), P_D)$ is *unimodal* in the P_{FA} range shown in Fig. 4.5. Therefore both line search algorithms converge to the global optimum of this function. Note also that the global optimum found by the closed-form solution slightly differs from that of the actual function. At this point, we seek answers to the following questions:

- Whether there is notable loss of tracking performance by solving the approximate optimization problem rather than the original one,
- If no such loss is observed, what is the amount of computational gain obtained by using a closed-form solution to the approximated problem as compared to iterative solution of the original problem.

To answer these questions, we configure an experiment that is described in this section. Firstly we note that the variation of both cost functions given in Fig. 4.5 is best viewed in log scale for P_{FA} axis. Use of a linear scale in P_{FA} squeezes the global optimum peaks in a very small interval so that they can not be observed. The same effect also slow down the line search algorithms hence causes unfair evaluation. This observation leads us to operate line search algorithms not in linear scale but in logarithmic scale. That is, it is much more efficient to search the global optimum over the exponent term of P_{FA} . Therefore, for the iterative methods based on Golden-Section and Fibonacci Search, we take the initial interval of uncertainty for the exponent of P_{FA} as $\mathcal{I}_e = [-8, 0]$ and the maximum error tolerance on the exponent as $\Delta_e = 0.01$.

We consider five constant SNR scenarios of 5, 8, 11, 14, 17 *dB* and perform 500 Monte Carlo runs for each scenario. The simulation results are given in Fig. 4.6. All systems exhibit similar performance in terms of RMS position error and TLP. Hence, as an answer to the first question above, we may conclude that the proposed closed-form solution does not imply a tracking performance penalty.

The superiority of PDAF-OP becomes obvious when we consider execution times¹¹ given in Fig. 4.6d. Note that PDAF-OP, which uses closed-form adaptation scheme in detector threshold optimization, clearly outperforms PDAF-OP-GOL and PDAF-OP-FIB approaches, which use one dimensional search algorithms for the same task. The computational gains are significant.

¹¹ All executions times are measured on the same hardware (i.e., computer) with all auxiliary processes killed.

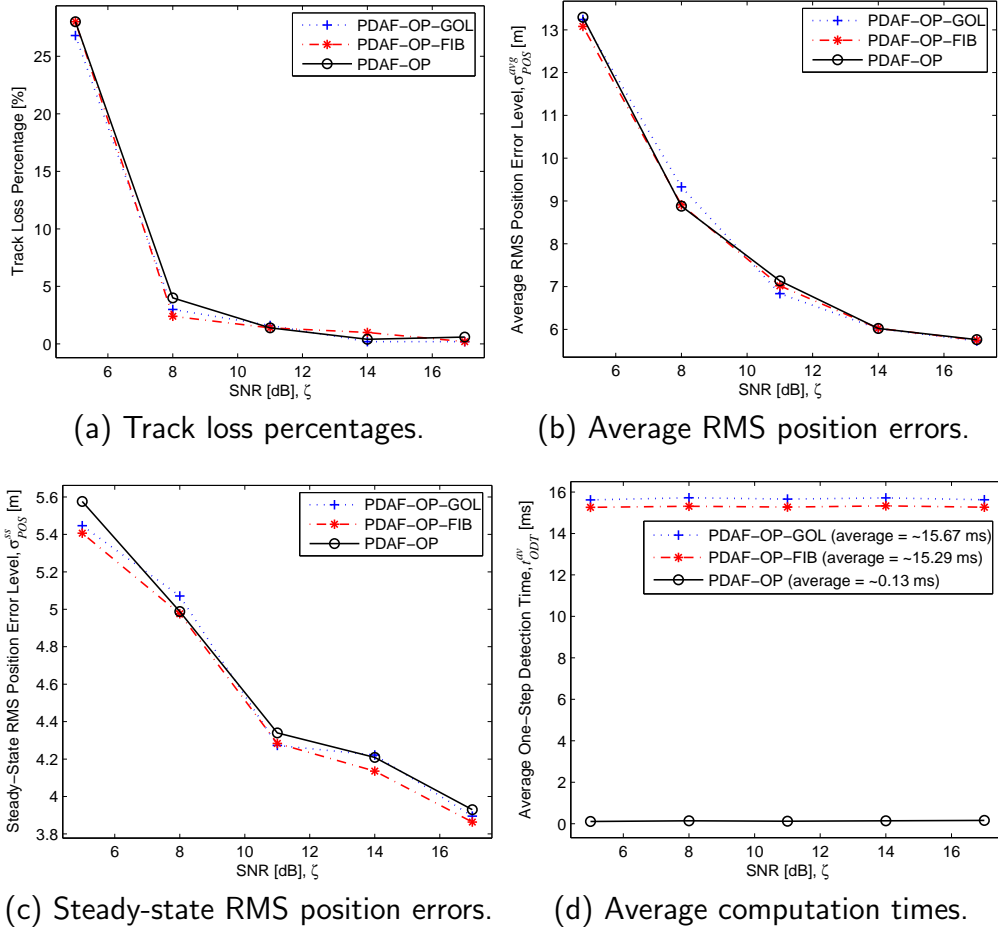


Figure 4.6: Comparison of tracking systems for $\mathcal{I}_e = [-8, 0]$ and $\Delta_e = 0.01$. Although there is no notable difference in terms of RMS position error and TLP, the closed-form approach (PDAF-OP) is computationally much more efficient than the iterative algorithms.

For the iterative search methods, the computation time critically depends on number of function evaluations which is determined by \mathcal{I}_e and Δ_e . In this particular selection of these parameters, the gain in terms of computational power is (approximately) as much as 115 times. To obtain a fairer comparison we attempted to observe the trade-off between tracking performance and computation times by changing the error tolerance parameter, Δ_e . Since we have already observed that the proper setting of P_{FA} becomes more crucial for low SNR conditions, a very low SNR scenario of (5 dB) is chosen for this comparison and the same experiment is repeated for $\mathcal{I}_e = [-8, 0]$ and error tolerance values of $\Delta_e = \{0.1, 1, 2, 3, 4\}$. The corresponding computational gains are approximately $\{85, 66, 64\}$ times for $\Delta_e = \{0.1, 1, 2\}$. For the other tolerance values $\Delta_e = \{3, 4\}$, line search algorithms produce unacceptable results and the optimization fails. Therefore, we conclude that even for the crude tolerance case of $\Delta_e = 2$, the closed-form solution is approximately 64 times more efficient than the iterative algorithms. Note that a very crude error tolerance usually obtains an arbitrary point near the mid-point of the initial search interval rather than the true maximum point. This behavior can be expected to impact performance especially when the maxima lies close to the interval boundaries, such as the one illustrated in Fig. 4.5.

4.6 Conclusion

In this chapter, we proposed a closed-form solution for the prior detector threshold optimization problem defined in [1]. This problem can also be viewed as an MRE-based DTOP (*DYNAMIC-MRE-CF*), explained in the previous chapter. Our proposed solution relies on a functional approximation for the IRF which was introduced previously in [62] but not applied to the problem. Compared with the existing iterative solution approaches (*DYNAMIC-MRE-LS* [1]), this led to a significantly more computationally efficient adaptation scheme with no observable performance degradation. Furthermore, a numeri-

cal analysis on the proposed expression shows that this solution brings a theoretical lower bound on the operating SNR concerning when the whole system should be switched to the track before detect (TBD) mode.

CHAPTER 5

EXTENSIONS TO MANEUVERING TARGET TRACKING CASE

In the previous chapters, we considered tracker-aware detection threshold optimization problem when tracking *non-maneuvering* targets in clutter. In this chapter, we relax this assumption and consider the same problem for now *maneuvering* targets.

5.1 Introduction

Up to now, we assumed that the model describing the state transition and measurement system is completely known to the filter. In other words, given the following state space representation

$$x(k+1) = F(k)x(k) + G(k)u(k) + v(k) \quad (5.1)$$

$$z(k) = H(k)x(k) + w(k), \quad (5.2)$$

where

$$v(k) \sim \mathcal{N}(0, Q(k)) \quad (5.3)$$

$$w(k) \sim \mathcal{N}(0, R(k)), \quad (5.4)$$

the matrices $F(k)$, $G(k)$, $H(k)$, $Q(k)$ and $R(k)$ and the input vector $u(k)$ are all assumed to be exactly known by the filtering algorithm. This means that,

no modeling uncertainty (or *modeling error*) is assumed. Indeed, this is one of the fundamental assumptions made in the derivation of the Kalman filter [18] in classical *state estimation*, as well as many other algorithms in *tracking*,¹ such as, the probabilistic data association filter (PDAF) [45], the joint PDAF (JPDAF) [70] and the multiple hypothesis tracking (MHT) [71] algorithm.

In practical problems, however, there are many cases that the dynamic system model related with the state transition and/or state measurement can not be known with certainty all times. For example, in a practical tracking scenario, this assumption may not be valid due to unknown target maneuver which appears as an *abrupt* change in the motion dynamics (*state transition model*). Similarly, in the field of fault diagnosis, the system is accepted to be in either a “faulty” or “non-faulty” operating mode and the unknown switching mechanism between these modes (e.g., failure of the system) is usually modeled by an abrupt change in the system output (*measurement model*).

In any case, when the filter-assumed state space model does not match the actual phenomena (target motion, system working mode, etc.), the filtering algorithm often produces unacceptable results leading to divergence or *track loss*.

In this chapter, our aim is to propose solutions for the problem of detector threshold optimization when tracking a maneuvering target in clutter. This problem contains both of two challenging issues in tracking, namely, the problem of *measurement origin uncertainty* or *data association* [4] and target motion uncertainty, i.e., *maneuver*. For the first issue, a popularly used solution is the *probabilistic data association* (PDA) filter (or PDAF) [45]. Unlike simple data association rules which make “hard” decisions, such as the nearest neighbor and the strongest neighbor approaches, the PDA is an *all-neighbor*

¹ In [18], tracking is defined as “the state estimation of a moving object using *remote sensors*.” Although tracking can be viewed as a special case of state estimation, it is wider in scope: Not only it uses all the tools from the state estimation theory, but also it requires the extensive use of statistical decision theory when some of the practical problems like *data association* [4] are considered.

approach – it uses all the validated measurements in the association process. By this feature, the PDA is often interpreted as a “soft” decision logic. The filter which uses this logic, called the PDAF, is proven to be very robust and *consistent*² [72], and produces much better results than simple hard-decision-based logics do. The details of the PDAF algorithm are given in Appendix B.

When the second issue, i.e., maneuver problem, comes into the picture, the PDAF alone is not competent to solve the problem due to the mentioned mismatch between the filter-assumed system model and true system mode. The literature related to solving this problem is abundant [4], [3], [73], [18]. However, methodologically, the proposed solutions can be categorized into a few broad categories [4].

In the first methodology, the maneuver is treated as a random process which enters the state dynamics given in (5.1) as an additional process noise. In this case, the problem turns out to be either readjusting the process noise level in a continuous space – *continuous level adjustment* or switching between several discrete noise levels – *discrete level adjustment* [18]. Relying on this crude noise assumption, this methodology usually results in poor tracking performance because a maneuver is, in general, not noise. The second methodology takes this fact into account and models the maneuver as a constant deterministic acceleration continuing over a certain period of time. Using this treatment, the unknown acceleration input is estimated either separately by another filter or simultaneously within the state. Then, the state estimation is corrected with this input estimation.

Different than the previous two methodologies, the third one uses multiple model filtering approach. In this solution approach, multiple filters each matched to a different motion model are run in parallel and their outputs are

² In general, a state estimator (filter) is called *consistent* if its state estimation error, $\tilde{x}(k|k) \triangleq x(k) - \hat{x}(k|k)$ has zero mean (i.e., the estimate is unbiased) and has a covariance matrix as calculated by the filter (i.e., the filter should be “honest”!) [18].

combined to obtain the global estimate. The algorithms in this category are proven to be better than the previous two approaches. In particular, the interacting multiple model (IMM) structure [64] provides a superior performance with less computation among its alternatives. The details of this algorithm can be found in Appendix C.

5.2 Proposed Optimization Schemes

As it is emphasized above, two elegant solutions for *clutter* and *maneuver* problems are the PDAF and multiple model filtering (and particularly IMM filter), respectively. For tracking maneuvering targets in clutter, a general approach is to use these solutions together. This can be achieved by running multiple model PDAFs in parallel and combine their estimates in forming the global estimate. In this section, we present two dynamic threshold optimization (DTOP) schemes for the detectors of the tracking systems which use multiple model PDAFs in their filtering side. The first scheme is a heuristic one in the sense that it is based on a heuristic filter. The second scheme, on the other hand, is a transparent extension of the DTOP schemes presented in Chapter 3 for a single model, to the multiple model filtering case.

5.2.1 A Heuristic Extension

Tracking maneuvering targets requires a good adaptation of the tracking filter to the changes in the state transition (or motion) model. One of the most attractive solution approaches is to use multiple model filtering where multiple tracking filters, each matched to a different motion model, are run in parallel and their estimates are fused to obtain the global estimate.

At this point, instead of fusing each elemental filter output, we try a heuristic filtering approach based on a *hard-decision* mechanism, so that at every

time step, the global estimate is produced by taking only one of the filter’s output. Let us assume that the target behaves according to one of the two modes: “Quiescent” and “maneuvering.” Then, basically, we have two elemental filters (PDAFs) corresponding to each mode. Provided that a reliable maneuver detection algorithm exists, we run only one of the filters together with its tracker-aware detector. This is the main motivation³ in this extension.

We prefer a DTOP scheme, so that the desired false alarm probability of the detector is determined optimally and fed to the detector at every time step. Without having any interaction between model-matched filters, the proposed approach closely resembles the *static multiple model estimator* approach [18], but with a difference that it does not even combine the estimates of each elemental filter in producing the final estimate.⁴

One may ask the natural question: “Why do we try such a filtering approach instead of, for example, the interacting multiple model (IMM) filter, which is already proven to be successful for the problem at hand?” The answer to this question is twofold.

First of all, this ad-hoc idea allows *direct*⁵ use of the DTOP schemes studied previously for single model PDAF case. So it is a quick solution approach worthwhile to try.

Secondly, we are motivated to investigate whether such a heuristic filtering structure with a tracker-aware detector performs better than a sophisticated filtering structure, such as IMM filter, but with a conventional detector.

Now, the question is: How do we detect a maneuver onset/termination, and so the criterion for switching between models? In a cluttered environment, it

³ As we have already shown that each individual tracking system (i.e., tracker-aware detector and single model tracking filter) provides very good performance over their conventional counterparts.

⁴ Fusing the output of each elemental filter is a common characteristic for all multiple model filtering schemes including the static multiple model estimator (see, e.g., [18]).

⁵ That is, without any further derivation efforts.

is very crucial to detect the onset/termination of the maneuver as quickly as possible. Since the only reliable as well as fast detection mechanism available is the IMM-PDAF, we use this filter not for the purpose of estimation but for the maneuver detection. So in this heuristic system architecture, there exists also an IMM-PDAF running continuously at the background, for detecting the maneuver onset and termination as quickly and reliably as possible.

We use the IMM-PDAF model probabilities, $\{\mu_j(k)\}$ in making the decision for switching between the quiescent and maneuvering models. Let us define three possible (exhaustive) events as

$$E_j(k) \triangleq \{\mu_j(k) \geq 1 - \epsilon\} \quad j = 1, 2, \quad (5.5)$$

and $E_0(k)$ being the complementary event of $\{E_1(k) \text{ or } E_2(k)\}$. Then, our tracking system has three operating modes corresponding to each of these events:

- E_1 : Quiescent model based tracker-aware detection and filtering,
- E_2 : Maneuvering model based tracker-aware detection and filtering,
- E_0 : Transition mode.

An example operation for the choice of $\epsilon = 0.1$ is illustrated over the IMM-PDAF model probabilities in Fig 5.1 where the white regions corresponds to the occurrence of E_0 .

5.2.1.1 Steps of the Algorithm

At each time step k , the algorithm makes a hard-switching between three operating modes according to the occurrence of the events $E_0(k)$, $E_1(k)$ and $E_2(k)$. One cycle of the algorithm is as follows.

- **Operating Mode E_1 :** This is the *quiescent* model based tracker-aware detection and filtering mode.

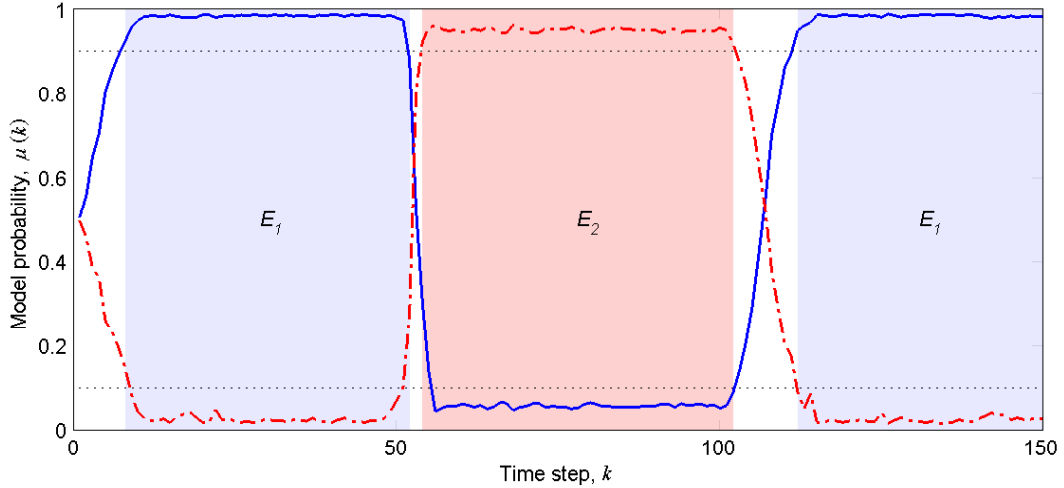


Figure 5.1: The operating modes of the proposed heuristic approach over the variation of model probabilities of the IMM-PDAF. The white regions corresponds to the transition mode E_0 .

– **Reinitialization of the Filter Based on the Quiescent Model:**

This is done by feeding the last estimation output and associated covariance of the overall system back to the PDAF based on the *quiescent* model as a new initial estimate and the associated, covariance. That is,

$$\hat{x}^Q(k-1|k-1) = \hat{x}(k-1|k-1) \quad (5.6)$$

$$P^Q(k-1|k-1) = P(k-1|k-1) \quad (5.7)$$

– **Dynamic TA-DTO Based on the Quiescent Model:** The desired false alarm probability, P_{FA}^d of the detector is set optimally by solving the optimization problem defined in (3.3) of Chapter 3, i.e.,

$$P_{FA}^d(k) = \arg \min_{P_{FA}} \left\{ f_S \left[\bar{P}_{NSPP}^Q(k|k) \right] \right\}, \quad \text{subject to} \quad (5.8)$$

$$P_D = f_{ROC}(P_{FA}, \zeta) \quad \text{and} \quad 0 \leq P_{FA} \leq 1$$

where as defined previously $f_S[\cdot]$ is any scalar measure that can be deduced from a matrix (such as, trace or determinant) and $\bar{P}_{NSPP}^Q(k|k)$ is an offline approximation of the covariance of the PDAF based on the quiescent model. Note that $\bar{P}_{NSPP}^Q(k|k)$ can

be obtained either of the NSPP methodologies for the PDAF, i.e., the MRE or HYCA algorithm.⁶

- **Detection:** In this step, given the desired false alarm probability, which is optimally set in the previous step, and the SNR, the detector operating point, (P_{FA}, P_D) , so the detection threshold is determined, and the measurements, $Z(k)$ are generated.
- **Quiescent Model Based Filtering:** Given the initial estimate, $\hat{x}^Q(k-1|k-1)$, the associated covariance, $P^Q(k-1|k-1)$, and the measurements, $Z(k)$, a probabilistic data association filtering (PDAF) algorithm which is based on the *quiescent* model is carried out to obtain the updated estimate and the associated covariance, $\hat{x}^Q(k|k)$ and $P^Q(k|k)$.
- **Outputting:** The global estimate and associated covariance of the overall system are taken as those produced by the *quiescent* model based filter as

$$\hat{x}(k|k) = \hat{x}^Q(k|k) \tag{5.9}$$

$$P(k|k) = P^Q(k|k) \tag{5.10}$$

- **Operating Mode E_2 :** This is the *maneuvering* model based tracker-aware detection and filtering mode. The steps of this mode are exactly the same as those of E_1 . The difference is the model used.

- **Reinitialization of the Filter Based on the Maneuvering Model:** This is done by feeding the last estimation output and associated covariance of the overall system back to the PDAF based on the *maneuvering* model as a new initial estimate and the asso-

⁶ For the MRE case, as mentioned in the previous chapter, instead of solving the optimization problem iteratively, one can use the closed-form expression (4.37) provided that the detector is of Neyman-Pearson type and the corresponding assumptions hold.

ciated covariance. That is,

$$\hat{x}^M(k-1|k-1) = \hat{x}(k-1|k-1) \quad (5.11)$$

$$P^M(k-1|k-1) = P(k-1|k-1) \quad (5.12)$$

- **Dynamic TA-DTO Based on the Maneuvering Model:** The desired false alarm probability, P_{FA}^d of the detector is set optimally by solving the optimization problem

$$P_{FA}^d(k) = \arg \min_{P_{FA}} \left\{ f_S \left[\bar{P}_{NSPP}^M(k|k) \right] \right\}, \quad \text{subject to}$$

$$P_D = f_{ROC}(P_{FA}, \zeta) \quad \text{and} \quad 0 \leq P_{FA} \leq 1 \quad (5.13)$$

where $\bar{P}_{NSPP}^M(k|k)$ is an offline approximation of the covariance of the PDAF based on the *maneuvering* model.

- **Detection:** In this step, given the desired false alarm probability, and the SNR, the detector operating point, (P_{FA}, P_D) , so the detection threshold is determined, and the measurements, $Z(k)$ are generated.
- **Maneuvering Model Based Filtering:** Given the initial estimate, $\hat{x}^M(k-1|k-1)$, the associated covariance, $P^M(k-1|k-1)$, and the measurements, $Z(k)$, a PDAF algorithm which is based on the *maneuvering* model is carried out to obtain the updated estimate and the associated covariance, $\hat{x}^M(k|k)$ and $P^M(k|k)$.
- **Outputting:** The global estimate and associated covariance of the overall system are taken as those produced by the *maneuvering* model based filter as

$$\hat{x}(k|k) = \hat{x}^M(k|k) \quad (5.14)$$

$$P(k|k) = P^M(k|k) \quad (5.15)$$

- **Operating Mode E_0 :** This is the *transition* mode between the quiescent and maneuvering modes.

- **Conventional Detection:** The desired false alarm probability, P_{FA}^d of the detector is set conventionally, i.e., to a maximum allowable value. Then given the SNR, the detector operating point, (P_{FA}, P_D) , so the detection threshold is determined, and the measurements, $Z(k)$ are generated.
- **Outputting:** The global estimate and associated covariance of the overall system are taken as those produced by the IMM-PDAF running at the background.

$$\hat{x}(k|k) = \hat{x}^{IMM-PDAF}(k|k) \quad (5.16)$$

$$P(k|k) = P^{IMM-PDAF}(k|k) \quad (5.17)$$

5.2.2 A Multiple Model Filter Integrated Extension

Although the previous heuristic extension of dynamic threshold optimization problem is a quick and reasonable approach, it is very cumbersome: It uses two detection blocks and four PDAFs for tracking two-modes target motion. It is not integrated into the multiple-model filtering rather it uses some heuristics and a hard-switching mechanism to favor the models. As a second extension, in this section, we try to integrate the threshold optimization within multiple model filtering. Our problem formulation is as follows. We seek an optimum operating false alarm probability such that

$$P_{FA}^*(k) = \arg \min_{P_{FA}} \left[\mathbb{E} \left[\|x(k) - \hat{x}(k|k)\|^2 \middle| Z^{k-1} \right] \right], \quad \text{subject to,}$$

$$P_D = f_{ROC}(P_{FA}, \zeta) \quad \text{and} \quad 0 \leq P_{FA} \leq 1 \quad (5.18)$$

where $x(k)$, called the *base state*, is the true target state at time step k , $\hat{x}(k|k)$ is the state estimated by a multiple model filtering algorithm which uses the PDAFs as *modules* [4] (or *elemental filters* [19]), such as IMM-PDAF, and

Z^{k-1} is the cumulative set of *commonly*⁷ validated measurements through time $k - 1$.⁸ Note that, this problem is a multiple model filtering extension of the problem defined in (4.21) in the previous chapter, where the same problem is formulated for single model (PDAF) case. Our aim is to find an optimum false alarm probability, which in turn determines the detection threshold for a given SNR value. The equality constraint of the optimization problem is the ROC relation and the inequality one is used to guarantee that the resulting false alarm is a valid probability.

The unconstrained part of the optimization problem can be rewritten as

$$P_{FA}^*(k) = \arg \min_{P_{FA}} \left[\mathbb{E} \left[\|x(k) - \hat{x}(k|k)\|^2 \middle| Z^{k-1} \right] \right] \quad (5.19)$$

$$P_{FA}^*(k) = \arg \min_{P_{FA}} \left[\mathbb{E} \left[\text{tr} \{ P(k|k) \} \middle| Z^{k-1} \right] \right] \quad (5.20)$$

$$P_{FA}^*(k) = \arg \min_{P_{FA}} \left[\text{tr} \left\{ \mathbb{E} \left[P(k|k) \middle| Z^{k-1} \right] \right\} \right] \quad (5.21)$$

where $\text{tr}\{\cdot\}$ is the trace operator. Let $M(k) \in \{1, 2, \dots, r\}$, called the *modal state* [43], is a discrete-time switching random process [75] which represents the *system mode* at k (i.e., the model in effect *during* the sampling period ending at time step k). Moreover, let $M_j(k) \triangleq \{M(k) = j\}$ denote the event that the j th model is in effect at time k . Assuming that the true system mode obeys only one of the r possible modes defined above, the events $M_j(k)$, $j = 1, 2, \dots, r$ are *mutually exclusive*, that is, $\Pr\{M_i(k), M_j(k)\} = 0$, $\forall i \neq j$ and *exhaustive*, that is,

$$\sum_{j=1}^r \Pr\{M_j(k)\} = 1. \quad (5.22)$$

⁷ Different techniques in obtaining a *common* validation region in multiple model filtering can be found, for example in [74].

⁸ As mentioned in the previous chapter, this can be also named as a *prior* [1] detection threshold optimization. In its *posterior* version the conditioning will be on Z^k .

So, we can apply *total expectation theorem* to (5.21) as

$$\begin{aligned}
P_{FA}^*(k) &= \arg \min_{P_{FA}} \left[\text{tr} \left\{ \sum_{j=1}^r \mathbb{E} \left[P(k|k) \middle| M_j(k), Z^{k-1} \right] \Pr \{ M_j(k) | Z^{k-1} \} \right\} \right] \\
P_{FA}^*(k) &= \arg \min_{P_{FA}} \left[\text{tr} \left\{ \sum_{j=1}^r \mathbb{E} \left[P^j(k|k) \middle| Z^{k-1} \right] \mu_j(k|k-1) \right\} \right] \\
P_{FA}^*(k) &= \arg \min_{P_{FA}} \left[\text{tr} \left\{ \sum_{j=1}^r \bar{P}^j(k|k) \mu_j(k|k-1) \right\} \right] \\
P_{FA}^*(k) &= \arg \min_{P_{FA}} \left[\sum_{j=1}^r \text{tr} \{ \bar{P}^j(k|k) \} \mu_j(k|k-1) \right] \tag{5.23}
\end{aligned}$$

where $\mu_j(k|k-1) \triangleq \Pr \{ M_j(k) | Z^{k-1} \}$, $j = 1, 2, \dots, r$ are the *predicted* model probabilities. The term $\bar{P}^j(k|k)$, which is a deterministic version of the model-conditioned covariance $P^j(k|k)$, can be further substituted by either MRE or HYCA approximations given in Chapter 2. For the MRE case, this term can be approximately written as [5]

$$\begin{aligned}
\bar{P}^j(k|k) &= \bar{P}_{MRE}^j(k|k) \triangleq \mathbb{E} [P^j(k|k) | Z^{k-1}] \\
&\approx P^j(k|k-1) - q_2(P_{FA} N_C^j(k), P_D) W^j(k) S^j(k) W^j(k)^T \tag{5.24}
\end{aligned}$$

where $q_2(\cdot)$ is the *information reduction factor* [4] (IRF). The terms $W^j(k)$ and $S^j(k)$ are respectively the Kalman gain and innovation covariance corresponding to the j th model-matched PDAF at time step k and

$$N_C^j(k) \triangleq \frac{V^j(k)}{V_C} = \frac{c_{nz} g^{n_z} |S^j(k)|^{1/2}}{V_C} \tag{5.25}$$

is the number of resolution cells enclosed by the validation gate defined by the j th model at time step k . Substituting (5.24) into (5.23), we have

$$\begin{aligned}
P_{FA}^*(k) &= \arg \min_{P_{FA}} \left[\sum_{j=1}^r \text{tr} \{ P^j(k|k) \} \mu_j(k|k-1) \right. \\
&\quad \left. - \sum_{j=1}^r q_2(P_{FA} N_C^j(k), P_D) \text{tr} \{ W^j(k) S^j(k) W^j(k)^T \} \mu_j(k|k-1) \right] \tag{5.26}
\end{aligned}$$

Note that the first summation does not depend on P_{FA} and therefore it can be removed from the optimization. Furthermore, the terms in the second

summation are all non-negative. So the final form of the problem can be expressed as

$$P_{FA}^*(k) = \arg \max_{P_{FA}} \left[\sum_{j=1}^r q_2(P_{FA} N_C^j(k), P_D) \text{tr} \{ W^j(k) S^j(k) W^j(k)^T \} \mu_j(k|k-1) \right]. \quad (5.27)$$

Note that the optimization problem defined in (5.27) is one dimensional. Assuming that the cost function is *unimodal*,⁹ the solution can be found using well-known one dimensional (line) search algorithms.

5.3 Simulation Results

We consider an Air Traffic Control (ATC) scenario, illustrated in Fig. 5.2. In this scenario, an aircraft with an initial position of $p_T(0) = [0 \ 25000]^T$ m, flights eastward with a speed of $\|v_T\| = 150$ m/s for a 150 s. Then, it performs a coordinated turn with a turn rate of $\Omega = 1$ deg/s (which amounts to ~ 0.26 g maneuver at this speed) for a 150 s. Finally, it flights straight towards southwest for a 150 s. In generating this motion, we use a white noise acceleration (WNA) model for the straight parts and a constant turn rate¹⁰ coordinated turn (CT) model for the maneuvering part. In both WNA and CT models, we assume a process noise with a standard deviation of $q = 0.01$ m/s² in linear portions of the state transition.

The radar is located at $l_R = [23400 \ 16400]^T$ m, which corresponds approximately to the center of the coordinated turn maneuver. We assume that the radar provides position only measurements for every $T = 3$ seconds with a *rectangular*¹¹ resolution cell of 50 m in each coordinate which implies that the resolution cell volume is constant and equal to $V_C = 2500$ m².

⁹ Experimentally, it can be observed that the cost function given in (5.27) satisfies this requirement.

¹⁰ We do not add any process noise component to the turn rate. In the case of adding a noise to the turn rate, the motion model is often referred to as *nearly coordinated turn* (NCT) model [18, p. 467]

¹¹ We assume rectangular resolution cells to have a linear measurement model.

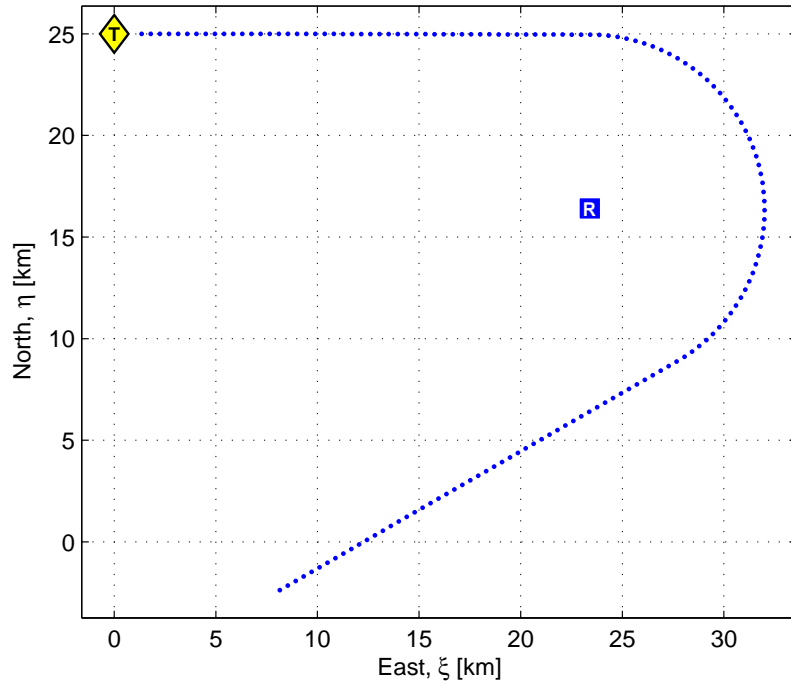


Figure 5.2: A sample Air Traffic Control (ATC) scenario: “T” and “R” denote initial aircraft (or target) position and radar location, respectively.

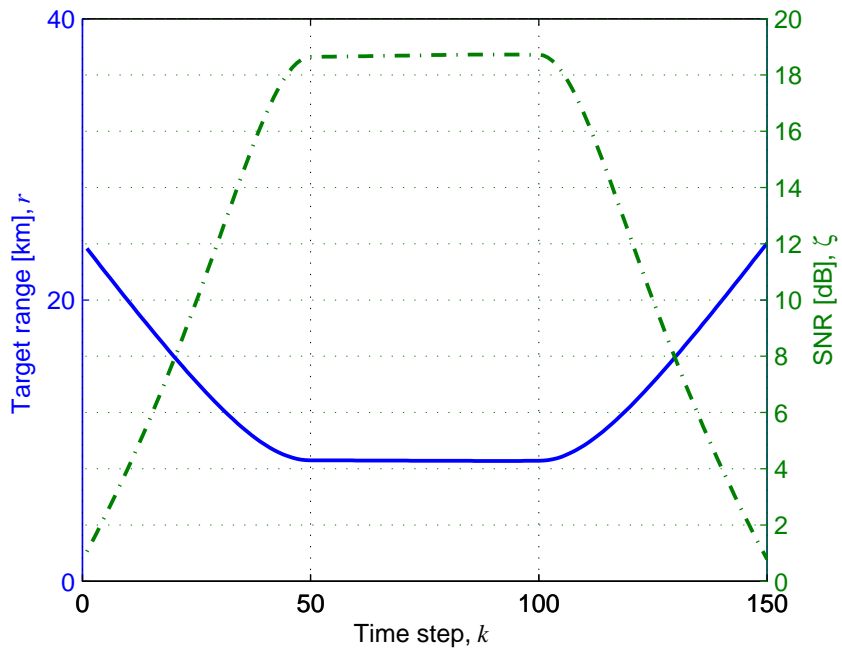


Figure 5.3: The variation of the range between target and radar, and that of SNR for $C_{\zeta} = 4 \times 10^{17}$ case.

Table 5.1: Minimum and maximum SNR values for different values of the SNR constant, C_ζ .

$C_\zeta [m^4]$	$\zeta_{min}[\text{dB}]$	$\zeta_{max}[\text{dB}]$
4×10^{17}	0.78	18.73
5×10^{17}	1.75	19.70
6×10^{17}	2.54	20.49
7×10^{17}	3.21	21.16
8×10^{17}	3.79	21.73
9×10^{17}	4.30	22.25
1×10^{18}	4.76	22.71

Similar to the experiments presented in the previous chapters, we assume that SNR depends only on range as

$$\zeta(r) = \frac{C_\zeta}{r^4} \quad (5.28)$$

where C_ζ is the SNR constant representing all the other factors in the SNR equation and r is the range to the target. The variation of the range between the radar and the aircraft and that of SNR for $C_\zeta = 4 \times 10^{17}$ case, are shown in Fig. 5.3. The minimum and maximum target range are reported to be as $r_{min} \approx 8.5 \text{ km}$ and $r_{max} \approx 24 \text{ km}$, respectively. Note that, at the beginning and end of the motion, SNR is very low as the target range is high. On the other hand, as the target approaches to the radar, SNR increases, and it reaches and stays at the maximum value during the coordinated turn maneuver. The minimum and maximum SNR values for different values of C_ζ are listed in Table 5.1. These are the different SNR conditions considered in the experiment. We chose deliberately very low ζ_{min} values to be able to see the effect of threshold optimization on the system performance more clearly.

As a detector, we consider a Neyman-Person type detector whose ROC relation, under $\text{HOG}_I^{\text{SQL}}$, is given by [63]

$$P_D = P_{FA}^{1/(1+\zeta)}. \quad (5.29)$$

The quantization errors induced by the finite resolution of the sensor is modeled by the measurement noise, $v(k)$. Assuming that the true measurement is uniformly distributed in the resolution cell [4, pp. 472], the error covariance of $v(k)$ is taken as

$$R = \begin{bmatrix} (\Delta r_\xi/\sqrt{12})^2 & 0 \\ 0 & (\Delta r_\eta/\sqrt{12})^2 \end{bmatrix} \quad (5.30)$$

for all k , where Δr_ξ and Δr_η are the range resolutions, assumed 50 m , in East and North directions, respectively.

We use two elemental PDAF filters, named as PDAF-Q001 and PDAF-Q3, which use a second order linear kinematic model (WNA) with process noise standard deviations of $q = 0.01 \text{ m/s}^2$ and $q = 3 \text{ m/s}^2$, respectively. Each filter is initialized with *two point differencing* [18] method. These elemental filters are used either stand alone as in the heuristic approach presented in Section 5.2.1, or as *modules* in a multiple model filtering structure. But in any case, they are designed to track the target in its quiescent and maneuvering modes, respectively.¹² Note that the maneuvering model filter, PDAF-Q3 is designed to match (conservatively) for the maximum maneuver expected, i.e., $\sim 2.6 \text{ m/s}^2$ in the scenario.

As a multiple model filtering structure, we use an IMM filter whose Markov chain transition matrix is given by

$$\Pi = \begin{bmatrix} 1 - 1/\text{E}[\tau_Q] & 1/\text{E}[\tau_Q] \\ 1/\text{E}[\tau_M] & 1 - 1/\text{E}[\tau_M] \end{bmatrix}. \quad (5.31)$$

where $\text{E}[\tau_Q]$ and $\text{E}[\tau_M]$ are the expected *sojourn times* [18, p. 487] (in unit of sampling interval) of the underlying Markov chain in quiescent and maneuvering modes, respectively. For our case, we take these values as $\text{E}[\tau_Q] = 100$ and $\text{E}[\tau_M] = 50$. The initial model probabilities are taken as $\mu(0) = \begin{bmatrix} 0.5 & 0.5 \end{bmatrix}^T$.

¹² To track the maneuvering mode, a better approach is to use a coordinated turn (CT) model. This model is nonlinear and hence it requires to use extended Kalman filter (EKF) based PDAF.

Table 5.2: Experiment-I: Compared tracking systems.

System Name	Desired False Alarm Probability, P_{FA}^d
IMM-PDAF-E8	$P_{FA}(k) = 10^{-8}$
IMM-PDAF-E6	$P_{FA}(k) = 10^{-6}$
IMM-PDAF-E4	$P_{FA}(k) = 10^{-4}$
IMM-PDAF-E2	$P_{FA}(k) = 10^{-2}$
SWITCHED-PDAF	$P_{FA}(k)$ is set as explained in Section 5.2.1
IMM-PDAF-OP	$P_{FA}(k)$ is set as given in (5.27)

5.3.1 Experiment1: Comparison of Proposed Methods with Conventional Approaches

In this experiment, we compare the proposed DTOP schemes with conventional approaches, where IMM-PDAFs are used with *conventional detectors*.¹³ The compared tracking systems are listed in Table 5.2.

The first four tracking systems are conventional and use heuristically selected desired false alarm probabilities ranging from 10^{-8} to 10^{-2} . SWITCHED-PDAF and IMM-PDAF-OP are DTOP schemes proposed in Section 5.2.1 and 5.2.2, respectively.¹⁴ We perform 100 Monte Carlo runs over the scenario presented in Fig. 5.2 for each of the SNR conditions listed in Table 5.1. We accept that the track is lost for the i th Monte Carlo run, if the average estimation error for the i th Monte Carlo run exceeds the average measurement error for the i th Monte Carlo run. Then, the track loss percentage (TLP) is defined as the ratio of the number of Monte Carlo runs for which the track is lost to the total number of Monte Carlo runs performed. The results are given in Fig. 5.4 for different values of C_ζ .

Relying on a hard-switching mechanism between two PDAFs, the system SWITCHING-PDAF has relatively high TLP and performs not so well. The

¹³ By the conventional detector, we mean the detector whose desired false alarm probability, P_{FA}^d is set heuristically to a constant value.

¹⁴ Note that, IMM-PDAF-OP is based on the MRE approach. A comparison with the HYCA-based approach is given in the next section.

System Name	SNR Constant, C_ζ						
	10×10^{17}	9×10^{17}	8×10^{17}	7×10^{17}	6×10^{17}	5×10^{17}	4×10^{17}
KF-BASELINE	0	0	0	0	0	0	0
IMM-PDAF-E8	96	94	98	100	100	99	100
IMM-PDAF-E6	80	80	85	95	97	100	100
IMM-PDAF-E4	42	57	61	80	81	92	96
IMM-PDAF-E2	67	73	81	92	93	99	99
SWITCHED-PDAF	78	84	82	95	92	100	99
IMM-PDAF-OP	40	41	51	73	75	90	97

System Name	SNR Constant, C_ζ						
	10×10^{17}	9×10^{17}	8×10^{17}	7×10^{17}	6×10^{17}	5×10^{17}	4×10^{17}
KF-BASELINE	12.3515	12.1405	12.1534	12.0800	12.0239	12.1279	12.1829
IMM-PDAF-E8	17.5725	19.0719	17.8586	N/A	N/A	17.4377	N/A
IMM-PDAF-E6	18.9671	18.8323	19.0789	19.7609	18.2498	N/A	N/A
IMM-PDAF-E4	19.2023	18.8086	19.4615	19.5313	19.5268	18.6406	19.6058
IMM-PDAF-E2	18.8176	19.5101	18.3066	19.3564	17.4124	18.9084	15.8702
SWITCHED-PDAF	18.0528	18.4181	18.5075	18.5876	19.1925	N/A	15.3165
IMM-PDAF-OP	18.2771	18.4509	18.8909	19.1967	18.7658	18.6134	16.4778

Figure 5.4: TLPs [%] (the above table), and average RMS position errors [m] (the below table) for different values of the SNR constant, C_ζ .

multiple model filtering integrated extension, IMM-PDAF-OP, on the other hand, shows a robust behavior in terms of TLP. Note that the average RMS position error values of the systems are very close to each other and do not give much differentiating information about performance of the algorithms.

The false alarm probabilities suggested by the proposed DTOP schemes are given in Fig. 5.5. Note that the suggested false alarm probabilities of the algorithms are close to each other. Since the heuristic approach, SWITCHING-PDAF sets its false alarm to 1×10^{-6} in its transition mode E_0 , there are jumps in these regions. Actually they are these jumps that make the heuristic algorithm prone to track loss. Another heuristic but better approach would be to use the most recent false alarm value in these regions. This may prevent the jumps in the suggested false alarm probability. Note that during the maneuvering part of the motion which corresponds to the time steps between 51 and 100, dynamic threshold optimizations suggest lower values for the desired false alarm probability as compared to non-maneuvering part. This is mainly due to an increase in the volume of the validation gate during the maneuver.

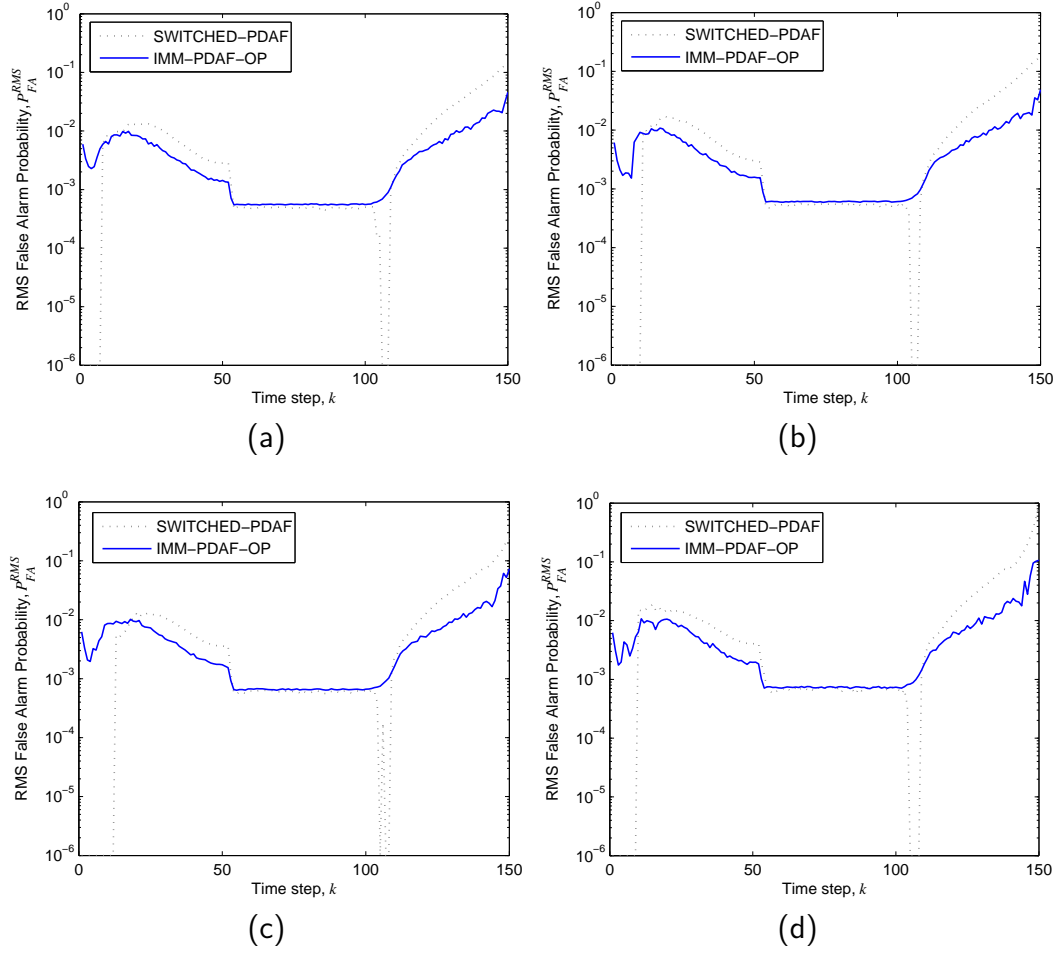


Figure 5.5: The false alarm probabilities suggested by the proposed DTOP schemes for (a) $C_\zeta = 1 \times 10^{18} m^4$, (b) $C_\zeta = 9 \times 10^{17} m^4$, (c) $C_\zeta = 8 \times 10^{17} m^4$ and (d) $C_\zeta = 7 \times 10^{17} m^4$ cases. Note that except from the transition mode, E_0 the false alarm probabilities suggested by SWITCHING-PDAF are close to those suggested by IMM-PDAF-OP algorithm.

Table 5.3: Experiment-II: Compared tracking systems.

System Name	Desired False Alarm Probability, P_{FA}^d
IMM-PDAF-OP-MRE	$P_{FA}(k)$ is set as given in (5.27)
IMM-PDAF-OP-HYCA	$P_{FA}(k)$ is set as given in (5.23) where $\bar{P}^j(k k) \triangleq \bar{P}_{HYCA}^j(k k)$

5.3.2 Experiment2: Comparison of MRE and HYCA Based Approaches

The optimal approach IMM-PDAF-OP in the previous experiment is based on MRE approach. As mentioned in Section 5.2.2, the one based on the HYCA approach is also possible. In this experiment, we compare these two approaches. The compared tracking systems are listed in Table 5.3.

We have conducted 100 Monte Carlo runs for $C_\zeta = 1 \times 10^{18}$ case. The performances of the algorithms are presented in Fig. 5.6. Note that MRE and HYCA based DTOP schemes have very similar performances and are superior to the heuristic extension, SWITCHING-PDAF and conventional approaches.

The suggested false alarm probabilities of the proposed dynamic optimization schemes are given in Fig. 5.7. Note that HYCA-based algorithm suggests consistently lower false alarm probabilities. This is advantageous because it leads to lower load for the radar data processor. However, this gain is compensated by the computational requirements of the HYCA-based optimization which is approximately 10 times higher than that of the MRE-based approach.

5.4 Conclusion

In this chapter, the ideas applied previously for optimization of detection thresholds in non-maneuvering target tracking in clutter are extended to maneuvering target tracking case.

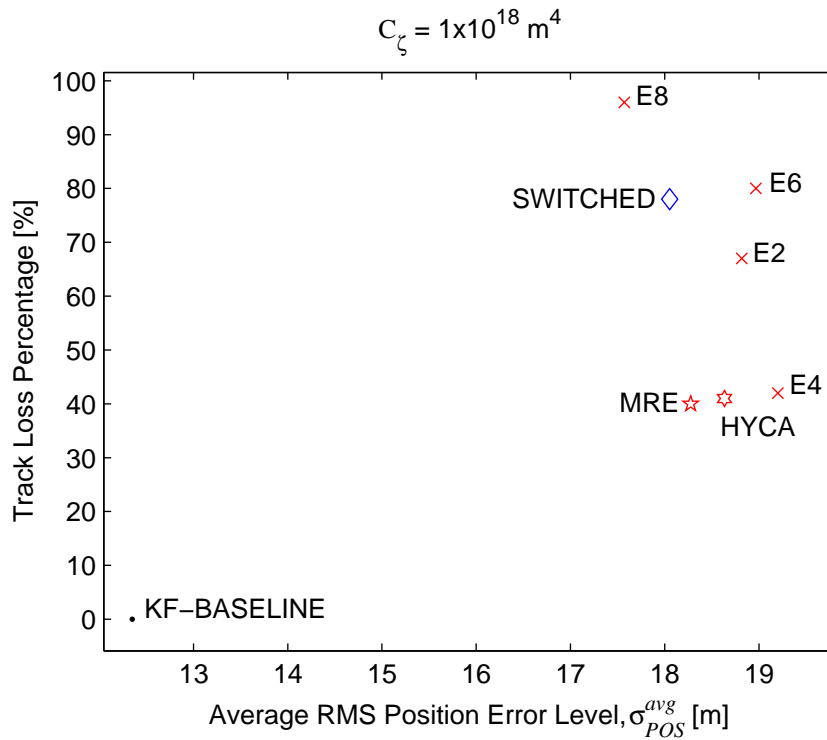


Figure 5.6: The performances of the algorithms in terms of TLP and average RMS position error. The point “EX” denotes the performance of the conventional system for which the desired false alarm probability is set to 10^{-X} .

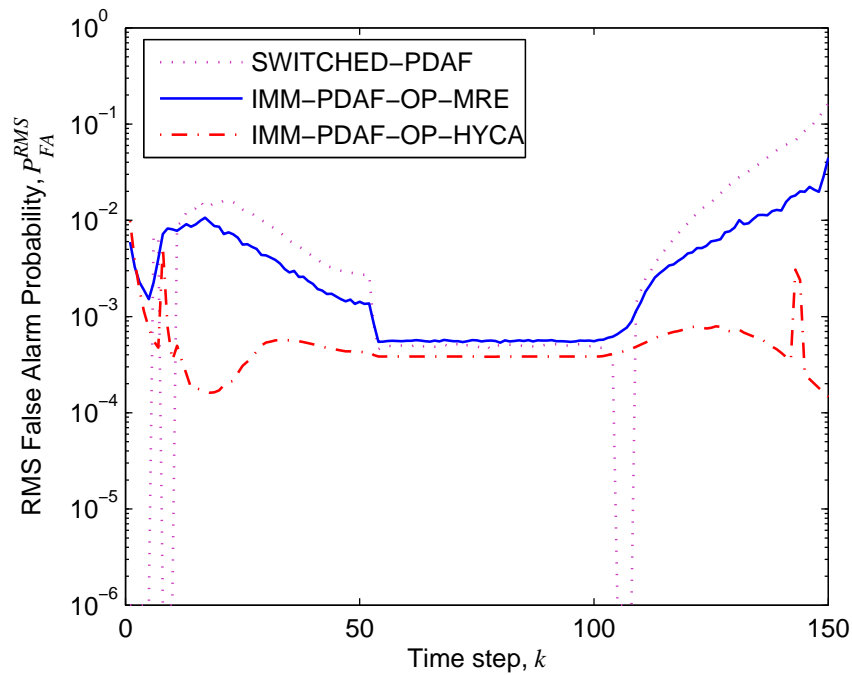


Figure 5.7: The suggested false alarm probabilities of the proposed solutions.

The first extension is a heuristic approach based on a *hard-switching* mechanism between two DTOP schemes for the PDAF. The second extension, on the other hand, is fully integrated into multiple model filtering structures and utilizes *soft* switching mechanism inherently available in them.

It is experimentally observed that the heuristic approach does not give better results than conventional approaches where the desired false alarm probabilities are kept constant. Although its suggested false alarm probability follows that of the fully integrated extension, it makes sharp jumps in its transition mode leading to high TLP. The integrated extension performs much better than the heuristic and conventional approaches and it makes the multiple model filtering algorithms more robust against *track loss*.

The integrated extension can be derived with either MRE or HYCA approximations. It is observed that this does not affect the final performance of the algorithm. Although HYCA-based integration results in lower false alarm probabilities, so less load for the radar to handle false tracks, this advantage may disappear due to higher computational requirements of HYCA-based optimization.

CHAPTER 6

DISCUSSION AND FUTURE WORK

In this thesis, a theoretical and an experimental framework has been presented for joint optimization of detector and tracker subsystems. More specifically, the optimal determination of the desired false alarm probability of the detector is investigated in a tracker-aware manner. This exciting problem, which can be considered within the context of more general topic of cognitive radar, is called *tracker-aware detection threshold optimization* (TA-DETOP) by the author. The problem and possible improvements are presented in two domains.

In the first domain, TA-DETOP problem is considered for non-maneuvering target tracking, particularly for the probabilistic data association filtering (PDAF) case. There were some prior attempts to this problem, but to the best of author's knowledge, comparison of these solution schemes is not available in the literature. After categorizing the existing and newly proposed solutions as *static* and *dynamic* optimization schemes, as the first contribution of the thesis, a comprehensive comparison of TA-DETOP schemes is presented in a unified experimental and theoretical framework. Contrary to expectations, the results concluded that only marginal gains can be achieved by HYCA-based approaches as compared to MRE-based ones. Moreover, it is observed that there exists a trade-off between having low track loss percentage (TLP) vs. having low steady-state tracking error.¹ The dynamic schemes are found to be well-located in this trade-off by providing considerably low TLP and low

¹ These measures can be seen also as transient vs. steady-state performance, respectively.

level of steady-state estimation error. The cost paid for this achievement is the computational complexity. Optimizing the false alarm probability at every time step, it turns out that dynamic schemes are computationally much more expensive than their static counterparts. As the second contribution of the thesis, an approximate closed-form solution is found for the MRE-based dynamic optimization scheme to partially overcome this issue. Although the solution is given only for the Neyman-Pearson (NP) detector case, in author's opinion, it can be applied for other practically used detection systems, which mimic asymptotically the NP detector, such as, cell averaging constant false alarm rate (CA-CFAR) system. Apart from its computational efficiency, the proposed closed-form solution also gives some useful insides into the problem. The most important implication is that it provides a theoretical lower bound on the detection SNR concerning when the whole tracking system should be switched to the track before detect (TBD) mode.

In the second domain of improvements, TA-DETOP problem is formulated for maneuvering target tracking. By extending the ideas of the first domain, two dynamic optimization schemes are presented. The first scheme is a heuristic approach and seems to not provide considerable improvement over the conventional systems where the false alarm is kept constant. The second scheme, on the other hand, is truly an extension of the dynamic optimization schemes applied to the PDAF to multiple model filtering structures. Experimental results show that this extension improves the robustness of the IMM-PDAF against track loss.

In addition to the contributions presented, this thesis also gives rise to new research directions for future studies. The ideas used in the detection threshold optimization sections of the thesis are based on MRE and HYCA methodologies for the PDAF. The NSPP algorithms for other tracking filters, such as, the nearest neighbor filter (NNF) or the strongest neighbor filter (SNF) are already available in the literature. So a quick idea may be to apply these NSPP techniques to the detection threshold optimization problem, if not applied yet.

Furthermore, new NSPP algorithms can also be proposed. Especially, the one for the IMM-PDAF deserve some attention. Then, it would be worthwhile to compare the optimization schemes relying directly on this NSPP methodology and the ones presented in this thesis.

An interesting and also a challenging extension is for the case of tracking multiple targets. When two tracks corresponding to two targets overlap, optimal determination of the detection threshold seems to be a challenging problem.

Another important point to note is the problem of unknown SNR situation. In all the detection optimization schemes, SNR is assumed to be known, but this is clearly not the case in practice. Therefore, SNR should be estimated. In this case, the TA-DETOP problem is coupled with the online SNR estimation which brings extra challenges to the problem.

REFERENCES

- [1] S. B. Gelfand, T. E. Fortmann, and Y. Bar-Shalom, "Adaptive detection threshold optimization for tracking in clutter," *IEEE Transactions on Aerospace and Electronic Systems*, vol. 32, pp. 514–523, April 1996.
- [2] M. A. Richards, *Fundamentals of Radar Signal Processing*. McGraw-Hill, 2005.
- [3] S. S. Blackman and R. Popoli, *Design and Analysis of Modern Tracking Systems*. Norwood, MA: Artech House, 1999.
- [4] Y. Bar-Shalom and X. R. Li, *Multitarget-Multisensor Tracking: Principles and Techniques*. Box U-157, Storrs, CT 06269-3157: YBS Publishing, 1995.
- [5] T. E. Fortmann, Y. Bar-Shalom, M. Scheffe, and S. Gelfand, "Detection thresholds for tracking in clutter – A connection between estimation and signal processing," *IEEE Transactions on Automatic Control*, vol. AC-30, no. 3, pp. 221–229, March 1985.
- [6] X. R. Li and Y. Bar-Shalom, "Stability evaluation and track life of the PDAF for tracking in clutter," *IEEE Transactions on Automatic Control*, vol. 36, pp. 588–602, May 1991.
- [7] —, "Detection threshold selection for tracking performance optimization," *IEEE Transactions on Aerospace and Electronic Systems*, vol. 30, pp. 742–749, July 1994.
- [8] P. Willett, R. Niu, and Y. Bar-Shalom, "Integration of Bayes detection with target tracking," *IEEE Transactions on Signal Processing*, vol. 49, no. 1, pp. 17–29, January 2001.
- [9] S. Haykin, "Cognitive radar networks," in *1st IEEE International Workshop on Computational Advances in Multi-Sensor Adaptive Processing*, December 2005, pp. 1–3.
- [10] N. A. Goodman, P. R. Venkata, and M. A. Neifeld, "Adaptive waveform design and sequential hypothesis testing for target recognition with active sensors," *IEEE Journal of Selected Topics in Signal Processing*, vol. 1, pp. 105–113, June 2007.
- [11] S. Haykin, "Cognitive radar: A way of the future," *IEEE Signal Processing Magazine*, vol. 23, pp. 30–40, January 2006.

- [12] D. J. Kershaw and R. J. Evans, "Optimal waveform selection for tracking systems," *IEEE Transactions on Information Theory*, vol. 40, no. 5, pp. 1536–1550, September 1994.
- [13] —, "Waveform selective probabilistic data association," *IEEE Transactions on Aerospace and Electronic Systems*, vol. 33, pp. 1180–1188, October 1997.
- [14] S.-M. Hong, R. J. Evans, and H.-S. Shin, "Optimization of waveform and detection threshold for range and range-rate tracking in clutter," *IEEE Transactions on Aerospace and Electronic Systems*, vol. 41, pp. 17–33, January 2005.
- [15] P. Willett, R. Niu, and Y. Bar-Shalom, *Multitarget-Multisensor Tracking: Applications and Advances Volume III*. Artech House, Inc., 2000, ch. 9, pp. 459–498.
- [16] B. D. O. Anderson and J. B. Moore, *Optimal Filtering*. Englewood Cliffs, NJ: Prentice-Hall, 1979.
- [17] P. R. Kumar and P. Varaiya, *Stochastic Systems: Estimation, Identification and Adaptive Control*. Englewood Cliffs, New Jersey: Prentice-Hall, Inc., 1986.
- [18] Y. Bar-Shalom, X. R. Li, and T. Kirubarajan, *Estimation with Applications to Tracking and Navigation*. John Wiley & Sons, Inc., 2001.
- [19] X. R. Li, *Multitarget-Multisensor Tracking: Applications and Advances Volume III*. Artech House, Inc., 2000, ch. 10, pp. 499–567.
- [20] X. R. Li and Y. Bar-Shalom, "A hybrid conditional averaging technique for performance prediction of algorithms with continuous and discrete uncertainties," in *Proceedings of the American Control Conference*, Maryland, June 1994, pp. 1530–1534.
- [21] J. H. Taylor, "The Cramér–Rao estimation error lower bound computation for deterministic nonlinear systems," *IEEE Transactions on Automatic Control*, vol. AC-24, no. 2, pp. 343–344, April 1979.
- [22] T. H. Kerr, "Status of cr-like lower bounds for nonlinear filtering," *IEEE Transactions on Aerospace and Electronic Systems*, vol. 25, no. 5, pp. 590–601, September 1989.
- [23] P. Tichavský, C. H. Muravchik, and A. Nehorai, "Posterior Cramér–Rao bounds for discrete-time nonlinear filtering," *IEEE Transactions on Signal Processing*, vol. 46, no. 5, pp. 1386–1396, May 1998.
- [24] A. Farina, B. Ristic, and L. Timmoneri, "Cramér-Rao bound for nonlinear filtering with $P_d < 1$ and its application to target tracking," *IEEE Transactions on Signal Processing*, vol. 50, pp. 1916–1924, August 2002.

- [25] Y. Boers and H. Driessen, “Modified Riccati equation and its application to target tracking,” *IEE Proceedings on Radar Sonar and Navigation*, vol. 153, pp. 7–12, February 2006.
- [26] —, “Results on the modified Riccati equation: Target tracking applications,” *IEEE Transactions on Aerospace and Electronic Systems*, vol. 42, pp. 379–384, January 2006.
- [27] M. Hernandez, B. Ristic, A. Farina, and L. Timmoneri, “A comparison of two Cramér-Rao bounds for nonlinear filtering with $P_d < 1$,” *IEEE Transactions on Signal Processing*, vol. 52, no. 9, pp. 2361–2370, September 2004.
- [28] I. Rapoport and Y. Oshman, “A Cramér-Rao-type estimation lower bound for systems with measurement faults,” *IEEE Transactions on Automatic Control*, vol. 50, no. 50, pp. 1234–1245, September 2005.
- [29] B. Sinopoli, L. Schenato, M. Franceschetti, K. Poola, M. I. Jordan, and S. S. Sastry, “Kalman filtering with intermittent observations,” *IEEE Transactions on Automatic Control*, vol. 49, pp. 1453–1464, September 2004.
- [30] C. Jauffret and Y. Bar-Shalom, “Track formation with bearing and frequency measurements in clutter,” *IEEE Transactions on Aerospace and Electronic Systems*, vol. 26, no. 6, pp. 999–1010, November 1990.
- [31] X. Zhang, P. Willet, and Y. Bar-Shalom, “Dynamic Cramér-Rao bound for target tracking in clutter,” *IEEE Transactions on Aerospace and Electronic Systems*, vol. 41, no. 4, pp. 1154–1167, October 2005.
- [32] M. L. Hernandez, A. Farina, and B. Ristic, “Pcrblb for tracking in cluttered environments: Measurement sequence conditioning approach,” *IEEE Transactions on Aerospace and Electronic Systems*, vol. 42, no. 2, pp. 680–704, April 2006.
- [33] T. Bréhard and J.-P. L. Cadre, “Closed-form posterior Cramér-Rao bounds for bearings-only tracking,” *IEEE Transactions on Aerospace and Electronic Systems*, vol. 42, no. 4, pp. 1198–1223, October 2006.
- [34] B. Xu, Z. Wu, and Z. Wang, “On the Cramér-Rao lower bound for biased bearings-only maneuvering target tracking,” *Elsevier Signal Processing*, vol. 87, no. 12, pp. 3175–3189, December 2007.
- [35] F. E. Daum, “Bounds on performance for multiple target tracking,” *IEEE Transactions on Automatic Control*, vol. 35, no. 4, pp. 443–446, April 1990.
- [36] B. Ristic, A. Farina, and M. Hernandez, “Cramér-Rao lower bound for tracking multiple targets,” *IEE Proceedings on Radar Sonar and Navigation*, vol. 151, pp. 129–134, 2004.

- [37] C. Hue, J.-P. L. Cadre, and P. Pérez, “Posterior Cramer–Rao bounds for multi-target tracking,” *IEEE Transactions on Aerospace and Electronic Systems*, vol. 42, no. 1, pp. 37–49, January 2006.
- [38] W. F. Leven, “Approximate Cramér-Rao bounds for multiple target tracking,” Ph. D. Thesis, Georgia Institute of Technology, May 2006.
- [39] M. L. Hernandez, B. Ristic, A. Farina, T. Sathyan, and T. Kirubarajan, “Performance measure for Markovian switching systems using best-fitting Gaussian distributions,” *IEEE Transactions on Aerospace and Electronic Systems*, vol. 44, no. 2, pp. 724–747, April 2008.
- [40] Y. Bar-Shalom, L. J. Campo, and P. B. Luh, “From receiver operating characteristic to system operating characteristic: Evaluation of a track formation system,” *IEEE Transactions on Automatic Control*, vol. 35, no. 2, pp. 172–179, February 1990.
- [41] S. R. Rogers, “Diffusion analysis of track loss in clutter,” *IEEE Transactions on Aerospace and Electronic Systems*, vol. 27, no. 2, pp. 380–387, March 1991.
- [42] S. Mori, K.-C. Chang, C.-Y. Chong, and K.-P. Dunn, “Prediction of track purity and track accuracy in dense target environments,” *IEEE Transactions on Automatic Control*, vol. 40, no. 5, pp. 953–959, May 1995.
- [43] X. R. Li and Y. Bar-Shalom, “Performance prediction of the interacting multiple model algorithm,” *IEEE Transactions on Aerospace and Electronic Systems*, vol. 29, no. 3, pp. 755–771, July 1993.
- [44] R. E. Kalman, “A new approach to linear filtering and prediction problems,” *Transactions of the ASME, Journal of Basic Engineering*, vol. 82, pp. 34–45, March 1960.
- [45] Y. Bar-Shalom and E. Tse, “Tracking in a cluttered environment with probabilistic data association,” *Automatica*, vol. 11, pp. 451–460, 1975.
- [46] C. W. Frei, “A comparison of parallel and sequential implementations of a multisensor multitarget tracking algorithm,” Master’s thesis, Northwestern University, Evanston, IL, May 1995.
- [47] X. R. Li and Y. Bar-Shalom, “Tracking in clutter with nearest neighbor filters: Analysis and performance,” *IEEE Transactions on Aerospace and Electronic Systems*, vol. 32, no. 3, pp. 995–1010, July 1996.
- [48] X. R. Li, “Tracking in clutter with strongest neighbor measurements – Part I: Theoretical analysis,” *IEEE Transactions on Aerospace and Electronic Systems*, vol. 43, no. 11, pp. 1560–1578, November 1998.

- [49] C. Rago, P. Willett, and Y. Bar-Shalom, "Detection-tracking performance with combined waveforms," *IEEE Transactions on Aerospace and Electronic Systems*, vol. 34, no. 2, pp. 612–624, April 1998.
- [50] S. P. Sira, A. Papandreou-Suppappola, and D. Morrell, "Dynamic configuration of time-varying waveforms for agile sensing and tracking in clutter," *IEEE Transactions on Signal Processing*, vol. 55, no. 7, pp. 3207–3217, July 2007.
- [51] L. Y. Pao and L. Trailović, "The optimal order of processing sensor information in sequential multisensor fusion algorithms," *IEEE Transactions on Automatic Control*, vol. 45, no. 8, pp. 1532–1536, August 2000.
- [52] U. D. Ramdaras and F. G. J. Absill, "Target tracking in sensor networks: Criteria for sensor selection," in *IEEE Radar Conference*, April 2007, pp. 192 – 196.
- [53] —, "Sensor selection: the modified Riccati equation approach compared with other selection schemes," in *International Conference on Information Fusion*, July 2007, pp. 1–6.
- [54] M. Kalandros and L. Y. Pao, "Multisensor covariance control strategies for reducing bias effects in interacting target scenarios," *IEEE Transactions on Aerospace and Electronic Systems*, vol. 41, no. 1, pp. 153–173, January 2005.
- [55] Y. H. Jung and S.-M. Hong, "Modeling and parameter optimization of agile beam radar tracking," *IEEE Transactions on Aerospace and Electronic Systems*, vol. 39, no. 1, pp. 13–33, January 2003.
- [56] M. Şamil Aslan, A. Saranlı, and B. Baykal, "Optimal tracker-aware radar detector threshold adaptation: A closed-form solution," in *International Conference on Information Fusion*, June 2008, pp. 470–477.
- [57] —, "A closed form optimum solution for the tracker-aware Neyman-Pearson detector," Submitted to *IEEE Transactions on Aerospace and Electronic Systems*.
- [58] M. Şamil Aslan and A. Saranlı, "A comparison of tracker-aware detector threshold optimization schemes for tracking in clutter," Submitted to *IEEE Transactions on Aerospace and Electronic Systems*.
- [59] —, "Tracker-aware detector threshold optimization for maneuvering targets in clutter," To be submitted to *IEEE Transactions on Aerospace and Electronic Systems*.
- [60] A. Houles and Y. Bar-Shalom, "Multisensor tracking of a maneuvering target in clutter," *IEEE Transactions on Aerospace and Electronic Systems*, vol. AES-25, no. 2, pp. 176–189, March 1989.

- [61] D. R. Vaughan, “A nonrecursive algebraic solution for the discrete Riccati equation,” *IEEE Transactions on Automatic Control*, pp. 597–599, October 1970.
- [62] D. J. Kershaw and R. J. Evans, “A contribution to performance prediction for probabilistic data association tracking filters,” *IEEE Transactions on Aerospace and Electronic Systems*, vol. 32, no. 3, pp. 1143–1148, July 1996.
- [63] P. K. Varshney, *Distributed Detection and Data Fusion*. Springer Verlag, New York, Inc., 1997.
- [64] H. A. P. Blom and Y. Bar-Shalom, “The interacting multiple model algorithm for systems with Markovian switching coefficients,” *IEEE Transactions on Automatic Control*, vol. 33, no. 8, pp. 780–783, August 1988.
- [65] S.-M. Hong and H.-S. Shin, “An analytic approximation of information reduction factor for performance prediction of PDA tracking,” in *Proceedings of the 41st SICE Annual Conference*, vol. 3, 2002, pp. 1447–1449.
- [66] M. Bazaraa, H. Sherali, and C. Shetty, *Nonlinear Programming Theory and Algorithms*. Wiley, 2006.
- [67] Y. Boers and J. N. Driessen, “Particle filter based detection for tracking,” in *Proceedings of the American Control Conference*, vol. 6, Arlington, VA, June 2001, pp. 4393–4397.
- [68] D. J. Salmond and H. Birch, “A particle filter for track-before-detect,” in *Proceedings of the American Control Conference*, vol. 5, Arlington, VA, June 2001, pp. 3755–3760.
- [69] M. K. Uner and P. K. Varshney, “Distributed CFAR detection in homogeneous and nonhomogeneous backgrounds,” *IEEE Transactions on Aerospace and Electronic Systems*, vol. 32, pp. 84–97, January 1996.
- [70] T. E. Fortmann, Y. Bar-Shalom, and M. Scheffe, “Sonar tracking of multiple targets using joint probabilistic data association,” *IEEE Journal of Ocean Engineering*, vol. OE-8, no. 3, pp. 173–184, July 1983.
- [71] D. B. Reid, “An algorithm for tracking multiple targets,” *IEEE Transactions on Automatic Control*, vol. AC-24, no. 6, pp. 843–854, December 1979.
- [72] Y. Bar-Shalom and K. Birmiwal, “Consistency and robustness of PDAF for target tracking in cluttered environments,” *Automatica*, vol. 19, pp. 431–437, July 1983.
- [73] Y. Bar-Shalom and W. D. Blair, Eds., *Multitarget-Multisensor Tracking: Applications and Advances Volume III*. Artech House, Inc., 2000.

- [74] X. Wang, S. Challa, and R. Evans, “Gating techniques for maneuvering target tracking in clutter,” *IEEE Transactions on Aerospace and Electronic Systems*, vol. 38, no. 3, pp. 1087–1097, July 2002.
- [75] U. Orguner, “Improved state estimation for jump markov linear systems,” Ph. D. Thesis, Middle East Technical University, Ankara, December 2006.
- [76] D. K. Barton, “Land clutter models for radar design and analysis,” *Proceedings of IEEE*, vol. 73, no. 2, pp. 198–204, February 1985.
- [77] D. A. Shnidman, “Comparison of low angle radar clutter models,” *IEEE Transactions on Aerospace and Electronic System*, vol. 41, no. 2, pp. 736–746, April 2005.
- [78] —, “Generalized radar clutter model,” *IEEE Transactions on Aerospace and Electronic System*, vol. 35, no. 3, pp. 857–865, July 1999.
- [79] E. Mazor, A. Averbuch, Y. Bar-Shalom, and J. Dayan, “Interacting multiple model methods in target tracking: A survey,” *IEEE Transactions on Aerospace and Electronic Systems*, vol. 34, no. 1, pp. 103–123, January 1998.

APPENDIX A

TRACKING AND FUSION SIMULATOR (TAFSIM)

This appendix presents the tracking and fusion simulator (TAFSIM) developed by the author as a part of the simulation studies conducted throughout the thesis. TAFSIM consists of a set of m-files written in MATLAB and a graphical user interface (GUI) for easy usage. It allows to do simulations about tracking non-maneuvering (or maneuvering), single (or multiple) target(s) in clutter (or in clutter-free environment) with single (or multiple) radar sensor(s).

The main functionalities of the simulator can be summarized as follows:

- Loading/saving specific scenarios (different target/radar configurations).
- Loading/saving problem specific filters running on radars.
- Doing animated simulations with pause/single-step options.
- Doing non-animated Monte Carlo simulations.
- Displaying the results of the simulations in various analysis plots, such as RMS position/velocity error, track loss percentage etc.

A snapshot view of the main simulator window is given in Fig. A.1.

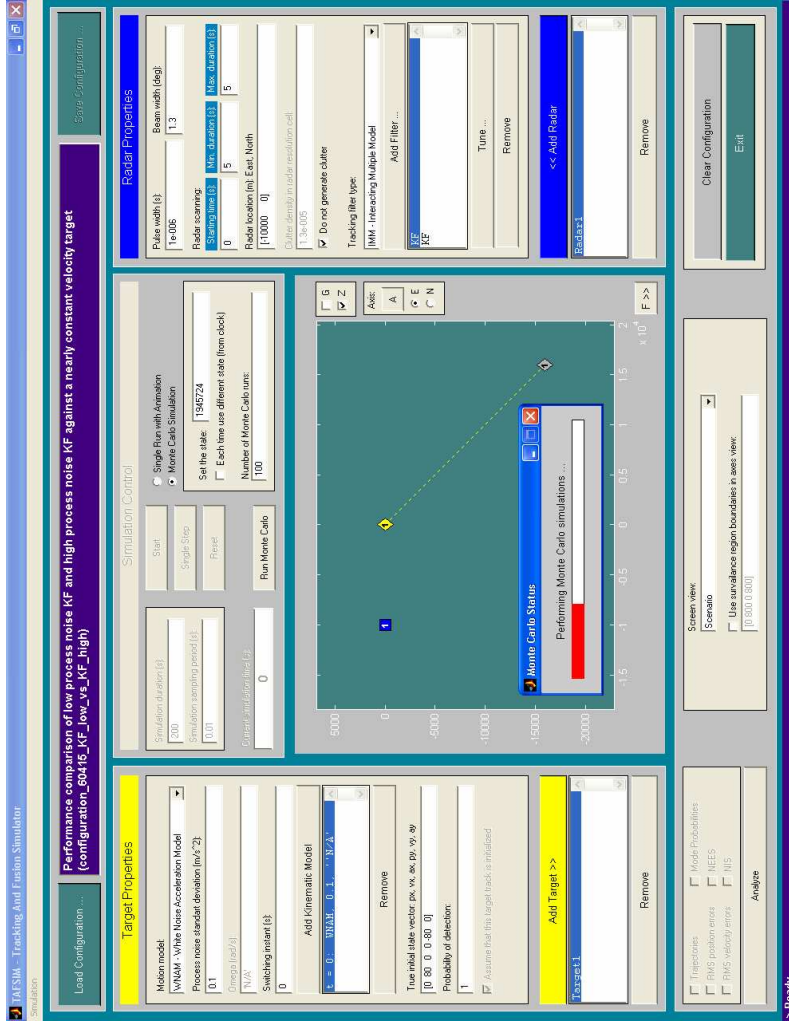


Figure A.1: Tracking and Fusion Simulator (TAFSIM): Main window. The right and the left part of the GUI is related with the radar and target properties, respectively. At the middle, there is a main tracking screen showing an animated target tracking if single simulation with animation is selected. The upper part of the GUI consists of some buttons for loading and saving the configuration. In the lower part, there exists analysis buttons which allows user to see and analyze some performance measures like RMS position error, RMS velocity error etc.

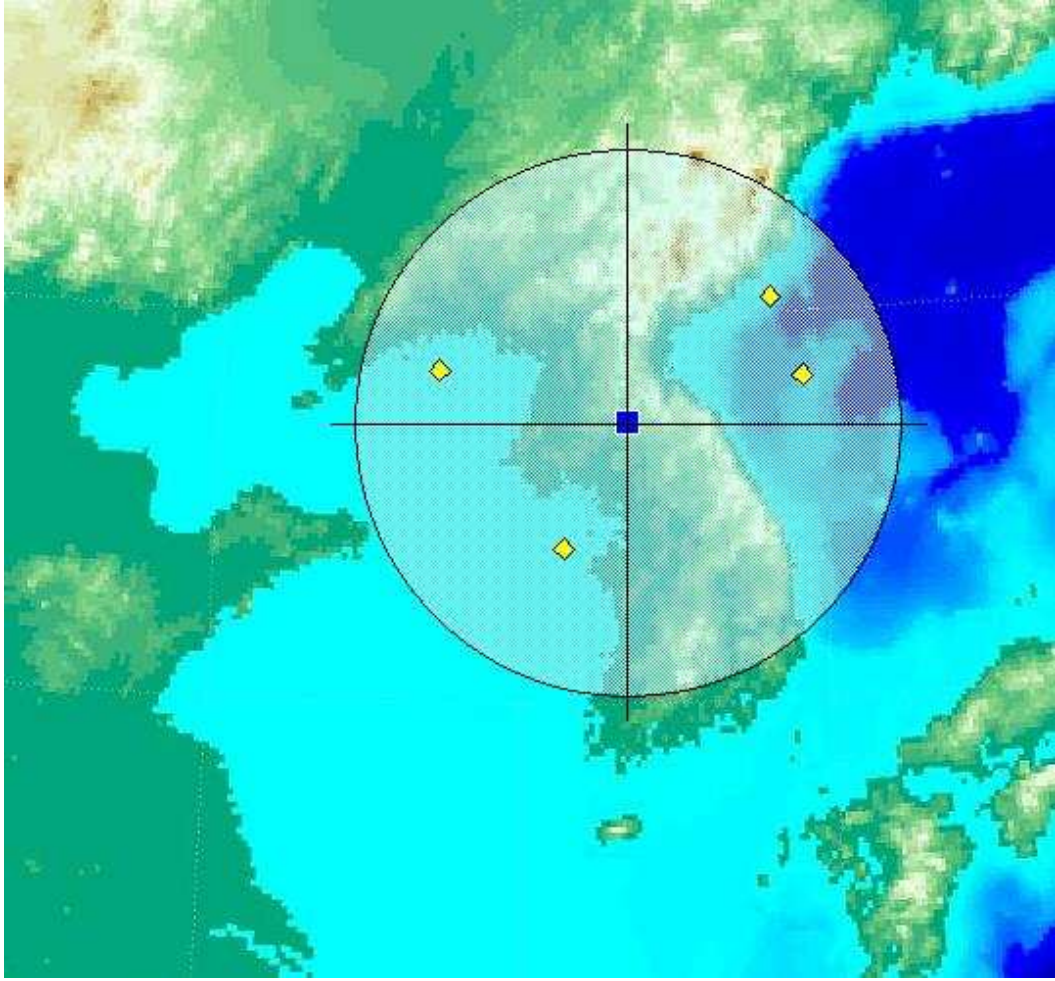


Figure A.2: 2D radar surveillance region, the square and diamond markers correspond to the radar and targets, respectively.

In TAFSIM, we model two dimensional (2D) rotating surveillance radars which periodically scan a *surveillance region*, defined as a circle centered at the radar location and with radius equal to the maximum range spec of the radar. An illustrative picture is shown in Fig. A.2.

Radar target tracking is accomplished by processing the detections obtained from scanning the surveillance region periodically. This type of radar operation is called *track-while-scan* (TWS). The radar measurements lie in a 2D measurement space where the dimensions are range and bearing (azimuth angle). In data generation, we have modeled radar-scanning, target originated measurement generation and clutter generation. In generating measurements,

a parametric modeling (rather than signal modeling) approach is considered. That is, we have just put some accepted models for each phenomenon and produced corresponding radar measurements.

A.1 Modeling Target Kinematics

In TAFSIM, target kinematics is modeled by a state space representation of the form

$$x(k+1) = F(k)x(k) + G(k)v(k) \quad (\text{A.1})$$

with process noise $v(k) \sim \mathcal{N}(0, Q(k))$. Here, $F(k)$ and $G(k)$ are state transition matrix and process noise gain matrix, respectively. Most common kinematic models which are used in the tracking literature [18], [4] are implemented in TAFSIM. These are listed as follows.

- White noise acceleration (WNA) model, which is used when tracking nearly constant velocity targets.
- Wiener process acceleration (WPA) model, which is used when tracking nearly constant acceleration targets.
- Coordinated turn (CT) model, which is used when tracking bank-to-turn maneuvering targets.
- Nearly coordinated turn (NCT) model, which is used when the turn rate is modeled noisy, i.e., with some process noise component.
- Linear coordinated turn (LCT) model, which is used when the turn rate is assumed to be known by the filtering algorithm.

Radar scanning:		
Starting time (s):	Min. duration (s):	Max. duration (s):
0	5	5

Figure A.3: Radar scanning parameters.

A.2 Modeling Radar Scanning

The radar is assumed to start scanning at a specified time and continue scanning until the end of the simulation. This scanning function is modeled by three parameters: Starting time (t_{start}), minimum duration (T_{min}), and maximum duration (T_{max}), as illustrated in in Fig. A.3.

Starting time is the time at which the radar starts scanning. By this definition, this parameter defines the “offset” between starting of scanning and simulation. Other parameters, minimum and maximum duration, define *scanning period* (T) of the radar. The scanning period (or usually called *sampling period*) is modeled as a random variable uniformly distributed between minimum and maximum duration values. If a constant sampling period is required in the simulation, minimum and maximum duration parameters should be set to the same value.

In our simulator, all the radar measurements are assumed to be available at the end of each scan. The radar is assumed to take a snapshot (sample) of the surveillance region at the end of each scan.¹ The time instants (or steps) at which the measurements are taken, denoted by t_k , $k = 1, 2, \dots$ can be expressed as

$$t_k = t_{k-1} + T_k \tag{A.2}$$

$$t_0 \triangleq t_{start} \tag{A.3}$$

where the k th sampling period is produced by

$$T_k = T_{min} + (T_{max} - T_{min})\tilde{a}_k. \tag{A.4}$$

¹ This is the usual approach in the research community and that is why the scanning period, T is often called “sampling” period.

Here, \tilde{a}_k is the k th realization of a random variable uniformly distributed between 0 and 1. Note that, when $T_{min} = T_{max} = T$, the sampling period becomes constant and equal to T .

A.3 Modeling Radar Measurements

The set of radar measurements taken during the k th scanning period is stored in $n_z \times m_k$ matrix defined by

$$Z(k) \triangleq \begin{bmatrix} z_1(k) & z_2(k) & \cdots & z_{m_k}(k) \end{bmatrix}^T. \quad (\text{A.5})$$

where $n_z = 2$ is the dimension of the measurement space and m_k is the number of received measurements during k th scanning period. Each column of this matrix corresponds to a single measurement (or detection) composed of range $[m]$ and bearing $[rad]$ components, i.e., $z_i(k) = \begin{bmatrix} r_i^m & \psi_i^m \end{bmatrix}^T$. At each time step k , the matrix $Z(k)$ is composed of two submatrices as

$$Z(k) \triangleq \begin{bmatrix} Z_T(k) & | & Z_C(k) \end{bmatrix}^T. \quad (\text{A.6})$$

where the first set of measurements $Z_T(k)$ denotes the target-originated measurements and the second set $Z_C(k)$ denotes the measurements due to clutter. Depending on the detection probabilities of each target and (spatial) clutter density, these matrices can be empty for an arbitrary time step.

A.3.1 Generating Target-Originated Measurements

Let us consider a specific simulation instant during the k th scanning period as illustrated in Fig.A.4a. *True range* (r) and *true bearing* (ψ) of the target at time step k are defined by

$$r(k) \triangleq \sqrt{\left(\xi^t(k) - \xi^r(k)\right)^2 + \left(\eta^t(k) - \eta^r(k)\right)^2} \quad (\text{A.7})$$

$$\psi(k) \triangleq \arctan\left(\frac{\eta^t(k) - \eta^r(k)}{\xi^t(k) - \xi^r(k)}\right), \quad (\text{A.8})$$

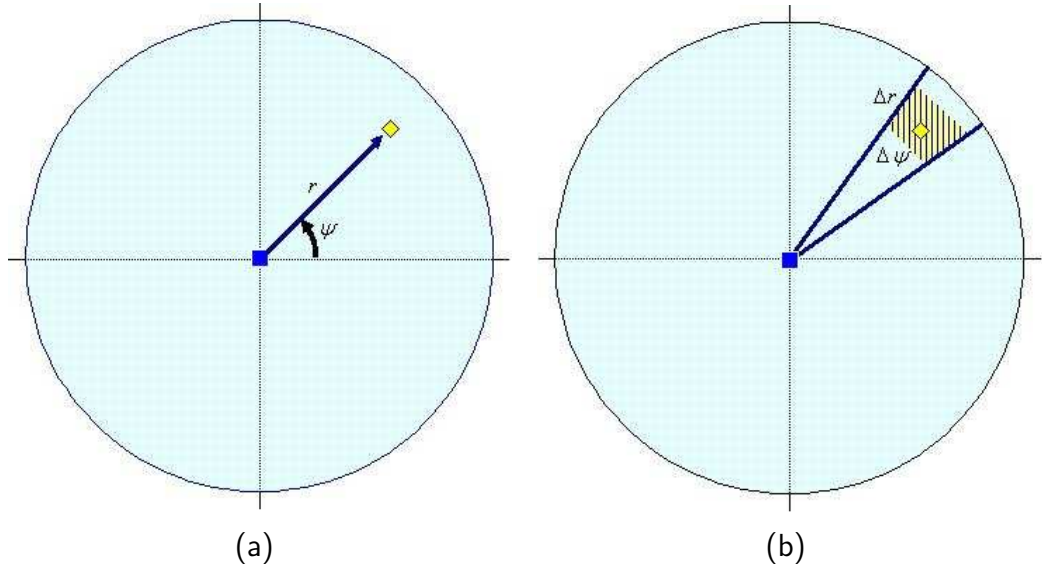


Figure A.4: Target-originated measurement: (a) True range, r and true bearing, ψ , and (b) radar resolution cell.

respectively where superscripts t and r refer to “target” and “radar”, respectively, and ξ and η correspond to East and North components of the position, respectively. In a realistic scenario, these true quantities may not be measured exactly due to finite range and angle resolutions of the radar and other system noises. This is illustrated in Fig. A.4b. The radar *resolution cell* is defined as a 2D closed region² describing the range and azimuth angle resolution of the radar. In TAFSIM, it is assumed that the true measurement is uniformly distributed in the resolution cell of the radar. Therefore, the standard deviations of the measurement error components in range and bearing are taken as $\sigma_r = \Delta r / \sqrt{12}$ and $\sigma_\psi = \Delta \psi / \sqrt{12}$. Here, the range resolution Δr is defined as

$$\Delta r \triangleq \frac{c \times \tau}{2} \quad (\text{A.9})$$

where $c \approx 3 \times 10^8$ m/s is the speed of light and τ is the radar pulse width. Furthermore, the azimuth angle resolution $\Delta \psi$ is taken as the horizontal beam width of the radar.

² In TAFSIM, we consider 2D radars whose measurement space consists of range and azimuth angle dimensions. For the radars whose measurement vector consists of some other components like elevation angle, Doppler frequency shift etc., the resolution cell should be defined accordingly.

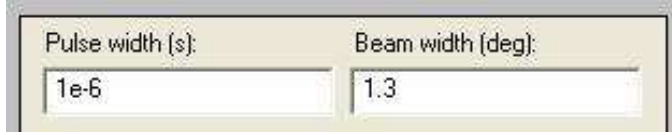


Figure A.5: Pulse and beam width parameters.

In TAFSIM, the user enters the pulse width and beam width parameters from the GUI as illustrated in Fig. A.5. Then, any target-originated measurement is produced by adding a measurement error noise vector to the true measurement vector as

$$z(k) \triangleq \begin{bmatrix} r^m(k) \\ \psi^m(k) \end{bmatrix} = \begin{bmatrix} r(k) \\ \psi(k) \end{bmatrix} + \begin{bmatrix} \tilde{r}(k) \\ \tilde{\psi}(k) \end{bmatrix} \quad (\text{A.10})$$

where $\tilde{r}(k)$ and $\tilde{\psi}(k)$ are the range measurement and azimuth measurement errors which are modeled as zero mean random variables with standard deviations, σ_r and σ_ψ , respectively.

Another point is that when the radar operates in fluctuating SNR situations, at some scanning periods, we may not get any measurement from a particular target or from all of the targets. Therefore, the target-originated measurement given in (A.10) may not always be available for the radar. This phenomenon is modeled by the probability of detection (P_D) parameter. In TAFSIM, the user can specify a detection probability P_D^t for each target $t = 1, 2, \dots, N_t$ where N_t is the number of targets. Then at each scanning period, the measurement originated from the target t is produced with a probability of P_D^t .

A.3.2 Generating the Measurements Due to Clutter

Clutter refers to unwanted radar returns. It may be caused by many reasons, like terrains, atmospheric conditions (rain), artificial objects (buildings), and even animals (birds). Modeling clutter is a wide topic and there are lots of work in the literature. Some of them are given in [76], [77], [78]. In these works, clutter is modeled from a signal-based perspective. Although such modeling of clutter is not considered in TAFSIM, we have adopted a reasonable clutter

model described in [4, p. 102] to be able to investigate real life target tracking problems. In this model, the whole phenomenon is modeled by two parameters:

- **Number of false detections:** The number of false detections (or false alarms) due to random clutter in the volume V , denoted by m_F , is modeled by a Poisson distribution random variable with probability mass function given by

$$\mu_F(m_F) \triangleq \frac{\exp(-\lambda V)(\lambda V)^{m_F}}{m_F!} \quad (\text{A.11})$$

where λ is the spatial clutter density and V is the volume of the measurement space under consideration.

- **Location of false detections:** Location of a false detection in the measurement space, denoted by z_F , is modeled by a random variable whose probability density function is given as

$$p(z_F) \triangleq \frac{1}{V}. \quad (\text{A.12})$$

In other words, any false detection is assumed to be uniformly distributed in the measurement space under concern.³

A.4 Implemented Tracking Filters

In TAFSIM various single sensor and multisensor tracking filters are implemented. These are listed below.

- **Single Sensor Filters:**
 - Kalman Filter (KF) with WNA and WPA models
 - Extended Kalman Filter (EKF) with NCT model

³ This is the region in which the measurement is known to lie. This can be, depending on the situation considered, either the radar's surveillance region or the target's validation region [4].

- Nearest Neighbor Filter (NNF)
- Probabilistic Data Association Filter (PDAF)
- Joint Probabilistic Data Association Filter (JPDAF)
- Interacting Multiple Model Filter (IMM)
- Interacting Multiple Model Probabilistic Data Association Filter (IMM-PDAF)
- Interacting Multiple Model Joint Probabilistic Data Association Filter (IMM-JPDAF)
- Interacting Multiple Model Nearest Neighbor Joint Probabilistic Data Association Filter (IMM-NNJPDAF)

- **Multisensor (Fusion-Capable) Filters:**

- Multisensor Probabilistic Data Association Filter (MSPDAF)
- Interacting Multiple Model Multisensor Probabilistic Data Association Filter (IMM-MSPDAF)

Before doing a simulation, the user can design the experiment either from the GUI, or from a configuration file. The configuration files are in the m-file format of MATLAB. These files allow the user to define his/her experiment from an easy-to-read text file and save it for future usage. A sample configuration file is shown in Fig. A.6. After the simulation is finished, the user can analyze the results over several performance measures such as RMS position error, RMS velocity error, model probabilities of IMM filter, etc.

APPENDIX B

PROBABILISTIC DATA ASSOCIATION FILTER

This appendix presents the assumptions and the algorithmic flow of the probabilistic data association filter (PDAF) [45], which is a single-scan cost-effective solution for tracking non-maneuvering targets in clutter.

B.1 Assumptions

The assumptions of the PDAF algorithm are as follows [4].

- The state of the target of interest, of dimension n_x , is assumed to make its transition in time according to the equation

$$x(k+1) = F(k)x(k) + v(k) \tag{B.1}$$

with the true (i.e., target originated) measurement, of dimension n_z , given by

$$z(k) = H(k)x(k) + w(k) \tag{B.2}$$

where $v(k)$ and $w(k)$ are zero-mean mutually independent white Gaussian noise sequences with known covariances $Q(k)$ and $R(k)$, respectively.

- At each time step k , the true measurement defined in (B.2) is available with a known detection probability possibly less than unity, i.e., $P_D < 1$, and in the presence of clutter, which gives rise to false measurements.

- The false measurements are assumed due to false alarm or clutter and are modeled as *independent identically distributed* (i.i.d.) with uniform spatial distribution over the measurement space under consideration, either the validation gate or the entire surveillance region.
- The number of false measurements (m_F) in the measurement space under consideration, either the validation gate or the entire surveillance region, is assumed to be a *Poisson* distributed random variable with probability mass function (pmf)

$$\mu_F(m_F) \triangleq \frac{\exp(-\lambda V) (\lambda V)^{m_F}}{m_F!} \quad (\text{B.3})$$

where λ is the spatial clutter density and V is the volume of the measurement space under consideration. This version of the PDAF is known as the *parametric* PDAF, as it requires the spatial clutter density parameter λ . The *non-parametric* PDAF is obtained either assuming a *diffuse* prior model for $\mu_F(\cdot)$ or simply replacing λ with m/V , where m is the number of validated measurements.

- At each time step k , the past information about the target state is summarized approximately by

$$p[x(k)|Z^{k-1}] = \mathcal{N}(x(k); \hat{x}(k|k-1), P(k|k-1)) \quad (\text{B.4})$$

where Z^{k-1} is the set of validated measurements through time $k-1$ and $\hat{x}(k|k-1)$ and $P(k|k-1)$ are the predicted state and predicted covariance, respectively.¹

B.2 Steps of the Algorithm

One cycle of the PDAF algorithm, whose block diagram is given in Fig. B.1, consists of the following steps:

¹ This is the fundamental assumption of the PDAF algorithm [6]. The actual pdf of the target state is a Gaussian mixture with exponentially growing number of terms with time.

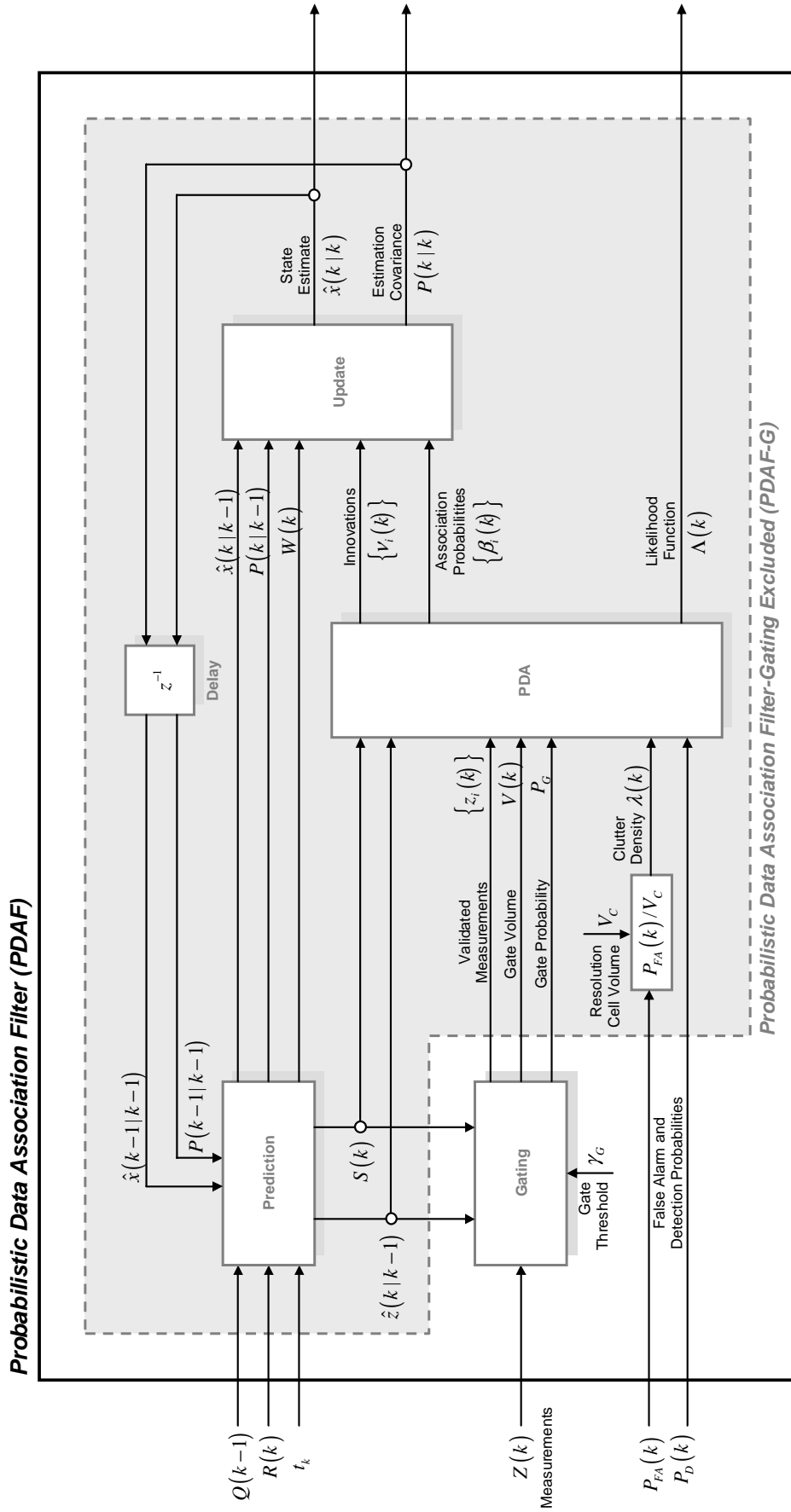


Figure B.1: Block diagram of the probabilistic data association filtering algorithm.

- **Prediction:** Prediction step of the PDAF is exactly the same as that of standard Kalman filter.

$$\hat{x}(k|k-1) = F(k-1)\hat{x}(k-1|k-1) \quad (\text{B.5})$$

$$\hat{z}(k|k-1) = H(k)\hat{x}(k|k-1) \quad (\text{B.6})$$

$$P(k|k-1) = F(k-1)P(k-1|k-1)F^T(k-1) + Q(k-1) \quad (\text{B.7})$$

$$S(k) = H(k)P(k|k-1)H^T(k) + R(k) \quad (\text{B.8})$$

$$W(k) = P(k|k-1)H^T(k)S^{-1}(k) \quad (\text{B.9})$$

- **Validation (Gating):** This step selects the measurements to be used in the update step. In this step, from the received measurement set $Z(k) = \{z_i(k), i = 1, 2, \dots, m_k\}$, only the measurements falling inside an ellipsoidal gate are selected. This selection can be mathematically described as

$$V_G(k, \gamma_G) \triangleq \left\{ z_i(k) : [z_i(k) - \hat{z}(k|k-1)]^T S^{-1}(k) [z_i(k) - \hat{z}(k|k-1)] \leq \gamma_G \right\} \quad (\text{B.10})$$

where γ_G is defined as the *gate threshold*. Any measurement $z_i(k)$ satisfying (B.10) is called a *validated measurement*. The volume of this hyper-ellipsoid gate is given by

$$V(k) \triangleq c_{n_z} \gamma_G^{n_z/2} |S(k)|^{1/2} \quad (\text{B.11})$$

where $c_{n_z} \triangleq \pi^{n_z/2} / \Gamma(n_z/2 + 1)$, with $\Gamma(\cdot)$ being gamma function, is the volume of the n_z -dimensional unit hypersphere ($c_1 = 2, c_2 = \pi, c_3 = 4\pi/3$, etc.).

- **Probabilistic Data Association (PDA):** This part is the heart of the PDAF algorithm. In the previous gating step, the measurements to be used in the update are already determined. The PDAF uses all these validated measurements in its update step by weighting (or mixing) them statistically. The weights, called *association probabilities*, are determined such that a measurement which is statistically closer to the predicted

one, i.e., $\hat{z}(k|k-1)$, gets higher association probability or vice versa. Association probabilities are calculated as follows.

$$\beta_i(k) = \begin{cases} \frac{e_i(k)}{b(k) + \sum_{j=1}^{m_k} e_j(k)} & i = 1, 2, \dots, m_k \\ \frac{b(k)}{b(k) + \sum_{j=1}^{m_k} e_j(k)} & i = 0 \end{cases} \quad (\text{B.12})$$

with

$$e_i(k) = \exp \left\{ -\frac{1}{2} \nu_i^T(k) S^{-1}(k) \nu_i(k) \right\} \quad (\text{B.13})$$

$$b(k) = \left(\frac{2\pi}{\gamma_G} \right)^{n_z/2} \frac{\lambda V(k)}{c_{n_z}} \frac{(1 - P_D P_G)}{P_D}. \quad (\text{B.14})$$

Here, $\beta_0(k)$ is defined as the probability that none of the validated measurements is target originated at time step k and $\beta_i(k)$ is the probability that the i th validated measurement is target originated at time step k .

In this step, one can also calculate the likelihood function of the PDAF which is the *uniform-Gaussian mixture* defined by

$$\Lambda(k) = [V(k)]^{m_k} \left[\gamma_0(m_k) + V(k) \sum_{i=1}^{m_k} P_G^{-1} \mathcal{N}(\nu_i(k); 0, S(k)) \gamma_i(m_k) \right] \quad (\text{B.15})$$

where

$$\gamma_i(m_k) = \begin{cases} \frac{P_D P_G}{[P_D P_G m_k + (1 - P_D P_G) \lambda V(k)]^{-1}} & i = 1, 2, \dots, m_k \\ \frac{(1 - P_D P_G) \lambda V(k)}{[P_D P_G m_k + (1 - P_D P_G) \lambda V(k)]^{-1}} & i = 0 \end{cases} \quad (\text{B.16})$$

- **Update:** Finally, the predicted state is updated as

$$\hat{x}(k|k) = \hat{x}(k|k-1) + W(k) \nu(k). \quad (\text{B.17})$$

Here, different from the Kalman filter, $\nu(k)$ is called the *combined innovation* and defined by

$$\nu(k) \triangleq \sum_{i=1}^{m_k} \beta_i(k) \nu_i(k), \quad (\text{B.18})$$

that is, a weighted summation of the innovations of each validated measurement. The weights are the association probabilities $\{\beta_i(k)\}$ calculated in the PDA step. This is the discriminating step of the PDAF from

the usual Kalman filter. The covariance corresponding to (B.17) is given as

$$P(k|k) = \beta_0(k)P(k|k-1) + (1 - \beta_0(k)) [P(k|k-1) - W(k)S(k)W^T(k)] + \tilde{P}(k) \quad (\text{B.19})$$

$$= P(k|k-1) - (1 - \beta_0(k))W(k)S(k)W^T(k) + \tilde{P}(k) \quad (\text{B.20})$$

where the (weighted) *spread of the innovations* term is

$$\tilde{P}(k) \triangleq W(k) \left[\sum_{i=1}^{m_k} \beta_i(k) \nu_i(k) \nu_i^T(k) - \nu(k) \nu^T(k) \right] W^T(k). \quad (\text{B.21})$$

APPENDIX C

INTERACTING MULTIPLE MODEL ESTIMATOR

This appendix presents the assumptions and the algorithmic flow of the interacting multiple model (IMM) estimator for discrete-time jump Markov linear systems (JMLSs).

The IMM estimator [64] is often considered to be the most significant advancement in target tracking since the Kalman filter [73]. This algorithm is used many real world problems especially in maneuvering target tracking [79] and has become well accepted in the tracking community as the best approach for this task when the performance and computational requirements of the alternatives are considered [73].

C.1 Assumptions

The assumptions of the IMM algorithm are as follows.

- The dynamic system under concern obeys one of a finite number of r modes and is modeled as a multiple-model *hybrid* system whose state-space representation is given by [4]

$$x(k) = F[M(k)]x(k-1) + v(k-1, M(k)) \quad (\text{C.1})$$

$$z(k) = H[M(k)]x(k) + w[k, M(k)] \quad (\text{C.2})$$

where $M(k) \in \{1, 2, \dots, r\}$ is a discrete-time switching random process [75] which represents the system mode at k (i.e., the model in effect *during* the sampling period ending at time step k), and $v(k)$ and $w(k)$ are white, uncorrelated and of known densities. Here, $x(k)$ and $M(k)$ are called the *base state* and the *modal state* [43], respectively. As $x(k)$ is continuous-valued and $M(k)$ is discrete-valued, the overall state $\phi(k) = [x(k)^T \ M(k)^T]^T$ is hybrid, hence the name *hybrid* system [19].

- The event that the model j is in effect at k is denoted by

$$M_j(k) \triangleq \{M(k) = j\} \quad (\text{C.3})$$

- The mode jump process $M(k)$ is a Markov chain with known transition probabilities

$$\Pr\{M(k) = j | M(k-1) = i\} \triangleq \Pr\{M_j(k) | M_i(k-1)\} = \pi_{ij} \quad (\text{C.4})$$

- A Bayesian framework is used: Starting with prior probabilities of each model being in effect, given by the vector

$$\mu(0) \triangleq \begin{bmatrix} \mu_1(0) & \mu_2(0) & \dots & \mu_r(0) \end{bmatrix}^T, \quad (\text{C.5})$$

where $\mu_i(0) \triangleq \Pr\{M_i(0)\}$, i.e., the prior probability that the i th model is in effect at time 0, the posterior model probabilities are obtained.

C.2 Steps of the Algorithm

One cycle of the IMM algorithm consists of the following steps:

- **Mixing Probability Calculation:** The probability that the model i is in effect at $k-1$ given that the model j is in effect at k conditioned on the cumulative set of measurements through $k-1$, i.e., Z^{k-1} , is calculated

for every possible combinations of i, j as

$$\mu_{i|j}(k-1|k-1) \triangleq \Pr\{M_i(k-1)|M_j(k), Z^{k-1}\} \quad (\text{C.6})$$

$$= \frac{1}{\mu_j(k|k-1)} \pi_{ij} \mu_i(k-1) \quad i, j = 1, 2, \dots, r \quad (\text{C.7})$$

where

$$\pi_{ij} \triangleq \Pr\{M_j(k)|M_i(k-1), Z^{k-1}\} \quad (\text{C.8})$$

$$\mu_i(k-1) \triangleq \Pr\{M_i(k-1)|Z^{k-1}\} \quad (\text{C.9})$$

$$\begin{aligned} \mu_j(k|k-1) &\triangleq \Pr\{M_j(k)|Z^{k-1}\} \\ &= \sum_{i=1}^r \pi_{ij} \mu_i(k-1) \quad j = 1, 2, \dots, r. \end{aligned} \quad (\text{C.10})$$

The probabilities $\mu_{i|j}(k-1|k-1)$, $i, j = 1, 2, \dots, r$, which are to be used in mixing the estimates and covariances of the previous time step, are called the *mixing probabilities*.

- **Interaction (Mixing):** The mode-conditioned estimates and covariances from the previous time step, $\hat{x}^i(k-1|k-1)$ and $P^i(k-1|k-1)$ are mixed to initialize each *elemental filter*¹ [19] at the current time step as

$$\hat{x}^{0j}(k-1|k-1) = \sum_{i=1}^r \mu_{i|j}(k-1|k-1) \hat{x}^i(k-1|k-1) \quad (\text{C.11})$$

$$\begin{aligned} P^{0j}(k-1|k-1) &= \sum_{i=1}^r \mu_{i|j}(k-1|k-1) \left\{ P^i(k-1|k-1) \right. \\ &\quad \left. + [\hat{x}^i(k-1|k-1) - \hat{x}^{0j}(k-1|k-1)] \right. \\ &\quad \left. \times [\hat{x}^i(k-1|k-1) - \hat{x}^{0j}(k-1|k-1)]^T \right\} \end{aligned} \quad (\text{C.12})$$

for $j = 1, 2, \dots, r$, where $\hat{x}^{0j}(k-1|k-1)$ and $P^{0j}(k-1|k-1)$ serve as an initial condition (or a *quasi-sufficient statistic* [19]) for the filter matched to the model j .

- **Model-Matched Filtering:** Using the initial condition (C.11) with

¹ Or in its more popularly known name, *mode-matched* (or *model-matched*) filters [18].

(C.12) and the measurement(s)² at the current time step, each model-matched filter is run separately to obtain the model-conditioned estimate $\hat{x}^j(k|k)$ and the associated covariance $P^j(k|k)$. Moreover, the likelihood function corresponding to each elemental filter is computed using the initial condition (C.11) and (C.12) as

$$\Lambda_j(k) \triangleq p[z(k)|M_j(k), Z^{k-1}] \quad (\text{C.13})$$

$$\approx p[z(k)|M_j(k), \hat{x}^{0j}(k-1|k-1), P^{0j}(k-1|k-1)]. \quad (\text{C.14})$$

Depending on the type of the elemental filters (or modules) used in the IMM structure, such as Kalman filters (KFs) or probabilistic data association filters (PDAFs), it is this stage (i.e., model-conditioned filtering) that differ in implementation. The other stages of the IMM algorithm are *almost*³ the same in implementation.

- **Model Probability Update:** The previous model probabilities $\mu_i(k-1)$, $i = 1, 2, \dots, r$ are updated as follows.

$$\begin{aligned} \mu_j(k) &\triangleq \Pr\{M_j(k)|Z^k\} \\ &= \frac{1}{c} p[z(k)|M_j(k), Z^{k-1}] \Pr\{M_j(k)|Z^{k-1}\} \\ &= \frac{1}{c} \Lambda_j(k) \sum_{i=1}^r \Pr\{M_j(k)|M_i(k-1), Z^{k-1}\} \Pr\{M_i(k-1)|Z^{k-1}\} \\ &= \frac{1}{c} \Lambda_j(k) \sum_{i=1}^r p_{ij} \mu_i(k-1) \\ &= \frac{1}{c} \Lambda_j(k) \mu_j(k|k-1) \quad j = 1, 2, \dots, r \end{aligned} \quad (\text{C.15})$$

where the normalizing constant is

$$c = \sum_{j=1}^r \Lambda_j(k) \mu_j(k|k-1) \quad (\text{C.16})$$

² Depending on type of the each elemental filter, we have either single measurement like for the Kalman filter or set of (validated) measurements like for the filters used in cluttered environments, such as the probabilistic data association filter (PDAF).

³ Of course, it may still be needed to do some modifications. For example, when using PDAFs as modules in an IMM structure, gating stage should be performed *commonly* outside of each elemental filter [60], [74]. This is different than stand-alone PDAF where the gating procedure is a part of the filtering algorithm.

- **Estimate and Covariance Combination:** This last step is only for output purposes, i.e., it is not part of the algorithm recursions [18]. It combines the model-conditioned estimates and covariances according to the mixture equations

$$\hat{x}(k|k) = \sum_{j=1}^r \mu_j(k) \hat{x}^j(k|k) \quad (\text{C.17})$$

$$P(k|k) = \sum_{j=1}^r \mu_j(k) \left\{ P^j(k|k) [\hat{x}^j(k|k) - \hat{x}(k|k)] [\hat{x}^j(k|k) - \hat{x}(k|k)]^T \right\} \quad (\text{C.18})$$

VITA

Murat Şamil Aslan was born in Tekirdağ, Turkey in 1979. He received his B.S. and M.S. degrees both in Electrical and Electronics Engineering from Middle East Technical University (METU), Ankara, Turkey in 2001 and 2003, respectively. Since 2004, he has been a research scientist at İLTAREN Research and Development Group operating under Scientific and Technological Research Council of Turkey-National Research Institute of Electronics and Cryptology (TÜBİTAK-UEKAE). His research interests include detection, estimation and tracking.

His publications are as follows:

Journal Papers

- M. Şamil Aslan and A. Saranlı, “A comparison of tracker-aware detector threshold optimization schemes for tracking in clutter,” Submitted to *IEEE Transactions on Aerospace and Electronic Systems*.
- M. Şamil Aslan, A. Saranlı, and B. Baykal, “A closed-form optimum solution for the tracker-aware Neyman-Pearson detector,” Submitted to *IEEE Transactions on Aerospace and Electronic Systems*.
- M. Şamil Aslan and A. Saranlı, “Tracker-aware detector threshold optimization for maneuvering targets in clutter,” To be submitted to *IEEE Transactions on Aerospace and Electronic Systems*.

Conference Papers

- M. Şamil Aslan, A. Saranlı, “An Optimal Radar Detector Threshold Adaptation for Maneuvering Targets in Clutter,” Submitted to *IEEE Signal Processing and Communications Applications*, Antalya, Turkey, April 2009.

- M. Şamil Aslan, A. Saranlı, and B. Baykal, “Optimal tracker-aware radar detector threshold adaptation: A closed-form solution,” in *International Conference on Information Fusion*, June 2008, pp. 470–477.
- M. Şamil Aslan, A. Saranlı, and B. Baykal, “Development of a closed form solution for instantaneous threshold optimization using modified Riccati equation,” in *IEEE Signal Processing and Communications Applications*, Didim, Turkey, April 2008.
- M. Şamil Aslan, A. Saranlı, and B. Baykal, “Development of a MATLAB based target tracking simulation environment,” in *IEEE Signal Processing and Communications Applications*, Antalya, Turkey, April 2006.
- M. Şamil Aslan, S. Gökhan Tanyer, A. Saranlı, and B. Baykal, “Ağ merkezli elektronik harp kapsamında veri tümleştirme radar ağ sistemi,” in *Savunma Teknolojileri Kongresi*, O.D.T.Ü, Ankara, Türkiye, Haziran 2006.